Duke Power℠

A Duke Energy Company

DUKE POWER COMPANY
MCGUIRE NUCLEAR STATION
CATAWBA NUCLEAR STATION

Nuclear Physics Methodology For Reload Design

DPC-NF-2010-A
Revision 1

SER Dated October 1, 2002

Nuclear Generation Department
Nuclear Engineering

Revision History

Revision	Description
DPC-NF-2010, Original Issue	Originally submitted to the NRC for approval in July 1984. Additional information was submitted to the NRC supplying responses to a request for additional information.
DPC-NF-2010-A, Original Issue	NRC approved version issued in May 1985.
DPC-NF-2010, Revision 1	Submitted to the NRC for approval in August 2001. This revision updates the report for completeness to indicate the use of NRC approved methods approved subsequent to the implementation of the original issue including the use of CASMO-3/SIMLUATE-3 reactor physics methods. This revision also removes unnecessary data including items not reviewed by the NRC in the original version and general fuel data not necessary for these methods. Also various editorial changes are made, including updating the Table of Contents. Changes associated with this revision are denoted by revision bars, except format changes.
DPC-NF-2010-A, Revision 1	NRC approved. SER issued October 1, 2002.

STATEMENT OF DISCLAIMER

This report was prepared by Duke Power Company ("Duke Power") for filing with the United States Nuclear Regulatory Commission ("USNRC") for the sole purpose of obtaining approval of Duke Power's PWR nuclear design methods at McGuire and Catawba. Duke Power makes no warranty or representation and assumes no obligation, responsibility, or liability with respect to the contents of this report or its accuracy or completeness. Any use of or reliance on the report or the information contained in this report is at the sole risk of the party using or relying on it.

ABSTRACT

This Technical Report describes Duke Power Company's Nuclear Design Methodology for the McGuire and Catawba Nuclear Station. The nuclear design process consists of mechanical properties used as nuclear design input, the nuclear code system and methodology Duke Power intends to use to perform design calculations and to provide operational support, and the development of statistical reliability factors.

TABLE OF CONTENTS

		Page
1.	INTRODUCTION	1-1
	1.1 General Nuclear Design Description	1-1
	1.2 Definition of Terms	1-3
2.	FUEL DESCRIPTION	2-1
3.	NUCLEAR CODE SYSTEM	3-1
	3.1 Introduction	3-1
	3.2 Sources of Input Data	3-1
	3.3 Cross Section Preparation	3-2
	3.3.1 Fuel Calculations	3-3
	3.3.2 Non-Fuel Calculations	3-3
	3.4 PDQ07 Models	3-4
	3.4.1 Colorset PDQ07 Modeling	3-4
	3.4.2 Quarter Core PDQ07 Model	3-5
	3.5 EPRI-NODE-P Model	3-7
	3.6 CASMO-3/SIMULATE-3 Model	3-8
4.	FUEL CYCLE DESIGN	4-1
	4.1 Preliminary Fuel Cycle Design - Initialization	4-1
	4.1.1 Review of Design Basis Information	4-1
	4.1.2 Determination of Cycle - Specific Operating Requirements	4-1
	4.1.3 Preliminary Loading Pattern and Reload Region Determination	4-2
	4.2 Final Fuel Cycle Design	4-2
	4.2.1 Fuel Shuffle Optimization and Cycle Depletion	4-3
	4.2.2 Rod Worth Calculations	4-3
	4.2.2.1 Control Rod Worths	4-4
	4.2.2.2 Shutdown Margin	4-4
	4.2.2.3 Rod Insertion Limit Verification	4-5
	4.2.2.4 Ejected Rod Analysis	4-5
	4.2.2.5 Dropped Rod Analysis	4-7
	4.2.3 Fuel Burnup Calculations	4-7

TABLE OF CONTENTS (CONT.)

		Page
4.2.4	Reactivity Coefficients and Deficits	4-7
4.2.4.1	Doppler Coefficient	4-8
4.2.4.2	Moderator Temperature Coefficient	4-8
4.2.4.3	Isothermal Temperature Coefficient	4-9
4.2.4.4	Power Coefficient and Power Defect	4-9
4.2.4.5	Miscellaneous Coefficients	4-11
4.2.4.6	Boron Related Parameters	4-11
4.2.4.7	Xenon Worth	4-11
4.2.4.8	Kinetics Parameters	4-12
4.2.5	Assessment of the Fuel Cycle Design	4-12
5.	NODAL ANALYSIS METHODOLOGY	5-1
5.1	Purpose and Introduction	5-1
5.2	Fuel Cycle Depletion	5-2
5.3	Rod Worth Analysis	5-2
5.3.1	Differential Rod Worth Analysis	5-3
5.3.2	Integral Rod Worth Analysis	5-3
5.4	Shutdown Margin Analysis	5-4
5.4.1	Shutdown Margin	5-4
5.4.2	Shutdown Boron Concentration	5-5
5.5	Rod Insertion Limit Assessment	5-5
5.6	Trip Reactivity Analysis	5-7
5.6.1	Minimum Trip Reactivity	5-7
5.6.2	Trip Reactivity Shape	5-8
5.7	Assessment of Nodal Analyses	5-8
6.	CALCULATION OF SAFETY RELATED PHYSICS PARAMETERS	6-1
6.1	Safety Analysis Physics Parameters	6-1
6.2	Core Power Distributions	6-1
6.3	Power Peaking and Reliability Factors	6-2
7.	3-D POWER PEAKING ANALYSIS	7-1
8.	RADIAL LOCAL ANALYSIS	8-1
8.1	Background	8-1

TABLE OF CONTENTS (CONT.)

	Page
8.2 Comparison of PDQ07 to CASMO-2 at Hot Full Power Condition	8-1
8.3 Comparisons of PDQ07 to Cold Criticals	8-2
8.4 BNL Benchmark Assembly Problem	8-2
8.5 Conclusion	8-3
9. DEVELOPMENT OF CORE PHYSICS PARAMETERS	9-1
9.1 Startup Test Predictions	9-1
9.1.1 Critical Boron Concentrations and Boron Worths	9-1
9.1.2 Xenon Worth and Defect	9-2
9.1.3 Rod Worths	9-3
9.1.3.1 Group Worths	9-3
9.1.3.2 Stuck Rod Worth	9-3
9.1.3.3 Dropped Rod Worth	9-3
9.1.3.4 Ejected Rod Worth	9-4
9.1.4 Reactivity Coefficients	9-4
9.1.4.1 HZP Coefficients	9-4
9.1.4.2 HFP Coefficients	9-5
9.1.5 Power Distribution	9-5
9.1.6 Kinetics Parameters	9-5
9.2 Startup and Operation Report	9-6
10.0 PHYSICS TEST COMPARISONS	10-1
10.1 Introduction	10-1
10.2 Critical Boron Concentrations	10-2
10.2.1 Measurement Technique	10-2
10.2.2 Calculational Technique	10-2
10.2.3 Comparison of Calculated and Measured Results	10-2
10.2.3.1 Hot Zero Power Comparison	10-2
10.2.3.2 Hot Full Power Comparison	10-3
10.2.4 Summary	10-3
10.3 Control Rod Worth	10-3
10.3.1 Measurement Techniques	10-3
10.3.2 Calculational Techniques	10-3
10.3.3 Comparisons of Calculated and Measured Results	10-4
10.3.4 Summary	10-4

TABLE OF CONTENTS (CONT.)

	Page
10.4 Ejected Rod Worths	10-5
10.4.1 Measurement Technique	10-5
10.4.2 Calculational Technique	10-5
10.4.3 Comparison of Calculated and Measured Results	10-5
10.5 Isothermal Temperature Coefficient	10-5
10.5.1 Measurement Technique	10-6
10.5.2 Calculational Technique	10-6
10.5.3 Comparison of Calculated and Measured Results	10-6
10.5.4 Summary	10-6
11. POWER DISTRIBUTION COMPARISONS	11-1
11.1 Introduction and Summary	11-1
11.1.1 Introduction	11-1
11.1.2 Summary	11-1
11.2 Measured Data	11-2
11.2.1 Measured Assembly Power Data	11-2
11.2.2 Measurement System Description	11-2
11.3 EPRI-NODE-P Power Distribution	11-3
11.3.1 EPRI-NODE-P Model	11-3
11.3.2 Fuel Cycle Simulation	11-3
11.3.3 Radial Power Methodology	11-5
11.3.4 Assembly Peak Axial Power Methodology	11-5
11.3.5 Conclusions	11-6
11.4 PDQ07 - Power Distribution Comparisons	11-6
11.5 Statistical Analysis	11-6
11.5.1 Observed Nuclear Reliability Factor Derivation	11-6
11.5.2 Normality Test Results	11-9
11.5.3 Observed Nuclear Reliability Factors for EPRI-NODE-P	11-10
11.5.4 Quantitative Comparison of EPRI-NODE-P to Measurement	11-11
11.5.5 Relative Percent Differences	11-12
11.5.6 Conclusions	11-13
12. REFERENCES	12-1

TABLE OF CONTENTS (CONT.)

APPENDIX A: Code Summary

APPENDIX B: NRC/DPC Correspondence Regarding NRC Request for Additional Information

APPENDIX C: Original Issue NRC SER

APPENDIX D: Revision 1 NRC SER

LIST OF TABLES

Table		Page
3-1	EPRI-CELL/CASMO-2 Cross Sections Calculation by Composition	3-9
4-1	Nuclear Design Data for Reload Design	4-13
4-2	Shutdown Margin Calculation	4-14
4-3	Typical Boron Parameters	4-15
5-1	BOC Trip Reactivity Calculation	5-9
8-1	Characteristics of 1/8th Assembly Simulations	8-4
8-2	Peak Pin Power Comparison	8-5
8-3	Statistical Summary of Percent Differences between PDQ07 and CASMO-2 for Pins in Assemblies with Powers Greater Than or Equal to 1.000	8-6
9-1	Critical Boron Concentrations (ppmB)	9-7
9-2	Boron Worth (pcm/ppmB)	9-8
9-3	Typical Core Physics Data	9-9
10-1	McGuire Critical Boron Concentrations at Hot Zero Power, BOC	10-7
10-2	McGuire 1 Cycle 1-1A Hot Full Power Critical Boron Concentration	10-8
10-3	McGuire Control Rod Worths at Hot Zero Power, BOC	10-9
10-4	McGuire Control Rod Worths at Hot Zero Power, BOC Using Boron EndPoints	10-10
10-5	McGuire PDQ07 Calculated Control Rod Worths vs. Measured Rod Worths at HZP, BOC	10-11
10-6	McGuire 1 Cycle 1 Ejected Rod Worths	10-12
10-7	McGuire Isothermal Temperature Coefficients at Hot Zero Power, BOC	10-13
11-1	McGuire Unit 1 Cycle 1 State Points	11-15
11-2	McGuire Unit 1 Cycle 1A State Points	11-16
11-3	Sequoyah Unit 1 Cycle 1 State Points	11-17

LIST OF TABLES (CONT.)

Table		Page
11-4	McGuire Unit 1 Cycles 1 and 1A and Sequoyah Unit 1 Cycle 1 State Points for PDQ07 Calculated and Measured Data	11-18
11-5	Difference Distribution Normality Tests for (C, M $\geq$ 1.0) - 5% Level of Significance	11-19
11-6	Calculated ORNFs and Associated Data	11-20
11-7	Difference, Means, and Standard Deviations for Assembly Radial Powers (C, M $\geq$ 1.0)	11-21
11-8	Difference, Means, and Standard Deviations for Assembly Peak Axial Powers (C, M $\geq$ 1.0)	11-22
11-9	Percent Difference Means (C,M $\geq$ 1.0) - Assembly Radial Powers	11-23
11-10	Percent Difference Means (C,M $\geq$ 1.0) - Assembly Peak Axial Powers	11-24

LIST OF FIGURES

Figure		Page
3-1	Nuclear Flow Chart For EPRI-ARMP	3-10
3-2	17x17 Assembly PDQ07 Colorset Geometry	3-11
3-3	PDQ07 Quarter Core Model Assembly Geometry	3-12
3-4	PDQ07 Quarter Core 17x17 Geometry	3-13
8-1	CASMO-2 and PDQ-7 Rod Power Comparison BOL HFP No Xenon Case Number 1	8-7
8-2	CASMO-2 and PDQ-7 Rod Power Comparison BOL HFP No Xenon Case Number 2	8-8
8-3	CASMO-2 and PDQ-7 Rod Power Comparison BOL HFP No Xenon Case Number 3	8-9
8-4	CASMO-2 and PDQ-7 Rod Power Comparison BOL HFP No Xenon Case Number 4	8-10
8-5	CASMO-2 and PDQ-7 Rod Power Comparison BOL HFP No Xenon Case Number 5	8-11
8-6	CASMO-2 and PDQ-7 Rod Power Comparison BOL HFP No Xenon Case Number 6	8-12
8-7	CASMO-2 and PDQ-7 Rod Power Comparison BOL HFP No Xenon Case Number 7	8-13
8-8	CASMO-2 and PDQ-7 Rod Power Comparison BOL HFP No Xenon Case Number 8	8-14
8-9	CASMO-2 and PDQ-7 Rod Power Comparison BOL HFP No Xenon Case Number 9	8-15
8-10	CASMO-2 and PDQ-7 Rod Power Comparison BOL HFP No Xenon Case Number 10	8-16
9-1	Boron Letdown Curve HFP, ARO	9-10
9-2	Differential Boron Worth HZP, BOL	9-11
9-3	Inverse Boron Worth HFP, ARO	9-12
9-4	Equilibrium Xenon Worth HFP	9-13
9-5	Xenon Reactivity Defect BOL	9-14
9-6	Integral Rod Worth HZP, BOL	9-15
10-1	McGuire 1 Cycle 1 Boron Letdown Curves	10-14
10-2	McGuire 1 Cycle 1A Boron Letdown Curves	10-15

LIST OF FIGURES (CONT.)

Figure		Page
11-1	Instrumented Fuel Assemblies McGuire and Sequoyah	11-25
11-2	Control and Shutdown Bank Locations McGuire Unit 1 Cycle 1	11-26
11-3	Core Loading Pattern McGuire Unit 1 Cycle 1	11-27
11-4	Control and Shutdown Bank Locations Sequoyah Unit 1 Cycle 1	11-28
11-5	Core Loading Pattern Sequoyah Unit 1 Cycle 1	11-29
11-6 to 11-30	McGuire 1 Cycle 1 Assembly Radial Powers Calculated vs. Measured	11-30 to 11-54
11-31 to 11-55	McGuire 1 Cycle 1 Assembly Peak Axial Powers Calculated vs. Measured	11-55 to 11-79
11-56 to 11-60	McGuire 1 Cycle 1A Assembly Radial Powers Calculated vs. Measured	11-80 to 11-84
11-61 to 11-65	McGuire 1 Cycle 1A Assembly Peak Axial Powers Calculated vs. Measured	11-85 to 11-89
11-66 to 11-72	Sequoyah 1 Cycle 1 Assembly Radial Powers Calculated vs. Measured	11-90 to 11-96
11-73 to 11-79	Sequoyah 1 Cycle 1 Assembly Peak Axial Powers Calculated vs. Measured	11-97 to 11-103
11-80 to 11-83	McGuire 1 Cycle 1 PDQ07 Assembly Radial Powers Calculated vs. Measured	11-104 to 11-107
11-84 to 11-86	Sequoyah 1 Cycle 1 PDQ07 Assembly Radial Powers Calculated vs. Measured	11-108 to 11-110

1. INTRODUCTION

1.1 General Nuclear Design Description

A commercial Pressurized Water Reactor (PWR) is designed to hold a constant number of nuclear fuel assemblies which are generally identical mechanically, but differ in the amount of fissile material content. During cycles subsequent to the initial cycle, fuel assemblies differ in burnup as well. Refueling occurs at intervals appropriate for the power production needed, for example 12, 18, or 24 months. At refueling, a predetermined number of irradiated fuel assemblies are discharged and the same number are loaded as fresh (reload region) or possibly irradiated assemblies. The fuel management scheme determines the locations of all fresh and irradiated assemblies.

This report describes some of the various aspects of nuclear design with principal emphasis placed upon development of a core loading pattern and nuclear calculations performed to evaluate safety and operational parameters. The following sections provide detailed discussion, including descriptions, of design methods, analytical formulations, and calculational procedures involved in the various nuclear design tasks for the McGuire and Catawba Nuclear Stations. The nuclear design is essentially a series of analytical calculations with the objective of designing the reload core in such a manner that the reactor can be operated up to a specified power level for a specified number of days within acceptable safety and operating limits. It consists of the development of the basic specifications of the reload region (fuel enrichment, number of assemblies, uranium loading, etc.); it sets forth the number and identity of each residual fuel assembly, selects the location of each fuel assembly in the core for the new fuel cycle, and establishes the core characteristics. The nuclear design used in conjunction with the thermal hydraulic and safety analyses establishes the operating limits, control rod limits, and protection system setpoints.

In arriving at the final nuclear design, the designer tries to meet the requirements imposed by the operational considerations, fuel economics

considerations, and safety considerations. These requirements are called nuclear design criteria and are as follows:

1. Initial core excess reactivity will be sufficient to enable full power operation for the desired length of the cycle, with appropriate allowance for any planned coastdown.

2. The fuel assemblies to be discharged at the end of the fuel cycle will attain maximum permissible burnup so that maximum energy extraction consistent with the fuel mechanical integrity criteria is achieved.

3. Values of important core parameters (moderator temperature coefficient, Doppler coefficient, ejected rod worth, boron worth, control rod worth, maximum linear heat rate of the fuel pin at various elevations in the core, and shutdown margin) predicted for the cycle are conservative with respect to the values assumed in the safety analysis of various postulated accidents. If they are not conservative, acceptable reevaluation or reanalysis of applicable accidents is performed, or the core is redesigned.

4. The power distributions within the reactor core for all possible (or permissible) core conditions that could exist during the operation of the cycle will not lead to exceeding the thermal design criteria of the fuel or exceeding the LOCA-limited peaking factors.

5. Fuel management will produce fuel rod power and burnup consistent with the mechanical integrity analysis of the fuel rod.

The nuclear design process described in this report consists of mechanical properties used as nuclear design input, the nuclear code system and methodology Duke Power intends to use to perform design calculations and to provide operational support, and the development of statistical reliability factors.

The nuclear design calculations described in this report are covered by the Duke Power Quality Assurance program (Reference 21).

1.2 Definition of Terms

Presented below are terms which will be needed throughout the text of the report:

a/o	atom percent
ARI	all rods in
ARO	all rods out
axial offset (AO)	$\frac{P_T - P_B}{P_T + P_B}$, where P_T is the integrated power in the top half of the core, and P_B is the integrated power in the bottom half of the core
β_i	delayed neutron fraction for group i
β_{eff}	effective delayed neutron fraction in core
BOL	beginning of life
BP	burnable poison
BU	fuel burnup
C_B	Chemical shim boron concentration in the main coolant
CZP	cold zero power
EOL	end of cycle life
EQXE	equilibrium xenon condition
GWD/MTU	Gigawatt days per metric ton of initial uranium metal, 1 GWD/MTU is 1000 MWD/MTU
HFP	hot full power
HZP	hot zero power

$\bar{I}$	delayed neutron importance factor
ΔI or Axial Flux Difference (AFD)	flux difference between the top and bottom halves of the core; in this report, ΔI is a calculated value, rather than a difference between measured signals from the excore detectors
K(z)	F_Q^T normalized to the maximum value allowed at any core height
ℓ^*	prompt neutron lifetime
MOL	middle of cycle life
MWD/MTU	measure of energy extracted per unit weight of initial uranium metal fuel; is equal to 1 megawatt times 1 day, divided by 1 metric ton of uranium
pcm	percent mille (a reactivity change that equals 10^{-5} $\Delta\rho$)
ppm	parts per million by weight; which specifies the amount of chemical shim boron present by weight in the main coolant system
radial local	ratio of assembly maximum rod to assembly average x-y power
RCCA	rod cluster control assembly; the type of control rod assembly used in McGuire and Catawba. (All RCCA are full length absorbers for both plants.)
ρ	reactivity
$\Delta\rho$	$\frac{K_1 - K_2}{K_1 \times K_2}$, where K_1 and K_2 are eigenvalues obtained from two calculations where only one parameter was varied
shutdown margin	amount of negative reactivity (ρ) by which a reactor core is maintained in a HZP subcritical condition after a control rod trip
step	unit of control rod travel equal to 0.625 inch
TMOD	moderator temperature; defined as the temperature corresponding to the average water enthalpy of the core
T_{res}	resonance temperature of the fuel
w/o	weight percent

Power distributions will be quantified in terms of hot channel factors. These factors are a measure of the peak pellet power and the energy produced in the coolant. The factors are:

Power density	thermal power produced per unit volume of the core (KW/liter)
Linear Power Density	thermal power produced per unit length of active fuel (KW/ft)
Average Linear Power Density	total thermal power produced in the core divided by the total active fuel length of all fuel rods in the core
Local Heat Flux	local heat flux on the cladding surface (BTU/ft^2/hr)
Rod Power or Integral Power	is the length integrated linear power density in one rod (KW)

Various hot channel factors are:

F_Q^T, Heat Flux Hot Channel Factor, the maximum local heat flux on the surface of a fuel rod divided by the average fuel rod heat flux, including conservatisms for fuel pellet and rod dimensional uncertainties.

F_Q^N, Nuclear Heat Flux Hot Channel Factor, is defined as the maximum local fuel rod linear power density divided by the average linear power density, assuming nominal fuel rod and pellet dimensions.

F_Q^E, Engineering Heat Flux Hot Channel Factor, is the allowance on heat flux required for manufacturing tolerances. The engineering factor allows for local variations in enrichment, pellet density and diameter. Combined statistically the net effect is typically a factor of 1.03 to be applied to calculated KW/ft.

$F_{\Delta H}^N$, Nuclear Enthalpy Rise Hot Channel Factor, is defined as the ratio of the integral of linear power along the rod with the highest integrated power to the average rod power.

2. FUEL DESCRIPTION

The reactor cores for McGuire and Catawba contain 193 fuel assemblies. Each fuel assembly consists of 264 fuel rods, 24 guide thimble tubes and 1 instrumentation thimble tube assembled in a square 17x17 lattice. The assembly structure consists of top and bottom nozzles and grid assemblies positioned axially along the fuel assembly. Each fuel rod contains a column of stacked fuel pellets.

Detailed design data for the fuel pellets, fuel rods, fuel assembly, and reactivity control components can be found in the Updated Final Safety Analysis Report[18,19] (UFSAR).

3. NUCLEAR CODE SYSTEM

3.1 Introduction

Nuclear design calculations performed for Westinghouse reactors employ the EPRI-ARMP code system[1] and the CASMO-2 code[2] or the CASMO-3/SIMULATE-3P code system. A summary description of each code is given in Appendix A. The ARMP/CASMO-2 and the CASMO-3/SIMULATE-3 code sequences have been reviewed and approved by the NRC for use in the design of reload cores for the McGuire and Catawba Nuclear Stations by Duke Power[28,32].

Presented in this section will be a description of the sequence, cross section preparation and parameterization, and reload design modeling procedures.

The nuclear calculational system enables the nuclear engineer to numerically model and simulate the reactor core. The ARMP/PDQ code system sequence used by Duke Power for McGuire and Catawba is outlined in Figure 3-1. The CASMO-3/SIMULATE-3 code system sequence is outlined in Reference 28.

3.2 Sources of Input Data

The determination of nuclear fuel loading patterns and core physics characteristics requires an accurate database consisting of:

1. Core operating conditions
2. Dimensional characteristics
3. Composite materials and mechanical properties
4. Nuclear cross sections

The UFSAR, supplemented by vendor reports and open literature, is the primary source of data for Items 1 to 3. These data are used as input to the cross section generators and core simulators. A secondary data source for the core simulators are estimates of fuel pellet volume-averaged temperatures which are calculated by fuel performance codes as a function of power and burnup.

The cross section generators CASMO-2 and EPRI-CELL[8] use processed ENDF/B libraries unique to each code.

EPRI-CELL is a unit cell lattice code which is used to calculate few-group cross sections for fuel and non-fuel compositions as shown in Table 3-1.

CASMO-2 uses a processed version[9] of the ENDF/B-3 library. Group cross sections of σ_a, σ_f, $\nu\sigma_f$, σ_{tr}, scattering kernels, resonance integrals, and fission product data are among the data contained in this library. The 69 group library is divided into 14 fast, 13 resonance, and 42 thermal energy range groups. A 25 group version of this library is also used.

The EPRI-CELL library is derived from the ENDF/B-4 library[10]. The 97 energy groups are divided into 62 fast groups and 35 thermal groups.

CASMO-3 cross section development for SIMULATE-3 is described in Reference 28.

3.3 Cross Section Preparation

In order to model the neutronics of a reload core, it is necessary to generate a set of cross sections for use in a diffusion theory code. CASMO-3, CASMO-2, and EPRI-CELL are the cross section generators that may be used.

Inputs which are provided to these codes are: lattice materials and geometry, temperatures for fuel, clad, and moderator, effective resonance temperature, fuel enrichment, soluble boron concentration, number of depletion steps, length of depletion steps, etc. Table 3.1 shows the core materials or compositions which are parameterized by CASMO-2 and EPRI-CELL.

PDQ requires pin cell cross sections calculated as described Sections 3.3.1 and 3.3.2.

Reference 28 describes the cross section and nuclear data requirements for SIMULATE-3.

3.3.1 Fuel Calculations

Calculations for fuel regions employ fixed fuel and moderator temperatures for the cell depletion. Restart calculations are performed at various burnups to parameterize fuel cell cross sections at varying moderator and fuel temperatures.

The output of EPRI-CELL and CASMO-2 consists of sets of broad group cross sections which characterize the regions of interest. Cross sections are then formatted into PDQ07 tableset structure using either NUPUNCHER[11] (1-dimensional parameterization), or MULTIFIT[12] (2 and 3 dimensional parameterization or g-factors). Cross sections from CASMO-2 are similarly formatted using CHART[13].

3.3.2 Non-Fuel Calculations

Cross sections for empty control rod guide tubes, reflector, instrument thimble, and the water gap are calculated with either EPRI-CELL or CASMO-2. Separate cross section sets are generated for various moderator temperatures.

Strong absorbers such as RCCA and BP require reaction rate matching to obtain diffusion theory equivalent cross sections. Calculations using CASMO-2 are performed for these strong absorbers where first a transport theory method determines absorption rates, and then a series of diffusion theory iterations are performed to calculate a g-factor such that the absorption rates agree between both types of flux solutions. These g-factors are then incorporated in the tabulated cross sections.

RCCA cross sections are evaluated at BOL HFP conditions, while BP cross sections are evaluated with an HFP depletion calculation.

In both types of g-factor calculations, lattices with expected core average enrichments are used. Core baffle cross sections are also calculated with CASMO-2. A lattice geometry is employed, with the baffle material density

modified to reflect real versus modeled thickness in the quarter core PDQ07 discrete pin model.

3.4 PDQ07 Models

The PDQ07 few-group diffusion-depletion code is employed for core modeling. Two different models are used.

The first is the assembly colorset model, which is used for calculating k_∞ and M^2 data for EPRI-NODE-P 3-D simulations. The second model is the quarter-core model, which is used for X-Y power distribution calculations and for normalization of EPRI-NODE-P radial power distributions.

Aspects which are common to both PDQ07 models are:

1. Discrete pin representation
2. Two-group cross sections
3. Mixed Number Density thermal group constants
4. Improved Removal Treatment removal cross sections
5. Microscopic cross section parameterization for uranium, plutonium, burnable absorber, soluble boron, xenon, samarium, and lumped fission products
6. Thermally expanded geometry - pin pitch and assembly pitch

3.4.1 Colorset PDQ07 Modeling

The colorset PDQ07 model consists typically of four quarter assemblies arranged such that a representative neutron spectrum is obtained. Figure 3-2 shows a typical colorset geometry.

To accommodate asymmetric burnable poison rod loadings, full or half assembly geometries are used. The EPRI-ARMP PWR Procedures[14] are used for modeling, and most of the conventions and guidelines are employed.

Fuel types are determined according to enrichment and BPRA loading. k_∞ and M^2 data for each fuel type are calculated by performing the following operations:

I. BOL Cases - 0 MWD/MTU

A. k_∞ and M^2 - unrodded vs. T_{mod} (Inlet, Average, Outlet)

B. k_∞ and M^2 - rodded vs. T_{mod} (Inlet, Average, Outlet)

C. Boron worth

D. Doppler worth

II. Depletion Data - Exposure dependent data

A. Nominal HFP depletion at constant Tmod, Tfuel

B. Branch cases from depletion

1. Boron worth
2. Control rod worth
3. Equilibrium Xenon worth
4. Doppler worth
5. Moderator temperature worth

In the above PDQ07 branch calculations, only one parameter is varied, allowing a partial derivative of reactivity with respect to that parameter to be calculated.

The parameterization procedure involves approximately 150-200 cases, depending on the number of depletion steps.

The output from the PDQ07 colorset cases is written to PDQ07 integral files which in turn are processed by the linking codes EPRI-FIT[15] and SUPERLINX[16] to yield B-constant data for EPRI-NODE-P.

3.4.2 Quarter Core PDQ07 Model

Two-dimensional X-Y core simulations are performed with a discrete pin PDQ07 model. Assembly average and maximum pin powers are calculated, along with

critical boron concentrations and other reactivity parameters. Moderator and Doppler feedbacks are incorporated in this model.

The geometry employed utilizes thermally expanded dimensions. Figure 3-3 shows a geometry of a fuel assembly and water gaps. Figure 3-4 shows the complete quarter core mesh layout.

The plane of solution used in quarter core analyses is the axial midplane or the six foot level of the active fuel. Moderator and Doppler feedbacks are employed as described in Reference 17.

The depletion calculation is used to determine burnup dependent parameters. The soluble boron concentration is modified at each timestep such that the reactor is approximately critical.

Timesteps are taken using point depletion so that the core average exposure advances by: 150, 500, 1000, 2000, ..., N * 2000 MWD/MTU until the end of cycle is reached.

PDQ07 depletion calculations are used to determine the following parameters:

1. Assembly average and maximum pin powers
2. Core reactivity
3. Nuclide reaction rates: Fission and absorption
4. Nuclide inventories
5. Neutron flux distributions

Other calculations performed with the quarter core model may include:

1. RCCA bank worths
2. Boron and xenon worths
3. Power deficits
4. Moderator and Doppler temperature coefficients

Cases 2, 3, and 4 are usually performed with a nodal code; however, these are shown to demonstrate the quarter core model's flexibility.

3.5 EPRI-NODE-P Model

EPRI-NODE-P is the nodal code employed for three-dimensional analyses and reactivity studies. A summary description of EPRI-NODE-P is given in Appendix A. Typical calculations which are performed with the Duke Power EPRI-NODE-P model are:

1. Full core ejected rod worths
2. Power deficits
3. Differential rod worths
4. Axial xenon transients
5. Three-dimensional power distributions, etc.

The quarter core model uses one radial node per assembly and eighteen axial nodes.

Each unique combination of enrichment and BPRA loading comprises a separate fuel type. The fuel type is parameterized by sets of fitting coefficients which determine reactivity due to control rods, exposure, soluble boron, xenon, etc. Doppler and moderator feedbacks are explicitly treated.

EPRI-NODE-P radial power distributions are normalized near the beginning of cycle. Assembly average powers are adjusted to match quarter core PDQ07 calculations with radial albedoes - α_H and an internal leakage factor - g_H. The axial power distribution, is adjusted using vertical leakage factors α_V determined from comparisons of calculated and measured axial power distributions from benchmark core follow calculations.

Sections 5, 6, 7, and 9 discuss in depth calculational procedures of EPRI-NODE-P. Sections 10 and 11 address benchmarking of EPRI-NODE-P and PDQ07 calculations to measured power and reactivity data.

3.6 SIMULATE-3 Model

The SIMULATE-3 methodology used by Duke Power Company is described in Reference 28.

TABLE 3-1

EPRI-CELL/CASMO-2 Cross Sections
Calculation by Composition

1. EPRI-CELL

   a. Uranium Fuel
   b. Empty Control Rod Guide Tube/Instrument Tube
   c. Reflector
   d. Water Gap

2. CASMO-2

   a. Burnable Poison Rod Assembly
   b. Gadolinia doped Uranium Fuel
   c. Control Rod - AgInCd or B_4C
   d. Baffle

FIGURE 3-1

Nuclear Flow Chart for EPRI-ARMP

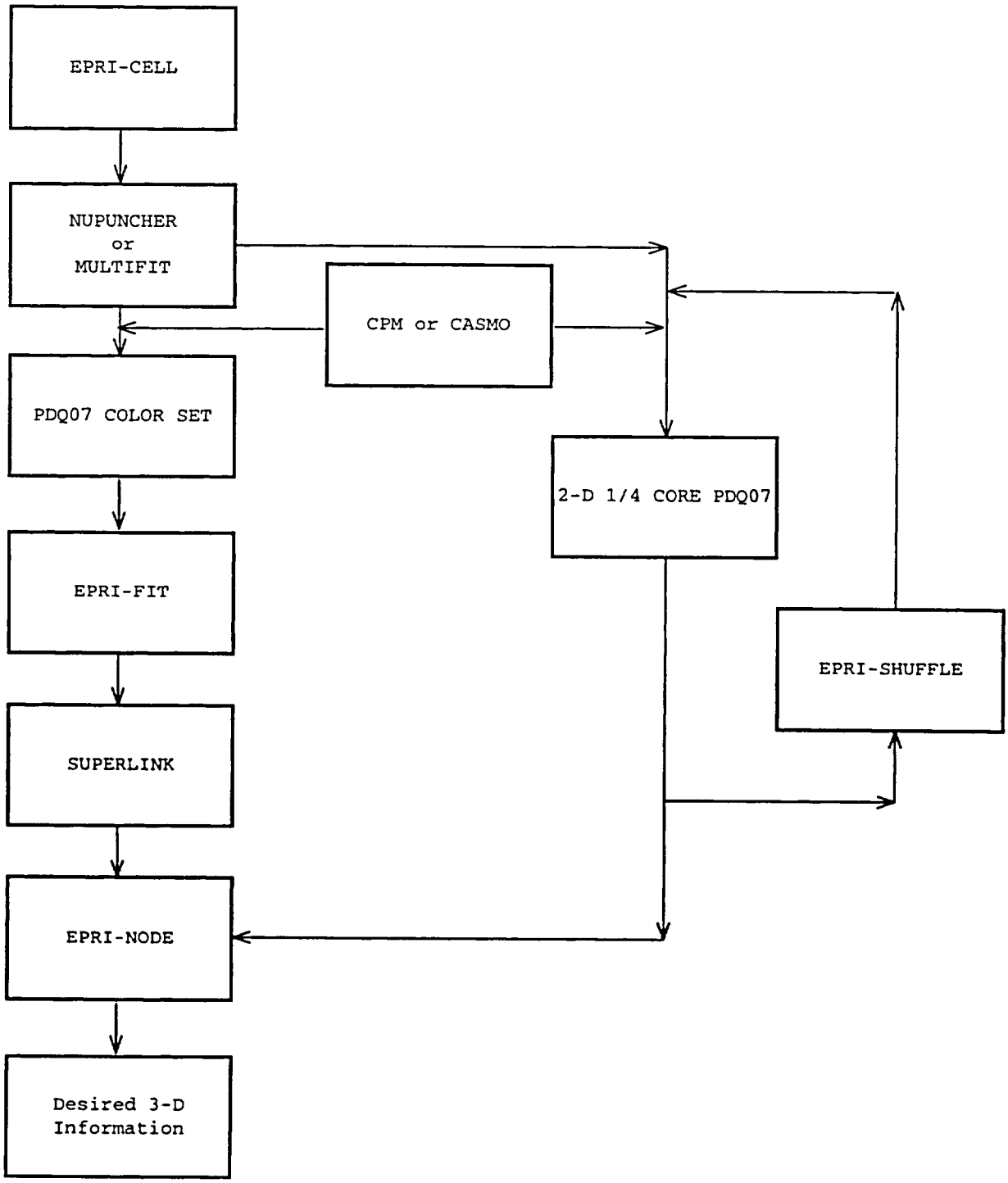

FIGURE 3-2

17 x 17 Assembly PDQ07 Colorset Geometry

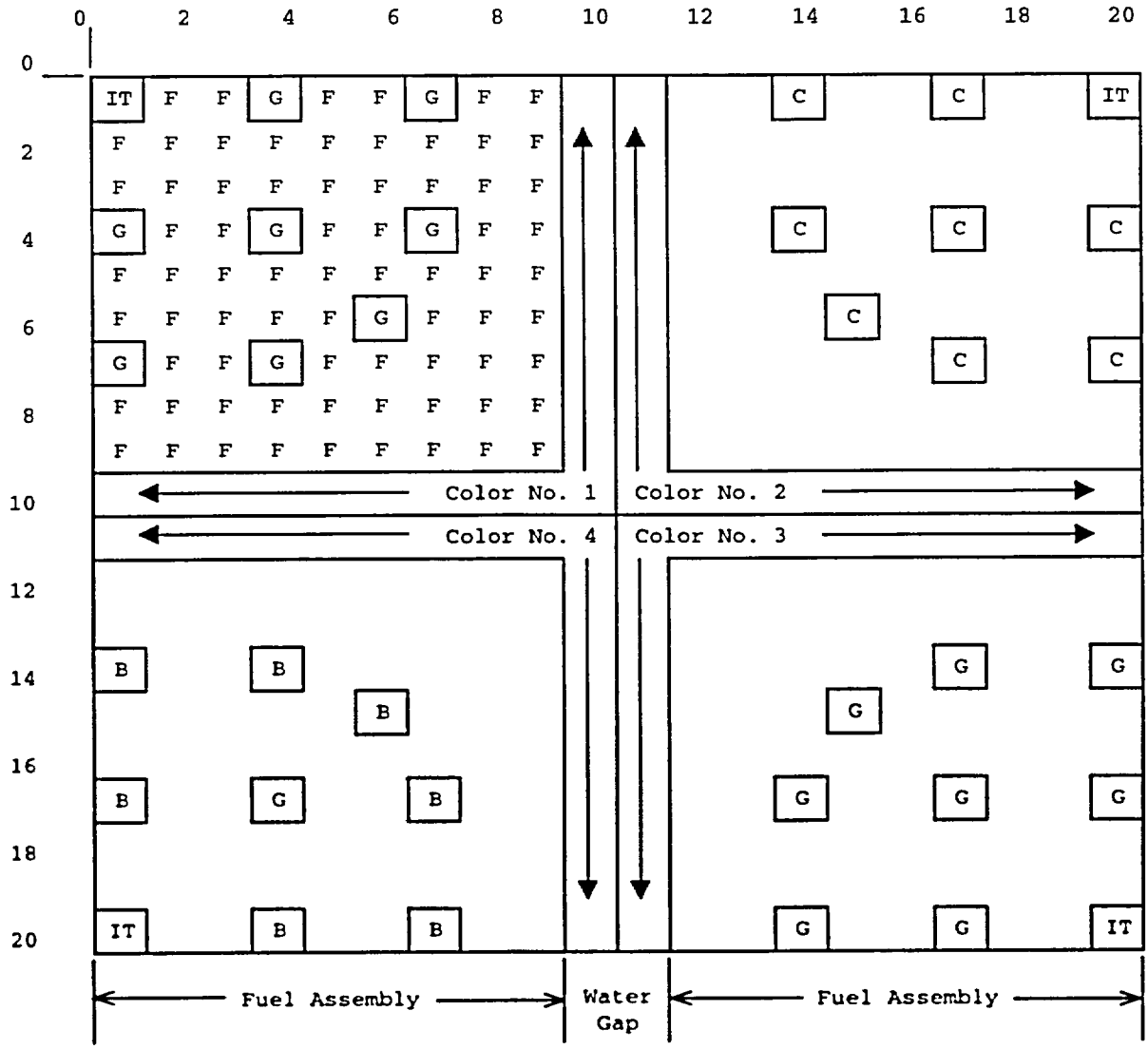

LEGEND:

IT Instrument Tube

C Guide Tube With Control Rod

B Guide Tube With Burnable Poison Rod

G Empty Guide Tube

F Fuel Rod

FIGURE 3-3

PDQ07 Quarter Core Model Assembly Geometry

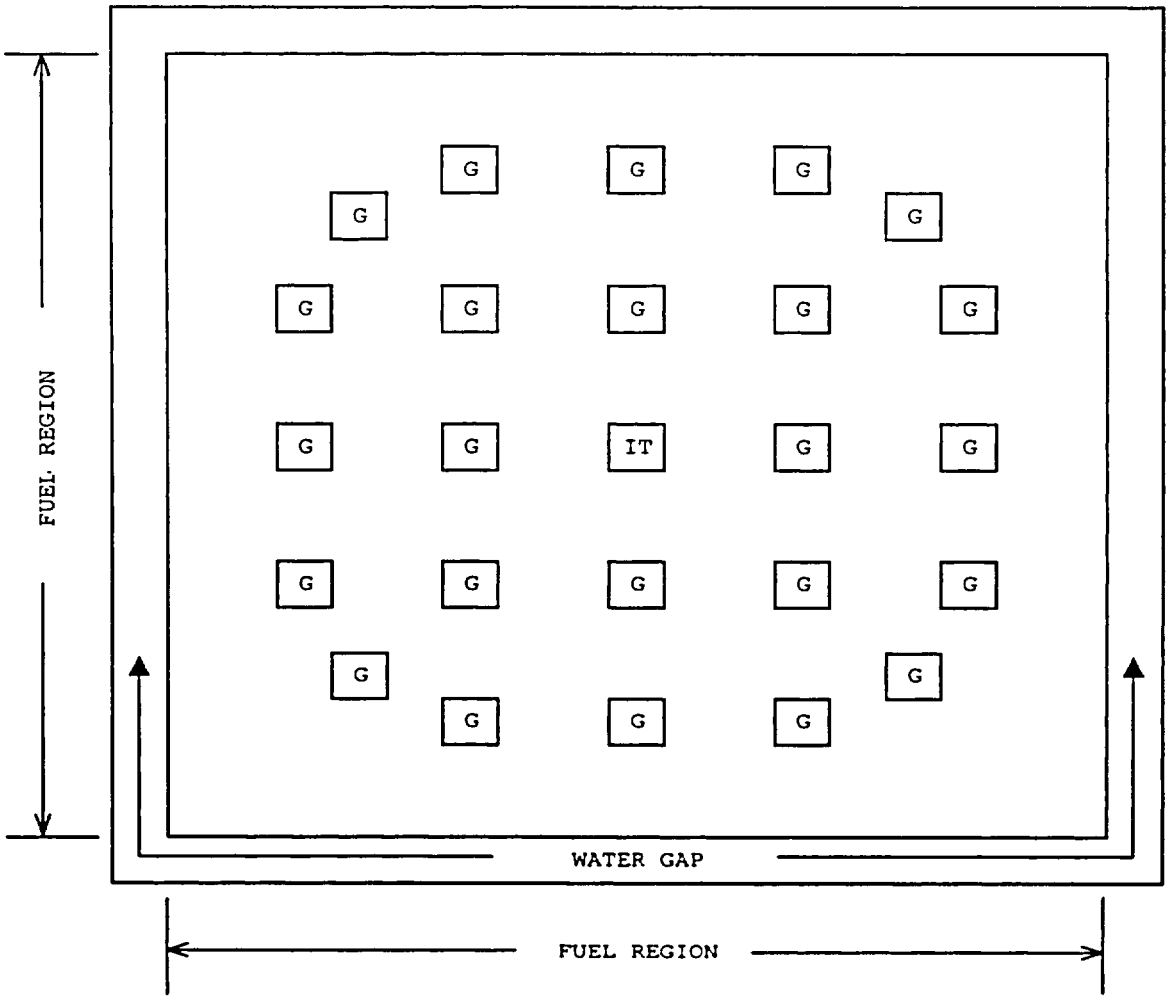

LEGEND:

IT Instrument Tube

G Control Rod Guide Tube

FIGURE 3-4

PDQ07 Quarter Core 17 x 17 Geometry

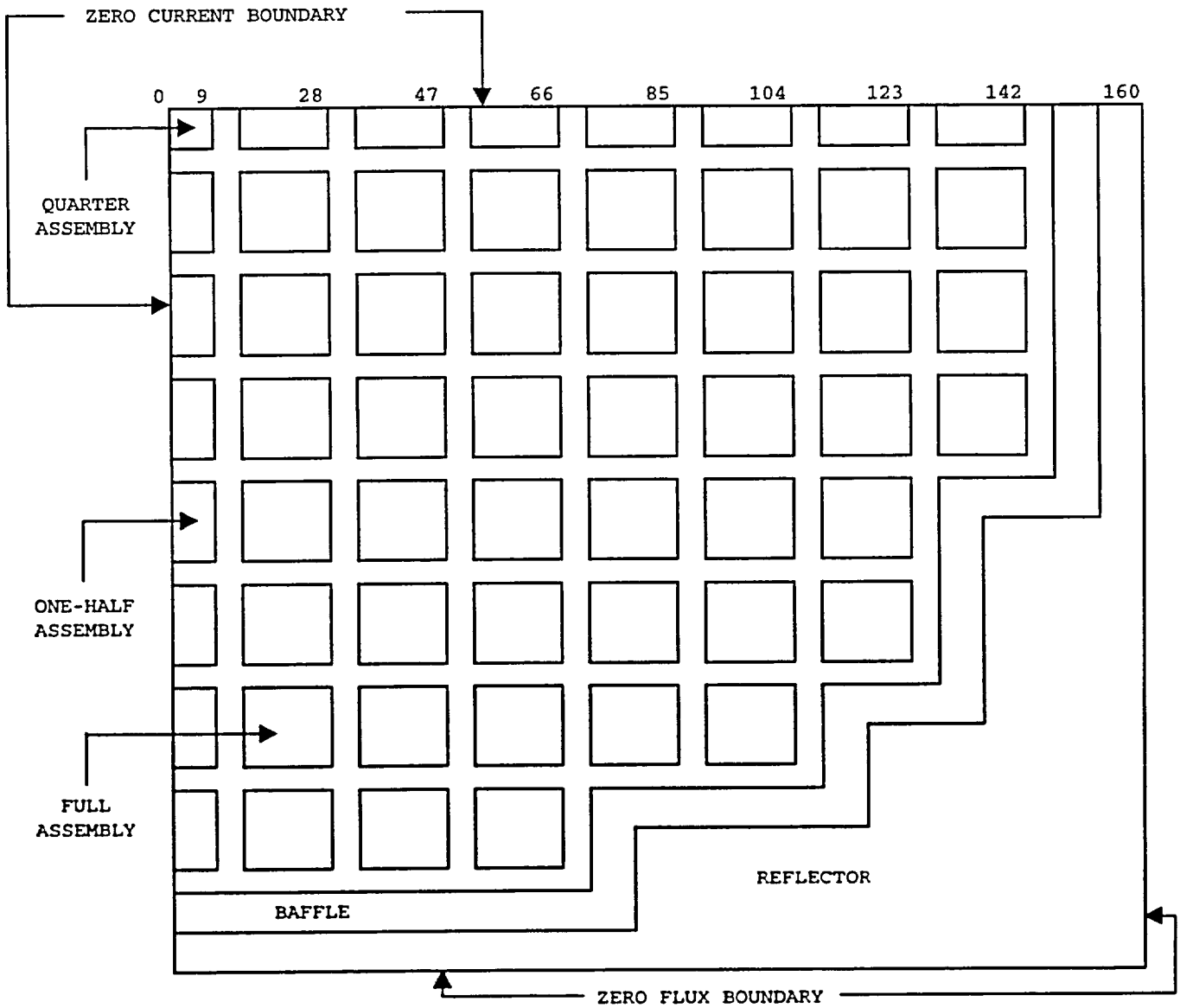

4. FUEL CYCLE DESIGN

4.1 Preliminary Fuel Cycle Design - Initialization

To commence the design of a reload, core operation requirements along with planned changes in reactor primary or secondary systems are assembled. A preliminary loading pattern is designed which meets operational requirements. Physics data from the preliminary design are compared with core operating requirements to determine the adequacy of the reload design. Likewise, physics data are compared to Technical Specifications to verify that the preliminary design will conform to existing limits.

4.1.1 Review of Design Information

The preliminary design procedure requires assembly of design information which in turn will determine the cycle's operational capabilities. Typical design data are shown on Table 4-1.

Table 4-1 and other pertinent nuclear design data are assembled and reviewed for consistency with previous sets of design data.

4.1.2 Determination of Cycle-Specific Operating Requirements

Design data from Table 4-1 uniquely determines expected operating requirements and capabilities. For instance, a longer than annual cycle may require a low leakage loading pattern and the use of burnable absorber rods. A larger energy requirement than can be provided by normal operation with a given reload enrichment may require a planned power coastdown at end of cycle. Similarly, other design considerations will govern the rest of the cycle-specific operational characteristics.

4.1.3 Preliminary Loading Pattern and Reload Region Determination

The purpose of a preliminary loading pattern analysis is to determine the uranium and separative work requirements to meet a desired cycle lifetime. The cycle lifetime is confirmed by modeling the depletion of a reload core. If the number of new fuel assemblies and the enrichment are known, this analysis will yield an estimate of the cycle lifetime.

4.2 Final Fuel Cycle Design

Having determined the number and enrichment of the fuel assemblies during the preliminary fuel cycle design, the final fuel cycle design (FFCD) concentrates on optimizing the placement of fresh and burned assemblies and burnable poison assemblies (if any) to result in an acceptable fuel cycle design. It must meet the following design criteria with appropriate reductions to account for calculational uncertainties:

1. $F^N_{\Delta H}$ must meet the limits specified in the Technical Specifications.
2. Moderator Temperature Coefficient must meet the limits specified in the Technical Specifications.
3. Maximum fuel burnup must be less than the limits applicable for the type of fuel being used.
4. Shutdown Margin must meet limits specified in the Technical Specifications.
5. Maximum linear rod power must meet the limit specified in the Technical Specifications.
6. UFSAR Chapter 15 related physics parameters must be validated.

A preliminary verification of the above is made in the FFCD. Final verification of the above is made in fuel mechanical performance analyses, thermal and thermal-hydraulic analyses, safety-analysis physics parameters analyses, and maneuvering analyses.

4.2.1 Fuel Shuffle Optimization and Cycle Depletion

The preliminary fuel shuffle scheme is modified to minimize power peaking. This is accomplished by a trial and error type search until an acceptable BOC power distribution results.

The reload design's "burnup window" is assessed to ensure that applicable safety criteria are met.

The cycle is then depleted to various times in the cycle to verify that power peaking versus burnup remains acceptable. The shuffling variations include rearranging the location of the burned or fresh fuel assemblies, BP placement, and rotation of the spent fuel assemblies. These calculations are typically performed assuming quarter core symmetry.

The core neutronic model resulting from the FFCD is the core model used for other nuclear design calculations.

The shuffle pattern determined in the FFCD may later need to be modified based upon results obtained in the remaining nuclear calculations.

4.2.2 Rod Worth Calculations

Control rods serve several functions in the McGuire and Catawba reactors. The primary function is to provide adequate shutdown capability during normal and accident conditions. They are also used to maintain criticality during power maneuvers and to maintain the Axial Flux Difference (AFD) within Technical Specification limits. Since the presence of control rods influences both power distributions and criticality, it is necessary in many calculations to evaluate not only the reactivity effect but also the perturbation that a given rod configuration has on the power distribution.

McGuire and Catawba are typically operated in the ARO or feed and bleed mode. All RCCA have full length absorber rods. During full power operation, Control

Bank D is typically inserted about six inches (215 steps withdrawn) in the active core. Control Bank D is used to control power during load follow maneuvers, and in conjunction with Control Banks B and C, to achieve criticality during startup.

Calculations of control rod worth and power peaking (F_Q) are used in the safety analysis of the reload core. The calculations discussed in subsequent sections include the following:

1. Control Rod Worths
2. Shutdown Margin
3. Ejected Rod Analysis
4. Dropped Rod Analysis

4.2.2.1 Control Rod Worths

RCCA bank locations in McGuire and Catawba usually are fixed and do not change from cycle to cycle. The worth of each control bank (A, B, C, D) is calculated at BOC and EOC, at HFP and HZP. The total rod worth (ARI) is calculated at BOC, EOC, and any limiting burnup at HZP only for use in the shutdown margin calculation.

4.2.2.2 Shutdown Margin

Searches for the highest worth stuck rod are performed at BOC, EOC, or any limiting burnup for HZP conditions using full core calculations.

Table 4-2 summarizes the results of a shutdown margin calculation. The total rod worth described in section 4.2.2.1 is shown as Item 1. Item 2 is the worth of the highest stuck rod. The total worth reduced by the stuck rod worth is shown as the net worth (Item 3). A calculational uncertainty of 10% is subtracted off in Step 4, and Step 5 shows the available rod worth.

The required rod worth is calculated next in Steps 6-9. The power deficit obtained by modeling the core at HFP and HZP (using constant boron and xenon) and subtracting the reactivities is shown as Item 6. This reactivity insertion accounts for Doppler and Moderator deficits. The maximum allowable inserted rod worth, Item 7, is obtained from the allowable rod insertion and the integral rod worth curve for that insertion. This accounts for the maximum allowed rod insertion at HFP. An axial flux redistribution occurs when the power level is reduced from HFP to HZP. This redistribution causes an increase in reactivity. If Item 6 is calculated using a 3-D model, no additional penalty is required. If Item 6 was calculated using a 2-D model, where redistribution effects are not modeled, an additional reactivity penalty is assessed as Item 8. The sum of these required worths (Item 9) is the total required worth.

Additional reactivity penalties are applied to both the power defect and the rod insertion allowance to account for xenon redistribution effects.

The shutdown margin is shown as Item 10 and is defined as the total available worth minus the total required worth. Shutdown margin requirements are specified in the Technical Specifications.

4.2.2.3 Rod Insertion Limit Verification

As part of the reload design procedure, the Rod Insertion Limits are verified for applicability in the reload core (see Section 5.5).

4.2.2.4 Ejected Rod Analysis

The UFSAR[18,19] presents the limiting criteria for the ejected rod accident. The accident has been analyzed at HFP and HZP conditions at BOL and EOL.

Ejected rod calculations are performed on a cycle-specific basis to verify that UFSAR accident analysis values are not exceeded.

Calculational limits are established using the methodology described in References 30 and 31.

To verify that the ejected rod parameters are within calculational limits, ejected rod calculations are performed at BOC and EOC or at other limiting times in cycle life at both HFP and HZP.

The HZP ejected rod calculations are performed using full core geometry with Control Banks B and C at their insertion limits in the core and with Control Bank D fully inserted. Single rods in Control Banks D, C, and B are removed in subsequent cases and the worth of the ejected rod is calculated by subtracting the reactivities of the cases before and after the rod was removed. The fuel and moderator temperature is held constant and equal to the HZP moderator temperature for these calculations. The highest worth calculated by the above procedure is the worst ejected rod at HZP. If the ejected rod worth exceeds the calculational limit, one of the following is performed: an evaluation, a revision to the rod insertion limits, a reanalysis of the Chapter 15 REA analysis, or a redesign of the core loading pattern.

The HFP ejected rod calculations are performed in a similar manner to the HZP calculations with the exceptions that only Control Bank D is inserted at the HFP insertion limit and that the fuel temperature and moderator temperatures correspond to those of HFP conditions. The HFP ejected rod worths are determined without thermal feedback to be conservative. If the ejected rod worth exceeds the calculational limit, one of the following is performed: an evaluation, a revision to the rod insertion limits, a reanalysis of the Chapter 15 REA analysis, or a redesign of the core loading pattern.

A parallel analysis, addressing core peaking, is performed at the same time as the rod worth analyses. Additional discussion of the rod ejection accident analysis methodology is contained in Reference 30.

4.2.2.5 Dropped Rod Analysis

The UFSAR[18,19] presents the limiting criteria for the dropped rod accident. The calculational limits are established using the methodology described in Reference 30.

A core model is used that evaluates pre-drop and post-drop physics parameters for possible dropped rod combinations. The physics parameters important to the dropped rod analysis are presented in Reference 30.

4.2.3 Fuel Burnup Calculations

The reload design must meet fuel burnup limits. This is confirmed during the final fuel cycle design. Depletion calculations yield core, assembly average, single fuel rod burnups, and peak local burnups which can be compared to the design limits.

4.2.4 Reactivity Coefficients and Defects

Reactivity coefficients define the reactivity insertion for small changes in reactor parameters such as moderator temperature, fuel temperature, and power level. These parameters are input to the safety analysis and used in modeling the reactor response during accidents and transients. Whereas reactivity coefficients represent reactivity effects over small changes in reactor parameters, reactivity defects usually apply to reactivity inserted from larger changes typical of HFP to HZP. An example of a reactivity deficit is the power defect from HFP to HZP used in the shutdown margin calculation. A different way of looking at the terms is that the coefficient when integrated over a given range yields the defect, or the coefficient is the partial derivative of reactivity with respect to one specific parameter.

Coefficients of reactivity are calculated using the core model. First a nominal case is established at some reference conditions. Then one parameter of interest is varied up and/or down by a fixed amount in another calculation

and the resulting change in core reactivity divided by the parameter change is calculated as the reactivity coefficient.

4.2.4.1 Doppler Coefficient

The Doppler Coefficient is the change in core reactivity produced by a small change in fuel temperature.

The major component of the Doppler Coefficient arises from the behavior of the Uranium-238 and Plutonium-240 resonance absorption cross sections. As the fuel temperature increases, the resonances broaden increasing the chance that a neutron will be absorbed and thus decreasing the core reactivity.

If Case 1 represents the reference case with an effective fuel temperature T_1 (and K^1 effective) and Case 2 represents a second case where the fuel temperature has been increased or decreased by approximately 50°F and is T_2 (and K^2 effective), the Doppler Coefficient is mathematically calculated from the following equation:

$$\alpha_D = \frac{\left(\frac{K^1_{eff} - K^2_{eff}}{K^1_{eff} \times K^2_{eff}}\right)}{(T_1 - T_2)} \times 10^5 = \Delta\rho \ \text{(pcm/°F)}$$

Doppler Coefficients are calculated at various core conditions to validate safety analysis assumptions.

4.2.4.2 Moderator Temperature Coefficient

The Moderator Temperature Coefficient (MTC) is the change in reactivity produced by a small change in moderator temperature. In McGuire and Catawba, the average core moderator temperature increases linearly as power is escalated from 0 to 100% HFP. Therefore, for accident and transient analyses it is necessary to know the moderator temperature coefficient over a range of moderator temperatures from CZP to HFP.

These analyses are performed by modeling changes in the core average moderator temperature. Cases are run changing the moderator temperature from the reference temperature. If the cases and resulting $K_{effective}$'s are identified as Case 1 (T_{MOD1}, K^1_{eff}) and Case 2 (T_{MOD2}, K^2_{eff}) the moderator temperature coefficient is calculated from the following equation:

$$\alpha_{T_{MOD}} = \frac{\left(\frac{K^1_{eff} - K^2_{eff}}{K^1_{eff} \times K^2_{eff}}\right)}{(T_{MOD1} - T_{MOD2})} \times 10^5 = \Delta\rho \ (\text{pcm}/^\circ\text{F})$$

Since the reload core is designed with a predetermined flexibility (burnup window), the MTC is verified to be within its design limit for the current cycle considering the burnup window of the previous cycle.

4.2.4.3 Isothermal Temperature Coefficient

The fractional change in reactivity due to a small change in core temperature is defined as the isothermal temperature coefficient (ITC) of reactivity. This is equal to the sum of the moderator and Doppler temperature coefficients and may be explicitly calculated at HZP for isothermal conditions (TFUEL=TMOD) by changing both the fuel and moderator temperatures from the reference HZP moderator temperature.

4.2.4.4 Power Coefficient and Power Defect

The power coefficient of reactivity is the core reactivity change resulting from an incremental change in core power level. The power defect is usually the total reactivity change associated with a power level change from HZP to HFP.

The power coefficient is defined by the following equation:

$$\alpha_P = \frac{\left(\frac{K^1_{eff} - K^2_{eff}}{K^1_{eff} \times K^2_{eff}}\right)}{(P_1 - P_2)} \times 10^5 = \Delta\rho \ (\text{pcm}/\%\text{FP})$$

where: K^1_{eff} is K-effective for the core at power P_1 (%)

K^2_{eff} is K-effective for the core at power P_2 (%)

Neglecting second order effects this equation is equivalent to the following:

$$\alpha_P = \alpha_{TMOD}\frac{\Delta TMOD}{\Delta P} + \alpha_D\frac{\Delta TFUEL}{\Delta P}$$

where: α_{TMOD} is the moderator temperature coefficient and α_D is the Doppler temperature coefficient.

Since the power coefficient should include flux redistribution effects resulting from axial variations in burnup and isotopics as well as non-uniform fuel temperature distributions, it should be performed using a 3-D simulator with thermal hydraulic feedback. If the calculation is performed using a 2-D model then it should be corrected for the 3-D effects.

A typical power coefficient calculation for HFP would proceed in the following manner: The HFP case is run, and the core Keff is calculated (K^1_{eff}). Then a second case is run with the core power level reduced while holding control rods, boron, and xenon constant. The K_{eff} from this case, K^2_{eff}, is used along with the results from the reference case to calculate the power coefficient:

$$\alpha_P = \frac{\left(\frac{K^1_{eff} - K^2_{eff}}{K^1_{eff} \times K^2_{eff}}\right)}{(P_1 - P_2)} \times 10^5 = \Delta\rho \text{ (pcm/\%FP)}$$

The power defect is calculated for use in the shutdown margin calculation (see Section 4.2.2.2) and is the reactivity change from HZP to HFP. This calculation should be performed in three dimensions to satisfactorily model the axial flux redistribution, however, a two dimensional calculation may be performed and corrected for this flux redistribution phenomenon. These calculations are usually performed at BOC and EOC.

Both HFP and the HZP cases should have the equilibrium xenon concentration corresponding to HFP. The power defect is calculated from the following equation:

$$\text{Power Defect (HFP to HZP)} = \left(\frac{K^1_{eff}-K^2_{eff}}{K^1_{eff}\times K^2_{eff}}\right)\times 10^5 = \Delta\rho \text{ (pcm)}$$

where: K^1_{eff} is K-effective at HZP and

K^2_{eff} is K-effective at HFP

4.2.4.5 Miscellaneous Coefficients

For reload design, certain other coefficients of reactivity are not routinely calculated. These include moderator density coefficient, moderator pressure coefficient, and moderator void coefficient. These coefficients can be calculated in an analogous manner by varying the appropriate core reactivity parameters.

4.2.4.6 Boron Related Parameters

Critical boron concentrations for various core conditions during cycle lifetime are calculated using the core model. Table 4-3 lists typical conditions that critical boron concentrations and boron worths are calculated. In addition to these, an ARO critical boron letdown curve is generated for HFP EQXE.

4.2.4.7 Xenon Worth

Xenon worth calculations are performed to support plant operation (e.g. startup after trip), rather than as a safety parameter. Xenon worth is calculated as a function of burnup. The equilibrium xenon worth is calculated as the difference in reactivities between the equilibrium and no xenon cases. The peak xenon worth is calculated as the difference between the peak and no xenon cases. The peak xenon worth is determined at approximately 8 hours following a reactor shutdown from HFP, equilibrium xenon conditions.

4.2.4.8 Kinetics Parameters

The kinetics behavior of the nuclear reactor is often described in terms of solutions to the kinetics equation for six effective groups of delayed neutrons. Transient and accident analyses often involve kinetic modeling of the reactor core. The rate of change in power from a given reactivity insertion can be calculated by solving the kinetics equations if the six group effective delayed neutron fractions, the six group precursor decay constants, and the prompt neutron lifetime are known.

PDQ07 and DELAY may be used to calculate these parameters[20]. PDQ07 is used to obtain spatially averaged isotopic fission rates as a function of burnup and DELAY calculates kinetics parameters and then uses these parameters to solve the Inhour equation and thereby relate the stable reactor period to the reactivity insertion. CASMO-3 data libraries contain delayed neutron data, and SIMULATE-3 is capable of calculating the core averaged kinetics parameters of interest.

Calculations are performed at BOL and EOL. The sum of the six group $\beta_i$effective, βeffective, for the new reload cycle is compared to those values used in the UFSAR.

4.2.5 Assessment of the Fuel Cycle Design

Once the FFCD calculations are performed, the resultant data are assessed for validity and consistency with core operation requirements as well as fuel design and safety analysis limits.

Design criteria for a reload design are outlined in Section 4.2. A preliminary verification of these criteria or parameters important to these criteria is made in the FFCD. Additional calculations that validate a reload design are described in Sections 5 - 7 of this report.

TABLE 4-1

Nuclear Design Data
For Reload Design

1. Power operation mode: load follow or base load.

2. Vessel internal or core component modifications.

3. Expected minimum and maximum cycle burnups.

4. Feed enrichment (if already contracted for).

5. Number and design of feed assemblies.

6. RCS hydraulic conditions.

TABLE 4-2

Shutdown Margin Calculation

		BOC, % Δρ
Available Rod Worth		
1.	Total rod worth, HZP	6.46
2.	Maximum stuck rod, HZP	-1.39
3.	Net Worth	5.07
4.	Less 10% uncertainty	.51
5.	Total available worth	4.56
Required Rod Worth		
6.	Power defect, HFP to HZP	.88
7.	Max allowable inserted rod worth	1.36
8.	Flux/Xenon redistribution	.63
9.	Total required worth	1.87
10.	Shutdown Margin (total avail. worth minus total required worth)	2.69

NOTE: Required shutdown margin is specified in the Technical Specifications.

TABLE 4-3

Typical Boron Parameters

Critical Boron - ppm

HZP, ARO, BOC, No Xenon

HZP, Bank D inserted, BOC, No Xenon

HZP, Bank D + C inserted, BOC, No Xenon

HFP, ARO, EQXE vs exposure

Boron Worth - ppm/%$\Delta\rho$

HFP, EQXE, ARO vs. exposure

HZP, NOXE, ARO vs. exposure

Boron Worth Versus Boron Concentration - HZP, NOXE

BOC

EOC

5. NODAL ANALYSIS METHODOLOGY

5.1 Purpose and Introduction

Nodal analysis allows for modeling of the reactor core in three-dimensions and for performing calculations which because of either code restraints or economic restraints cannot be performed by any other means. Examples of nodal code capabilities include:

1. Calculations which need a three-dimensional geometry such as differential rod worths, axial xenon transients and three-dimensional power distributions.

2. Calculations which need a full-core geometry such as stuck and ejected rod worths.

This section addresses the role of a nodal code in performing cycle depletions, generating rod worth data, determining shutdown margins and shutdown boron concentrations, setting control rod insertion limits, and determining trip reactivity worths and shapes.

A nodal code is also used to calculate many of the startup test parameters and core physics parameters described in Section 9 of this report.

The nodal codes used for McGuire and Catawba analyses are EPRI-NODE-P and SIMULATE-3. (See descriptions in Section 3 and Appendix A).

EPRI-NODE-P can be run with either a quarter-core or a full-core geometry. The McGuire and Catawba models utilize one radial node per assembly and twelve to eighteen axial nodes. EPRI-NODE-P radial powers are normalized to the two-dimensional PDQ07 assembly powers near the beginning of each cycle.

The SIMULATE-3 model is described in Reference 28.

5.2 Fuel Cycle Depletion - Nodal Code

A fuel cycle depletion is performed for each cycle using nodal analysis. For EPRI-NODE-P, the nodal radial powers are normalized to the two-dimensional quarter core PDQ07 or SIMULATE-3 powers at various conditions. SIMULATE-3 does not require normalization. The nodal core model is then depleted from BOC to EOC at appropriate burnup intervals. This depletion is typically performed in the critical boron search mode, with nominal rod insertion (usually 215 SWD) and equilibrium xenon.

Data files may be saved at each burnup step throughout the cycle depletion. These files contain records of the power, exposure, and xenon concentration for each node in the core.

As a result of the nodal core depletion, the following data is obtained:

1. Two and three-dimensional power distributions at each burnup step.

2. A boron letdown curve, i.e., critical boron concentrations as a function of burnup.

3. Axially-dependent parameters such as offset or axial flux difference as a function of burnup.

4. Assembly exposures as a function of core-averaged burnup.

5.3 Rod Worth Analysis

Nodal analysis is used to calculate various rod worths which require three-dimensional capabilities. These calculations include differential rod worths and integral rod worths.

5.3.1 Differential Rod Worth Analysis

Differential rod worths are calculated as a function of rod insertion. The differential rod worth is defined as the change in reactivity associated with a small change in rod position. This rod worth is determined by running two cases at different rod insertions with all other parameters held constant (power, burnup, xenon, boron) and then by dividing the reactivity difference by bank height difference.

Differential rod worths for the control banks are calculated at HZP and HFP, at BOC and EOC, and at no xenon, equilibrium xenon, and peak xenon conditions. The rod banks are inserted both sequentially and in 50% overlap.

5.3.2 Integral Rod Worth Analysis

Integral rod worths are defined as the integral of the differential rod worth data. Integral rod worths are determined by summing up the reactivities resulting from the differential rod worth analysis. Total integral rod worths for a rod bank can be calculated either with a two-dimensional or three-dimensional code by subtracting the reactivities resulting from cases where the rod bank is out and then in (other parameters held constant). However, in order to get the integral rod worth as a function of rod position, i.e., the shape of the rod worth curve, the three-dimensional nodal code is used.

Integral rod worth calculations for the control banks are performed at HZP and HFP, at BOC and EOC, and at no xenon, equilibrium xenon, and peak xenon conditions. The rod banks are inserted sequentially with 50% overlap. The total rod worth (ARI) is calculated at BOC, EOC, and any limiting burnup at HZP for use in the shutdown margin calculation.

5.4 Shutdown Margin Analysis

5.4.1 Shutdown Margin

Shutdown margin calculations are described in Section 4.2.2.2. Table 4-2 summarizes the results of a shutdown margin calculation.

The calculation consists of:

1. The total rod worth (ARI) at HZP, BOC, and EOC (Item 1 in Table 4-2). This worth is determined by running cases at ARO and ARI (with constant boron and xenon) and subtracting the reactivities.

2. The maximum stuck rod worth at HZP, BOC, and EOC (Item 2 in Table 4-2). Utilizing full-core capabilities, the worth of the worst stuck rod is determined by subtracting the reactivities between two cases, one with ARI, the other with ARI and the stuck rod out.

3. The power deficit from HFP to HZP, at BOC and EOC (Item 6 in Table 4-2). This deficit is determined by running cases at HFP and HZP (with constant boron and xenon) and subtracting the reactivities. This reactivity insertion accounts for Doppler and Moderator deficits, and for axial flux redistribution.

4. The maximum allowable inserted rod worth at HFP, BOC, and EOC (Item 7 in Table 4-2). This worth is obtained by reading the integral rod worth curve at the rod insertion limits (See Section 5.3.2).

Additional reactivity penalties are applied to both the power defect and the rod insertion allowance to account for xenon redistribution effects.

5.4.2 Shutdown Boron Concentration

The shutdown boron concentration is another parameter that is determined using three-dimensional nodal analysis. Since the shutdown margin is determined based on the worst case stuck rod out of the core with all other rods in, the full-core capability of the nodal code is needed.

The nodal code is first used to determine the worst case stuck rod by calculating the worth of various rods in the core. After the worse case stuck rod is determined, a boron search case is performed at the ARI-stuck rod out conditions. This boron concentration is adjusted based on boron worth results until the core reactivity reflects the appropriate margin (1.3% $\Delta\rho$ for temperatures greater than 200°F, 1.0% $\Delta\rho$ for temperatures less than or equal to 200°F). The resulting boron concentration is the shutdown boron concentration required for the conditions modeled in the nodal code. This calculated boron concentration is conservatively increased by a boron equivalent of 10% of the ARI-stuck rod out worth and by at least an additional 100 ppm.

A shutdown boron concentration can be determined for any moderator temperature provided the input cross sections remain valid. Typical average moderator temperatures for which shutdown boron concentrations are provided are 68°F, 200°F, 500°F, and the HZP average moderator temperature (approximately 557°F).

5.5 Rod Insertion Limit Assessment

Control rod insertion limits define how deep the control rods may be inserted into the core during normal operation as a function of the power level. It is a Technical Specification requirement that the rods not be inserted deeper than the established limits. This analysis is usually a verification that the Rod Insertion Limits from cycle N-1 are adequate for cycle N.

The control rod insertion limits are determined based on:

1. Maintaining the required minimum shutdown margin, as specified in the Technical Specifications, throughout the cycle life.

2. Maintaining the maximum calculated power peaking factors within the limit specified in the Technical Specifications.

3. The acceptability of the UFSAR Chapter 15 accident analyses.

Determining control rod insertion limits involves an iterative process based on satisfying the above criteria. This process begins with insertion limits from the previous cycle.

The first requirement for insertion limits is that of satisfying the reactivity constraints, i.e., maintaining the required shutdown margin. The insertion limits from the previous cycle, along with integral rod worth curves for control banks in ~50% overlap for the current cycle, are used to calculate the maximum allowable inserted rod worth for input into the shutdown margin calculation. The shutdown margin is calculated at BOC, EOC, and any limiting burnup in order to determine if the control rod insertion limits are acceptable. If the shutdown margin criteria is not satisfied, the insertion limits are adjusted until satisfactory margin is obtained or the core is redesigned.

The insertion limits also have to satisfy the peaking factor constraints. For ARMP methods, the nodal powers are synthesized with discrete pin PDQ07 pin powers to give values of power peaking at various power levels from HZP to HFP. For SIMULATE-3, power peaking factors are calculated directly. The power peaking values are then compared to the Technical Specification limits. If the Technical Specification limits are not satisfied, the control rod insertion limits are adjusted until satisfactory power peaking values are obtained, or the core is redesigned

In addition to satisfying reactivity and peaking factor constraints during normal operation, the control rod insertion limits may need to be modified based on the worst case consequences of an ejected RCCA, a dropped RCCA or a statically misaligned RCCA. Evaluations are performed with the nodal code to identify the worst case rod configuration during a withdrawal or misalignment event, that is, to identify the single RCCA which produces the maximum peaking factor (control rods held at insertion limits). The results of the three-dimensional nodal analysis with these worst case rod configurations are compared to the design criteria associated with each event. The acceptability of the control rod insertion limits is dependent on the criteria being satisfied.

5.6 Trip Reactivity Analysis

The minimum trip reactivity and the shape of the trip reactivity insertion curve (inserted rod worth as a function of rod position) are both generated using nodal analysis. These parameters are needed to perform the safety analysis for various UFSAR Chapter 15 accidents/transients.

5.6.1 Minimum Trip Reactivity

The minimum trip reactivity is the minimum amount of reactivity available to be inserted into the core in the event of a reactor trip. It is evaluated for each reload core to ensure that the previously set limits are still valid.

The minimum trip reactivity is calculated at BOC and EOC at HFP and HZP conditions. The minimum trip reactivity is the total rod worth reduced by (1) the most reactive stuck rod worth, (2) a 10% uncertainty on available rod worth, and (3) the rod insertion allowance including applicable penalties to account for xenon redistribution. The rod insertion allowance is the amount of reactivity associated with the control rod insertion limits. It is the difference in reactivity between an ARO case and one with control rods at their insertion limits. A sample BOC calculation is shown in Table 5-1.

5.6.2 Trip Reactivity Shape

The shape of the trip reactivity insertion curve defines the inserted rod worth as a function of rod position. The most limiting shape is the one which defines the minimum inserted rod worth as a function of rod position. This most limiting shape is evaluated each reload cycle to ensure that the values for the minimum inserted rod worth vs. rod position used in the safety analysis are still applicable.

The most limiting trip reactivity shape typically corresponds to the most bottom-skewed axial power shape. HFP axial power distributions are examined from BOC to EOC, with control rods at the full power rod insertion limits and the most reactive rod stuck out of the core. After the most limiting power shape is found, the N-1 control rods are inserted into the core in a stepwise manner. The results of this insertion yield the minimum inserted rod worth vs. position curve.

5.7 Assessment of Nodal Analyses

Once the nodal calculations are performed, the resultant data are assessed for validity and consistency with core operation requirements and safety limits.

TABLE 5-1

Example BOC Trip Reactivity Calculation

Trip Reactivity	HFP % Δρ
Minimum Available N-1 Rod Worth	6.18
10% Rod Worth Uncertainty	-0.62
Total Available Rod Worth	5.56
Rod Insertion Allowance	-1.13
Xenon Redistribution Penalty	-0.08
Minimum Trip Reactivity	4.35

6. CALCULATION OF SAFETY RELATED PHYSICS PARAMETERS

6.1 Safety Analysis Physics Parameters

With a reload of fresh fuel, a reactor core's physics characteristics are altered in three major areas:

1. Power distribution
2. Control rod worths
3. Kinetics

Each of the above has its own subset of specific parameters. These core physics parameters are considered in the UFSAR Chapter 15 safety analyses. The core physics parameters whose values have an important influence on the course or the consequences of the accidents analyzed in the UFSAR are designated as safety analysis physics parameters. Reference 30 identifies these parameters, describes the approach for calculating the values of these parameters, and discusses the manner in which the reload values are evaluated for acceptability with respect to the accident analysis assumptions.

6.2 Core Power Distributions

As part of the reload design, detailed analyses of the core power distributions are performed for core conditions of normal operation and anticipated transient conditions. These analyses are performed:

1. to confirm that the power peaking factors assumed as initial conditions for certain accidents remain valid,
2. to verify that certain transient induced power peaks will be acceptable for the fuel design thermal limits, and
3. to facilitate the selection of the operating limits and protection system setpoints.

The methodology for performing these analyses is presented in Reference 29.

6.3 Power Peaking Factors and Reliability Factors

Power peaking factors to be compared to a design limit are conservatively increased by total peaking reliability (or uncertainty) factors. The peaking reliability factor is determined by statistically combining manufacturing and calculation uncertainties. Additional potential power peaking uncertainties may be included for things such as rod bowing, etc.

The general formulation for the peaking reliability factor is:

$$\text{Peaking Reliability Factor} = 1+\text{BIAS}+\sqrt{(UC^2+Ux1^2+Ux2^2+...)} \qquad (6\text{-}1)$$

Where:

UC - Calculation Uncertainty

For the Pin Total Peak (F_Q): $UC^2 = UT^2 + URL^2$

For the Pin Radial Peak ($F_{\Delta H}$): $UC^2 = UR^2 + URL^2$

For the Assembly Axial Peak (F_Z): $UC^2 = UA^2$

UT - Total Peaking Uncertainty

URL - Assembly Radial Local (or Pin) Power Peaking Uncertainty

UR - Assembly Radial Power Peaking Uncertainty

UA - Assembly Axial Power Peaking Uncertainty

Uxi - Additional Uncertainties, e.g. manufacturing tolerance, rod bow, etc.

BIAS - Calculation Bias

For the PDQ07 code methodology, Section 8 contains the calculation of the radial local uncertainty factor. For the EPRI-NODE-P code based on ARMP methodology, Section 11 contains the calculation of the assembly and pin total peak and assembly and pin radial peak uncertainty factors. When the EPRI-NODE-P code is based on the CASMO-3/SIMULATE-3 methodology, Reference 28 presents the uncertainty factors. For the CASMO-3/SIMULATE-3 code methodology, Reference 28 contains the calculation of the uncertainty factors.

7. 3D POWER PEAKING ANALYSIS

As part of the reload design, detailed analysis of the core power distribution for normal operation and anticipated transient conditions are made. These analyses are performed (1) to confirm that the initial condition power peaking factors for certain accidents remain valid, (2) to verify that certain transient induced power peaks will satisfy the fuel design limits, and (3) to facilitate the selection of operating limits and RPS setpoints. The methods for performing these analyses are outlined in Reference 29.

8. RADIAL LOCAL ANALYSIS

8.1 Background

The radial local is an important factor in fuel cycle design because of its significant influence on LOCA and DNB analysis. The premise for performing this analysis is to evaluate the ability of PDQ07 to predict the radial local. The radial local is defined as the ratio of the maximum pin power, to the assembly average planar (x-y) power. It is used to calculate pin power by combining assembly power (F_Q or $F_{\Delta H}$) from the nodal analysis with the radial local factor by the equation shown below.

Pin Power = Nodal Power x Radial Local Factor

In the ARMP methodology, PDQ07 and CASMO-2 may be used to calculate radial local factors. PDQ07 is a 1, 2, or 3 dimensional two neutron energy group diffusion theory code, whereas CASMO-2 is a 2-dimensional multigroup transport theory code, which utilizes transport probabilities in the solution of the transport equation. The 2-dimensional PDQ07 code is the primary calculational tool used to model reactor cores (for additional information concerning the use of this code, refer to Section 3.4). Energy and burnup dependent Mixed Number Density (MND) cross sections used by PDQ07 are developed in accordance with ARMP[14] procedures. CASMO-2 is used primarily to generate multigroup constants (i.e., control rod and burnable absorber cross sections), and as a benchmark code.

SIMULATE-3 is capable of calculating pin power peaking directly and does not require the use of radial local factors (Reference 28).

8.2 Comparison of PDQ07 to CASMO-2 at Hot Full Power Condition

The predictive capability of PDQ07 was assessed by performing a series of eighth assembly calculations using both PDQ07 and CASMO-2. A typical Westinghouse 17x17, 3.2 w/o Uranium-235 optimized fuel assembly was modeled

using these codes.

All simulations were performed at beginning of life (BOL), hot full power (HFP), no xenon conditions, for at this time severe pin power peaking is most prominent. Simulations were performed for a variety of burnable absorber loadings and soluble boron concentrations. Table 8-1 contains a summary of the cases that were investigated.

Figures 8-1 through 8-10 contain 1/8 assembly pinwise power comparisons between PDQ07 and CASMO-2. Results from these comparisons indicate that PDQ07 conservatively overpredicts the maximum CASMO-2 pin power. This overprediction ranges from 0.86% to 2.26%. PDQ07 also correctly identifies the location of the CASMO-2 maximum pin power. Comparisons between PDQ07 and CASMO-2 maximum pin powers for each case are tabulated in Table 8-2.

The predictive capability of PDQ07 was assured by performing a statistical analysis over all pins in the problem and for pins with powers greater than or equal to 1.000. The average and average absolute differences and respective standard deviations are presented in Table 8-3 for all cases investigated.

8.3 Comparisons of PDQ07 to Cold Criticals

The ability of PDQ07 to predict pin powers at cold conditions was assessed by performing a series of simulations based on the B&W uranium criticals. In all simulations, PDQ07 conservatively and accurately predicted the maximum pin power. For additional specifics concerning the comparisons of PDQ07 to the B&W uranium criticals, refer to Reference 3.

8.4 BNL Benchmark Assembly Problem

The BNL evaluation of the Duke solution to the BNL benchmark assembly problem determined that PDQ07 methods overpredict the peak pin power by just over 1% at BOC and underpredict the peak pin power by approximately 1% at 40,000 MWD/MTU with the cross over occurring at approximately 15,000 MWD/MTU.

8.5 Conclusion

Comparisons between PDQ07 and CASMO-2 at HFP conditions indicate that PDQ07 conservatively predicts maximum pin powers. PDQ07 comparisons to B&W cold criticals also indicate that PDQ07 conservatively predicts maximum pin powers. However, the solution to the BNL benchmark problem shows an underprediction at high burnups. Therefore, an uncertainty of 2% is applied to the predicted pin peaking factors (see Appendix B).

TABLE 8-1

Characteristics of 1/8th Assembly Simulations

CASE	ENRICHMENT W/O U-235	BURNABLE ABSORBER LOADING	BORON CONCENTRATION (PPMB)
1	3.2	0	0
2	3.2	0	950
3	3.2	4	0
4	3.2	4	950
5	3.2	12	0
6	3.2	12	950
7	3.2	16	0
8	3.2	16	950
9	3.2	20	0
10	3.2	20	950

TABLE 8-2

Peak Pin Power Comparison

CASE	PDQ07 PEAK PIN POWER	CASMO PEAK PIN POWER	DIFFERENCE PDQ07-CASMO	% DIFFERENCE (P-C)/C
1	1.053	1.042	0.011	1.056
2	1.051	1.039	0.012	1.155
3	1.055	1.046	0.009	0.860
4	1.053	1.043	0.010	0.959
5	1.152	1.131	0.021	1.857
6	1.137	1.119	0.018	1.609
7	1.188	1.163	0.025	2.150
8	1.170	1.149	0.021	1.828
9	1.178	1.152	0.026	2.257
10	1.164	1.140	0.024	2.105

TABLE 8-3

Statistical Summary of Percent Differences between PDQ07 and CASMO-2 for Pins in Assemblies with Powers Greater Than or Equal to 1.000

CASE	$\bar{D}$ *	$\overline{ABS\ (D)}$	STANDARD DEVIATION (D)	S.D. [ABS (D)]
1	0.4450	0.5566	0.5524	0.4339
2	0.4657	0.5554	0.5627	0.4697
3	0.2151	0.3470	0.4098	0.3010
4	0.2109	0.3595	0.4215	0.2987
5	0.8916	1.0620	0.8705	0.6396
6	0.7936	0.9548	0.7733	0.5503
7	0.9321	1.1509	1.0832	0.8311
8	0.8057	1.0241	0.9635	0.7107
9	0.7130	0.8202	0.8885	0.7851
10	0.6458	0.7530	0.8109	0.7069

Statistical Summary of Percent Differences between PDQ07 and CASMO-2 For All Pins Within An Assembly

CASE	$\bar{D}$ *	$\overline{ABS\ (D)}$	STANDARD DEVIATION (D)	S.D. [ABS (D)]
1	0.0030	0.6395	0.7867	0.4463
2	0.0066	0.6572	0.8119	0.4648
3	-0.0255	0.4606	0.6328	0.4281
4	-0.0066	0.4520	0.6280	0.4298
5	0.0616	1.0682	1.2511	0.6310
6	0.0394	0.9801	1.1449	0.5713
7	0.0585	0.9416	1.2120	0.7499
8	0.0398	0.8436	1.0926	0.6819
9	0.0268	0.8776	1.1696	0.7604
10	0.0293	0.8059	1.0732	0.6972

* NOTE: D = [(PDQ07 - CASMO-2)/CASMO-2] *100

$$\bar{D} = \sum_{i=1}^{N} D_i/N$$

FIGURE 8-1

CASMO-2 AND PDQ-7
ROD POWER COMPARISON
BOL HFP NO XENON
3.2 w/o U-235 OPT 17x17 FA
CASE NUMBER 1

	PDQ-7	CASMO-2
PPMB	950	950
NUMBER BA	0	0
K-INFINITY	1.3486	1.3479
*MAX ROD POWER	1.053	1.042

0.0 0.0								
1.020 1.024	1.002 1.009							
1.021 1.024	1.002 1.009	1.002 1.010						
0.0 0.0	1.024 1.025	1.026 1.027	0.0 0.0					
1.020 1.023	1.002 1.009	1.004 1.013	1.033 1.037	1.023 1.045				
1.018 1.021	1.000 1.007	1.002 1.011	1.033 1.038	1.042 1.053	0.0 0.0	CASMO-2 PDQ-7		
0.0 0.0	1.018 1.017	1.020 1.019	0.0 0.0	1.030 1.037	1.014 1.010	0.976 0.975		
1.008 1.006	0.990 0.993	0.990 0.994	1.011 1.006	0.986 0.989	0.970 0.964	0.959 0.947	0.955 0.940	
0.986 0.982	0.985 0.979	0.985 0.979	0.985 0.980	0.979 0.973	0.972 0.961	0.966 0.953	0.967 0.954	0.981 0.971

FIGURE 8-2

CASMO-2 AND PDQ-7
ROD POWER COMPARISON
BOL HFP NO XENON
3.2 w/o U-235 OPT 17x17 FA
CASE NUMBER 2

	PDQ-7	CASMO-2
PPMB	950	950
NUMBER BA	0	0
K-INFINITY	1.2122	1.2077
*MAX ROD POWER	1.051	1.039

0.0 0.0								
1.017 1.021	1.000 1.007							
1.018 1.021	1.000 1.007	1.000 1.008						
0.0 0.0	1.021 1.022	1.023 1.024	0.0 0.0					
1.018 1.021	1.000 1.007	1.002 1.011	1.030 1.035	1.020 1.042				
1.016 1.020	0.999 1.006	1.001 1.010	1.030 1.035	* 1.039 1.051	0.0 0.0	CASMO-2 PDQ-7		
0.0 0.0	1.017 1.016	1.019 1.018	0.0 0.0	1.029 1.036	1.014 1.011	0.979 0.977		
1.007 1.006	0.990 0.993	0.990 0.994	1.011 1.007	0.988 0.991	0.973 0.966	0.963 0.950	0.960 0.945	
0.987 0.983	0.987 0.980	0.986 0.980	0.987 0.982	0.982 0.975	0.975 0.964	0.971 0.957	0.972 0.959	0.986 0.976

FIGURE 8-3

CASMO-2 AND PDQ-7
ROD POWER COMPARISON
BOL HFP NO XENON
3.2 w/o U-235 OPT 17x17 FA
CASE NUMBER 3

	PDQ-7	CASMO-2
PPMB	0	0
NUMBER BA	4	4
K-INFINITY	1.2978	1.2956
*MAX ROD POWER	1.055	1.046

0.0 0.0								
1.011 1.013	0.988 0.991							
1.006 1.003	0.975 0.972	0.933 0.915						
0.0 0.0	0.989 0.977	0.893 0.890	0.0 0.0					
1.011 1.009	0.980 0.979	0.940 0.925	0.905 0.908	0.964 0.963				
1.022 1.027	0.998 1.006	0.989 0.992	1.011 1.008	1.032 1.040	0.0 0.0	CASMO-2 PDQ-7		
0.0 0.0	1.034 1.036	1.033 1.034	0.0 0.0	* 1.046 1.055	1.036 1.039	1.005 1.011		
1.033 1.037	1.014 1.024	1.015 1.023	1.037 1.036	1.014 1.022	1.000 1.000	0.992 0.987	0.990 0.983	
1.015 1.018	1.015 1.015	1.015 1.014	1.016 1.016	1.011 1.010	1.005 1.001	1.002 0.996	1.004 0.999	1.019 1.018

FIGURE 8-4

CASMO-2 AND PDQ-7
ROD POWER COMPARISON
BOL HFP NO XENON
3.2 w/o U-235 OPT 17x17 FA
CASE NUMBER 4

	PDQ-7	CASMO-2
PPMB	950	950
NUMBER BA	4	4
K-INFINITY	1.1757	1.1672
*MAX ROD POWER	1.053	1.043

0.0 0.0								
1.012 1.014	0.990 0.993							
1.007 1.004	0.977 0.975	0.937 0.919						
0.0 0.0	0.991 0.980	0.898 0.896	0.0 0.0					
1.011 1.010	0.982 0.981	0.943 0.928	0.909 0.912	0.965 0.965				
1.021 1.026	0.998 1.006	0.989 0.993	1.010 1.009	1.030 1.039	0.0 0.0	CASMO-2 PDQ-7		
0.0 0.0	1.031 1.035	1.031 1.032	0.0 0.0	* 1.043 1.053	1.034 1.037	1.005 1.010		
1.031 1.035	1.013 1.022	1.013 1.021	1.035 1.034	1.013 1.020	1.000 0.999	0.992 0.987	0.991 0.983	
1.013 1.016	1.013 1.013	1.013 1.013	1.015 1.015	1.010 1.009	1.005 1.001	1.002 0.996	1.005 1.000	1.020 1.018

FIGURE 8-5

CASMO-2 AND PDQ-7
ROD POWER COMPARISON
BOL HFP NO XENON
3.2 w/o U-235 OPT 17x17 FA
CASE NUMBER 5

	PDQ-7	CASMO-2
PPMB	0	0
NUMBER BA	12	12
K-INFINITY	1.2073	1.2029
*MAX ROD POWER	1.152	1.131

0.0 0.0								
* 1.131 1.152	1.108 1.132							
1.123 1.144	1.099 1.123	1.088 1.109						
0.0 0.0	1.109 1.123	1.093 1.102	0.0 0.0					
1.093 1.109	1.063 1.081	1.036 1.045	1.019 1.014	0.946 0.937				
1.076 1.085	1.038 1.047	0.980 0.970	0.905 0.906	0.864 0.855	0.0 0.0	CASMO-2 PDQ-7		
0.0 0.0	1.043 1.041	0.930 0.934	0.0 0.0	0.860 0.849	0.876 0.867	0.932 0.908		
1.055 1.062	1.020 1.028	0.967 0.956	0.907 0.906	0.930 0.910	0.950 0.934	0.973 0.959	0.996 0.989	
1.035 1.046	0.026 1.032	1.004 1.000	0.984 0.976	0.983 0.973	0.992 0.984	1.007 1.000	1.024 1.023	1.048 1.054

FIGURE 8-6

CASMO-2 AND PDQ-7
ROD POWER COMPARISON
BOL HFP NO XENON
3.2 w/o U-235 OPT 17x17 FA
CASE NUMBER 6

	PDQ-7	CASMO-2
PPMB	950	950
NUMBER BA	12	12
K-INFINITY	1.1010	1.0941
*MAX ROD POWER	1.137	1.119

0.0 0.0								
* 1.119 1.137	1.097 1.118							
1.112 1.130	1.090 1.110	1.080 1.099						
0.0 0.0	1.100 1.112	1.086 1.094	0.0 0.0					
1.086 1.100	1.058 1.074	1.032 1.041	1.018 1.013	0.949 0.941				
1.070 1.079	1.035 1.044	0.981 0.970	0.909 0.911	0.871 0.864	0.0 0.0	CASMO-2 PDQ-7		
0.0 0.0	1.041 1.039	0.933 0.937	0.0 0.0	0.868 0.858	0.884 0.876	0.938 0.915		
1.052 1.059	1.019 1.027	0.969 0.958	0.912 0.912	0.936 0.917	0.956 0.940	0.977 0.964	0.999 0.992	
1.034 1.044	1.026 1.030	1.005 1.001	0.987 0.980	0.987 0.978	0.996 0.988	1.010 1.004	1.025 1.024	1.049 1.054

FIGURE 8-7

CASMO-2 AND PDQ-7
ROD POWER COMPARISON
BOL HFP NO XENON
3.2 w/o U-235 OPT 17x17 FA
CASE NUMBER 7

	PDQ-7	CASMO-2
PPMB	0	0
NUMBER BA	16	16
K-INFINITY	1.1629	1.1576
*MAX ROD POWER	1.188	1.163

0.0 0.0								
* 1.163 1.188	1.138 1.166							
1.150 1.173	1.125 1.152	1.111 1.137						
0.0 0.0	1.123 1.138	1.110 1.124	0.0 0.0					
1.072 1.080	1.051 1.065	1.040 1.052	1.035 1.034	0.966 0.962				
0.950 0.952	0.975 0.962	0.966 0.953	0.915 0.918	0.885 0.879	0.0 0.0	CASMO-2 PDQ-7		
0.0 0.0	0.909 0.906	0.904 0.902	0.0 0.0	0.882 0.874	0.905 0.900	0.966 0.946		
0.922 0.919	0.949 0.934	0.948 0.933	0.916 0.918	0.955 0.937	0.983 0.971	1.010 1.001	1.036 1.035	
0.992 0.989	0.993 0.993	0.995 0.993	0.996 0.993	1.009 1.004	1.027 1.023	1.046 1.046	1.066 1.071	1.093 1.105

FIGURE 8-8

CASMO-2 AND PDQ-7
ROD POWER COMPARISON
BOL HFP NO XENON
3.2 w/o U-235 OPT 17x17 FA
CASE NUMBER 8

	PDQ-7	CASMO-2
PPMB	950	950
NUMBER BA	16	16
K-INFINITY	1.0655	1.0581
*MAX ROD POWER	1.170	1.149

0.0 0.0								
* 1.149 1.170	1.126 1.150							
1.138 1.157	1.114 1.137	1.102 1.125						
0.0 0.0	1.113 1.127	1.102 1.115	0.0 0.0					
1.067 1.074	1.047 1.059	1.037 1.048	1.033 1.033	0.968 0.965				
0.952 0.953	0.976 0.963	0.968 0.955	0.919 0.923	0.890 0.886	0.0 0.0	CASMO-2 PDQ-7		
0.0 0.0	0.913 0.911	0.909 0.907	0.0 0.0	0.888 0.881	0.910 0.906	0.969 0.950		
0.927 0.925	0.953 0.939	0.953 0.938	0.921 0.923	0.959 0.943	0.986 0.974	1.011 1.002	1.035 1.033	
0.995 0.993	0.996 0.996	0.997 0.997	0.999 0.996	1.011 1.006	1.027 1.024	1.045 1.044	1.064 1.068	1.088 1.099

FIGURE 8-9

CASMO-2 AND PDQ-7
ROD POWER COMPARISON
BOL HFP NO XENON
3.2 w/o U-235 OPT 17x17 FA
CASE NUMBER 9

	PDQ-7	CASMO-2
PPMB	0	0
NUMBER BA	20	20
K-INFINITY	1.1206	1.1148
*MAX ROD POWER	1.178	1.152

0.0 0.0								
* 1.152 1.178	1.121 1.148							
1.132 1.151	1.094 1.112	1.036 1.034						
0.0 0.0	1.084 1.087	0.967 0.977	0.0 0.0					
1.061 1.064	1.026 1.033	0.971 0.958	0.899 0.898	0.903 0.877				
0.952 0.956	0.972 0.959	0.951 0.931	0.891 0.887	0.873 0.865	0.0 0.0	CASMO-2 PDQ-7		
0.0 0.0	0.923 0.924	0.916 0.915	0.0 0.0	0.898 0.891	0.929 0.928	0.998 0.984		
0.948 0.950	0.976 0.964	0.975 0.962	0.943 0.948	0.985 0.971	1.017 1.010	1.048 1.046	1.077 1.084	
1.025 1.027	1.027 1.030	1.029 1.031	1.031 1.032	1.045 1.046	1.065 1.069	1.087 1.095	1.109 1.124	1.136 1.160

FIGURE 8-10

CASMO-2 AND PDQ-7
ROD POWER COMPARISON
BOL HFP NO XENON
3.2 w/o U-235 OPT 17x17 FA
CASE NUMBER 10

	PDQ-7	CASMO-2
PPMB	950	950
NUMBER BA	20	20
K-INFINITY	1.0315	1.0238
*MAX ROD POWER	1.164	1.140

0.0 0.0								
* 1.140 1.164	1.112 1.136							
1.123 1.140	1.087 1.103	1.032 1.029						
0.0 0.0	1.078 1.082	0.967 0.977	0.0 0.0					
1.058 1.062	1.025 1.031	0.973 0.960	0.905 0.904	0.909 0.885				
0.954 0.958	0.974 0.962	0.954 0.936	0.897 0.894	0.880 0.873	0.0 0.0	CASMO-2 PDQ-7		
0.0 0.0	0.927 0.928	0.921 0.920	0.0 0.0	0.903 0.898	0.932 0.932	0.998 0.984		
0.951 0.953	0.978 0.967	0.978 0.966	0.946 0.951	0.986 0.973	1.016 1.010	1.045 1.043	1.072 1.077	
1.025 1.028	1.027 1.031	1.029 1.031	1.031 1.031	1.044 1.044	1.062 1.065	1.082 1.089	1.102 1.115	1.127 1.149

9. DEVELOPMENT OF CORE PHYSICS PARAMETERS

Upon completion of the Final Fuel Cycle Design, physics parameters such as boron concentrations and worths, power distributions, etc. are calculated primarily for HFP and some HZP conditions. The purpose of this stage of developing core physics parameters is to provide additional calculations to supplement those already performed. The results of these calculations are used for startup test predictions and core physics parameters throughout the cycle.

9.1 Startup Test Predictions

After each refueling, the reactor undergoes a startup test program aimed at verifying that the reactor core is correctly loaded and to verify reactor behavior is as predicted by the nuclear simulators which were used in generating the data used in the plant's safety analysis.

9.1.1 Critical Boron Concentrations and Boron Worths

Critical boron concentrations and boron worths at a variety of rod configurations, at HZP and HFP, as a function boron concentration, at different xenon concentrations, and at different times in the fuel cycle are calculated. EPRI-NODE-P and SIMULATE-3 are capable of performing critical boron search calculations. The method used for PDQ07 is to correct the input boron concentration to the critical boron concentration using a calculated boron worth and the calculated reactivity.

Table 9-1 shows some of the critical boron calculations normally performed for startup physics tests. These calculations are performed after the sequential insertion of each control or shutdown bank and are sometimes referred to as boron endpoints.

Critical boron concentrations at HZP and HFP with all rods out are also calculated as a function of cycle burnup. An example of how boron changes

with burnup is shown in Figure 9-1. These curves are referred to as boron letdown curves.

The boron worths are usually calculated by running two identical cases except that the soluble boron concentration is different. The differential boron worth is calculated by subtracting the reactivities and dividing by the boron difference. Differential boron worths are usually quoted in PCM/PPMB. The inverse boron worth is the inverse of the differential boron worth and is usually quoted in PPMB/%Δρ.

Table 9-2 shows the soluble boron worths usually performed for startup physics tests. Similar to critical boron concentrations, these worths are calculated with sequential bank insertions.

Differential boron worth (or inverse boron worth) can also be calculated as a function of boron concentration and as a function of cycle burnup. Figures 9-2 and 9-3 show the results of a typical differential boron worth calculation vs. boron concentration and vs. burnup, respectively.

9.1.2 Xenon Worth and Defect

Xenon worth is calculated as a function of cycle burnup. The nominal HFP depletion cases with equilibrium xenon are used as input to a second set of cases where the xenon concentration is set to zero (or the xenon cross sections are set to zero). The difference in reactivities between the equilibrium xenon and no xenon cases equals the equilibrium xenon worth at HFP. Figure 9-4 shows the results of a typical equilibrium xenon worth calculation.

Xenon worth can also be presented as a function of power level. Worths presented in this manner are usually referred to as the equilibrium xenon reactivity defect and are quoted in either pcm or %Δρ. Figure 9-5 shows the results of a typical xenon defect calculation.

9.1.3 Rod Worths

9.1.3.1 Bank Worths

The worth of the shutdown and control banks are calculated at BOC HZP for use in the zero power physics testing. The rod banks are sequentially inserted or withdrawn assuming no control rod overlap. The bank worth is the difference in reactivity between the fully inserted case and the fully withdrawn case.

Integral rod worth curves are calculated at BOC HZP for Control Banks B, C and D. The rod banks are inserted both sequentially and with 50% overlap. Figure 9-6 shows the results of a typical integral rod worth calculation.

Control bank worths with sequential insertion and integral rod worth curves with 50% overlap are calculated at HFP equilibrium xenon both at BOC and EOC.

9.1.3.2 Stuck Rod Worth

The maximum worth of a single control rod stuck out of the reactor core at HZP is calculated. The worth of the stuck rod is used by the site engineers in the reactivity balance procedures to guarantee shutdown margin. If the stuck rod worth is to be measured during the startup test program, then a recalculation of the worth is performed simulating the test conditions. This worth would then be provided as a startup test prediction.

9.1.3.3 Dropped Rod Worth

The maximum worth of a single control rod dropped into the reactor core is calculated. If this parameter is to be measured during the startup test program, then a recalculation of the worth is performed simulating the test conditions. This worth would then be provided as a startup test prediction.

9.1.3.4 Ejected Rod Worth

The maximum ejected control rod worth is calculated. If this parameter is to be measured during the startup test program, then a recalculation of the worth is performed simulating the test conditions. This worth would then be provided as a startup test prediction.

9.1.4 Reactivity Coefficients

9.1.4.1 HZP Coefficients

At HZP the isothermal temperature coefficient is measured by varying the average moderator temperature and determining the corresponding reactivity change. The calculations for predicting the isothermal temperature coefficient should be performed by changing the average moderator temperature in the core model. The resulting reactivity change is then divided by the temperature change to yield the HZP isothermal temperature coefficient.

The Doppler or fuel temperature coefficient at HZP can be calculated by varying the fuel temperature while maintaining the no load moderator temperature. The resulting reactivity change divided by the change in fuel temperature is the Doppler coefficient at HZP.

The predicted moderator coefficient is calculated by subtracting the Doppler coefficient from the isothermal coefficient. It is compared to the (inferred) measured moderator coefficient obtained by subtracting the predicted Doppler coefficient from the measured isothermal coefficient.

Alternately, the moderator temperature coefficient can also be explicitly calculated.

9.1.4.2 HFP Coefficients

Both a temperature coefficient of reactivity and a power Doppler coefficient of reactivity are calculated at HFP. The temperature coefficient is calculated by running one equilibrium HFP case at BOC (4 EFPD) and a second case where the moderator temperature is changed. The difference in reactivity divided by the temperature change is the temperature coefficient. To calculate the power Doppler coefficient, a third case is performed where the power level is reduced. All other parameters are kept at the HFP equilibrium values. The difference in reactivity between the HFP and the reduced power cases divided by change in power is the power Doppler coefficient.

9.1.5 Power Distribution

Power distributions, both assembly radial and total peaking factors, are measured at various power levels as identified in the test procedures for McGuire/Catawba reload startups. Calculations are performed at these power levels and nominal conditions to provide predicted power distributions for comparison.

9.1.6 Kinetics Parameters

Kinetics parameters are calculated using the methodology and codes as discussed in Section 4.2.4.8. These parameters include the six group βi effective and λi, total β effective and l^*. These kinetics parameters are generated for both BOC HZP and BOC HFP conditions with ARO. A second set of delayed neutron data may be generated at EOC.

9.2 Startup and Operation Report

The purpose of the Startup and Operation Report is to document the predicted behavior of the reactor core as a function of burnup and power level. It is intended to be used for operator guidance and to aid the site engineer.

This report will include sufficient information to calculate reactivity balance throughout the cycle. Table 9-3 lists items typical of what will be calculated for this report.

TABLE 9-1

Critical Boron Concentrations (ppmB)

HZP, NOXE, 0 EFPD

ARO

Bank D in

Banks D + C in

Banks D + C + B in

Banks D + C + B + A in

Banks D + C + B + A + S_E in

Banks D + C + B + A + S_E + S_D in

Banks D + C + B + A + S_E + S_D + S_C in

Banks D + C + B + A + S_E + S_D + S_C + S_B in

Banks D + C + B + A + S_E + S_D + S_C + S_B + S_A in

HFP, NOXE, 0 EFPD

ARO

HFP, EQXE, 4 EFPD

ARO

Bank D in

HFP, EQXE, EOC

ARO

TABLE 9-2

Boron Worth (pcm/ppmB)

HZP, NOXE, 0 EFPD

ARO

Bank D in*

Banks D + C in

Banks D + C + B in

Banks D + C + B + A in

ARI

HFP, EQXE, 4 EFPD

ARO

HFP, EQXE, EOC

ARO

* Note: When bank worths are determined using interchange (swap) with the reference control bank, the boron worth with the reference bank only inserted is evaluated in place of sequential insertions.

TABLE 9-3

Typical Core Physics Data

A. Critical Boron Concentrations
   1. ARO HFP Versus Burnup
   2. ARO HZP Versus Burnup

B. Shutdown Boron Concentrations Required for Shutdown with Highest Worth Rod Stuck Out (NoXe)
   1. HZP Versus Burnup
   2. 500°F, 200°F and 68°F Versus Burnup

C. Differential Boron Worth HFP, HZP Versus Burnup

D. Power Distributions from the Cycle Depletion

E. Rod Worths BOC, EOC, HFP and HZP

F. Xenon Worth Versus Power Level

G. Xenon Worth Versus Burnup

H. Reactivity Coefficients Versus Temperature, Power Level and Burnup

FIGURE 9-1

Boron Letdown Curve
HFP, ARO

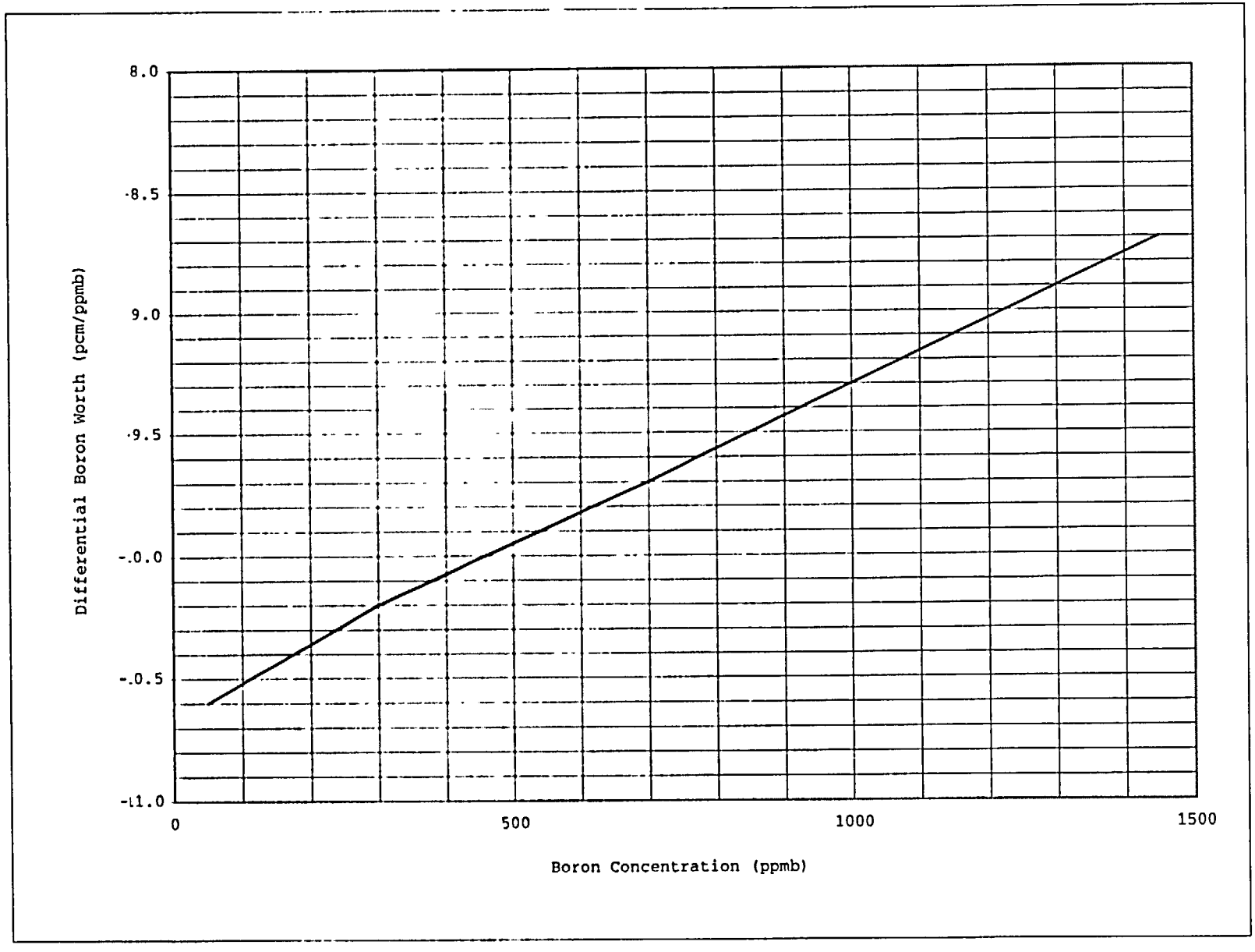

FIGURE 9-2

Differential Boron Worth
HZP, BOL

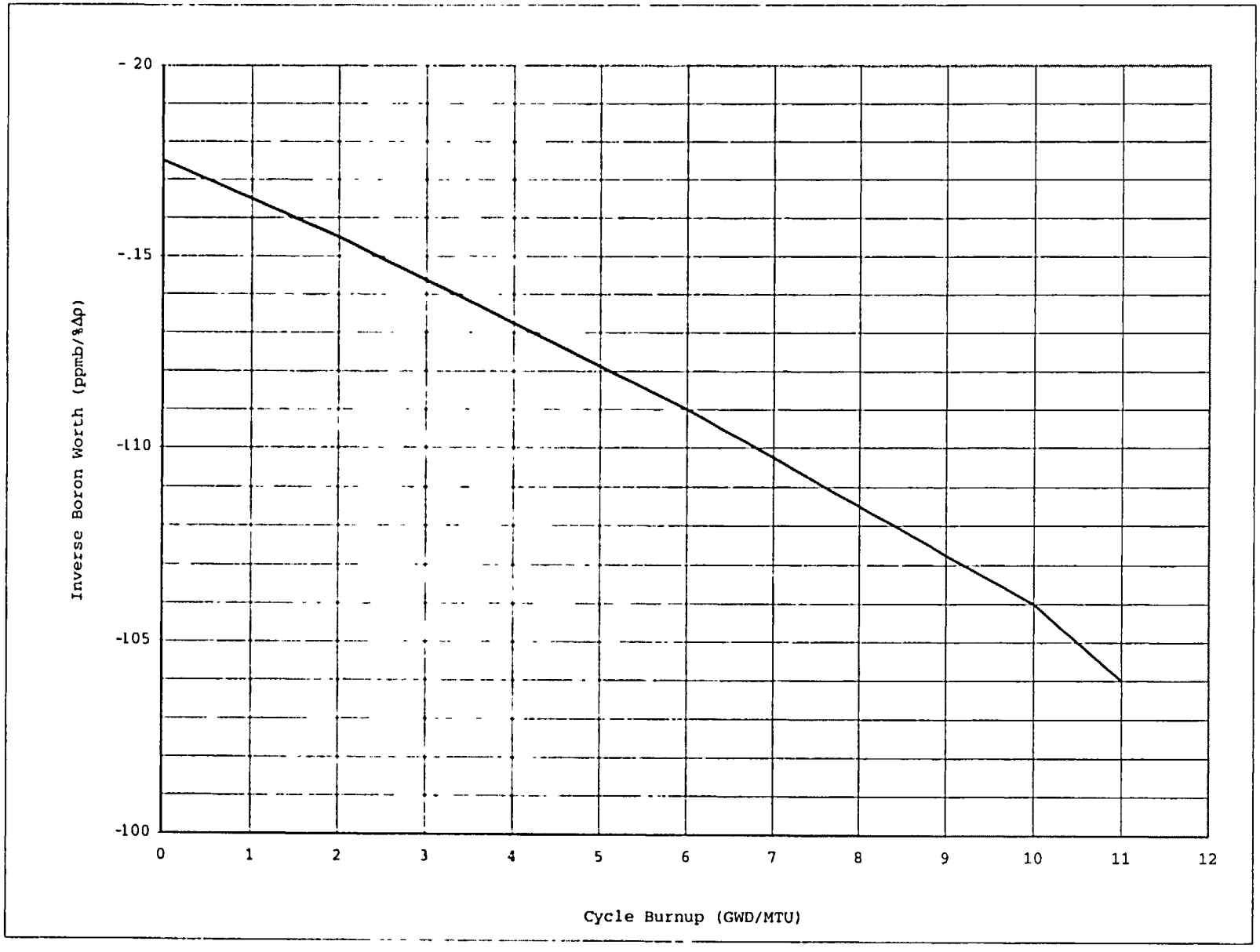

FIGURE 9-3

Inverse Boron Worth
HFP, ARO

FIGURE 9-4

Equilibrium Xenon Worth
HFP

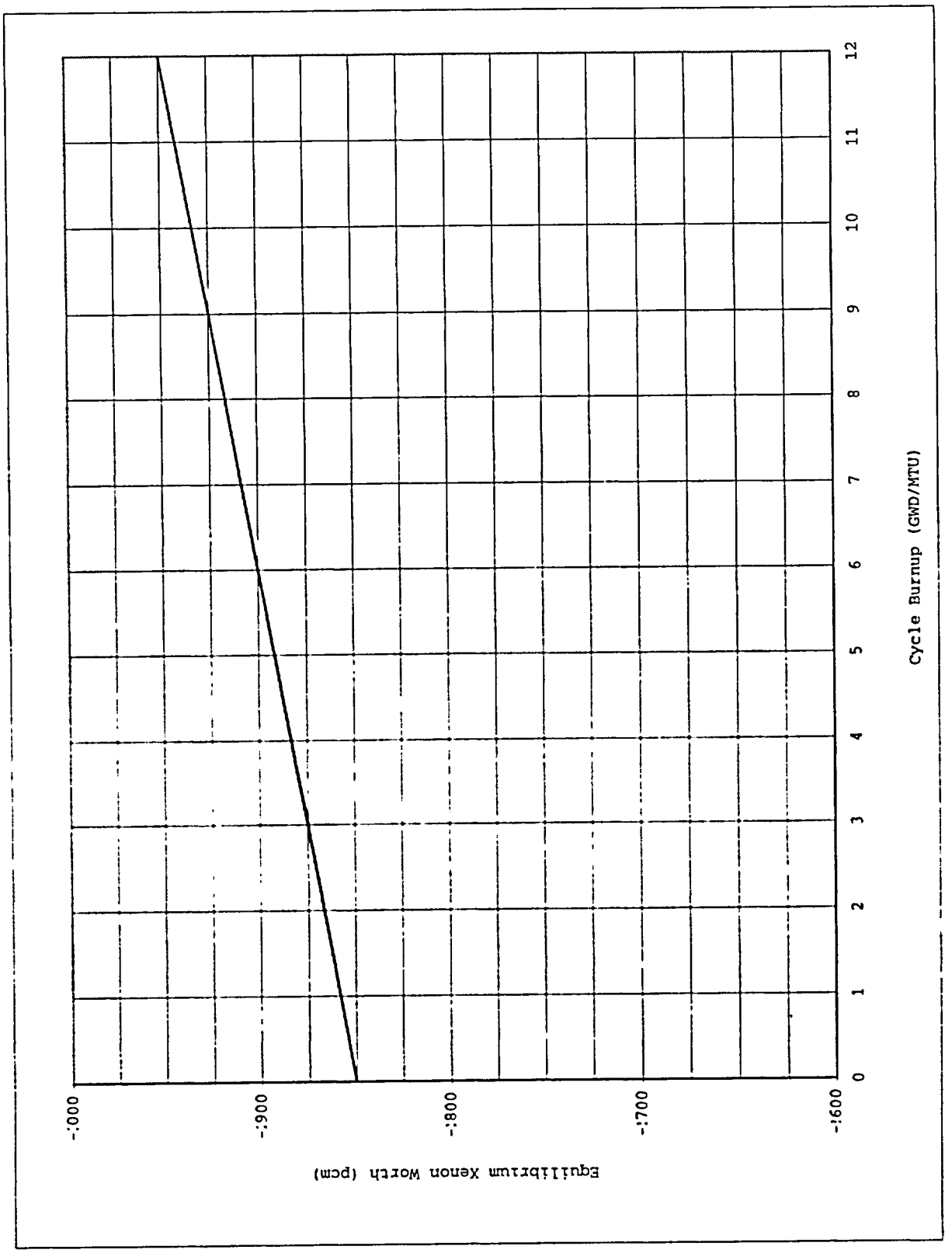

FIGURE 9-5

Xenon Reactivity Defect
BOL

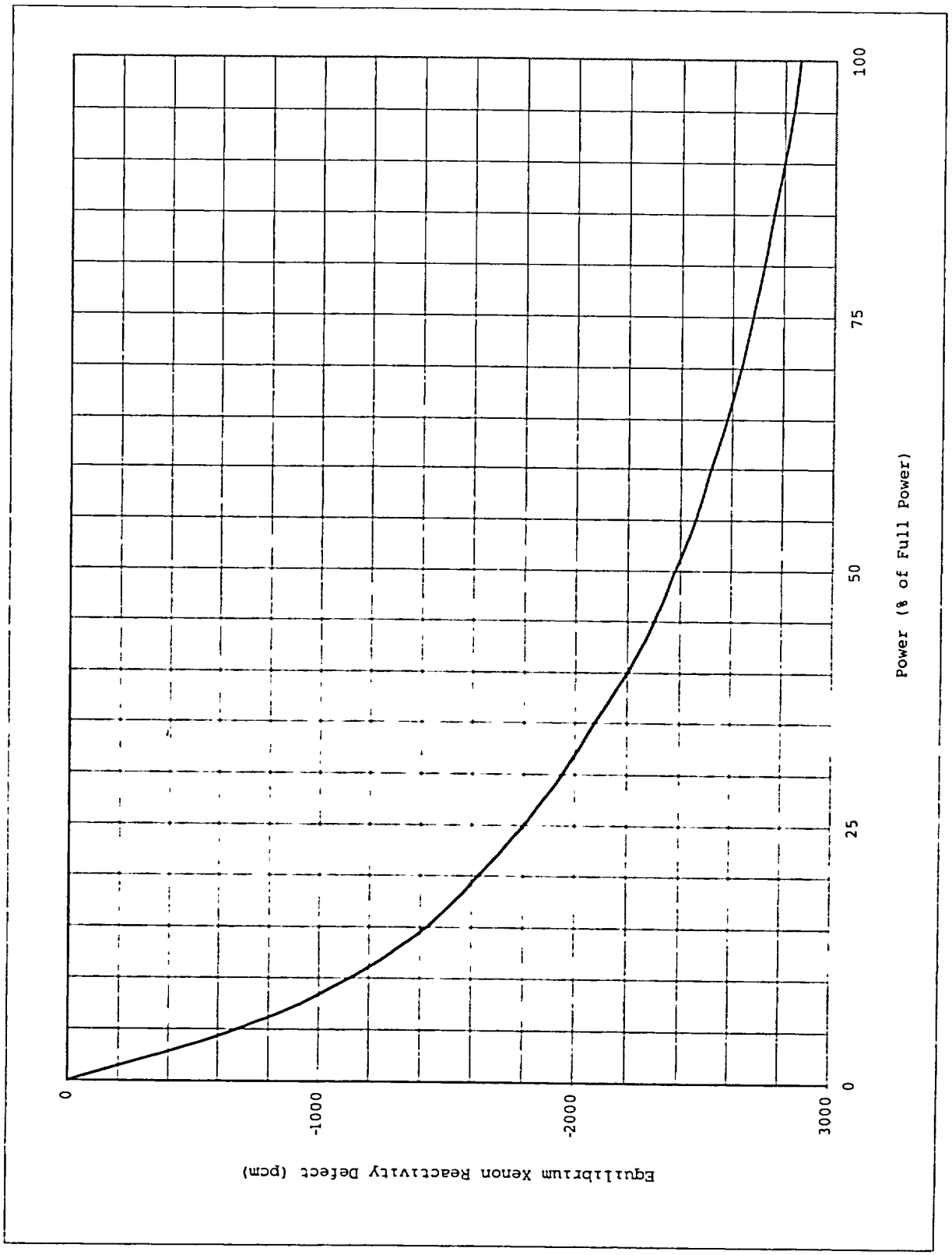

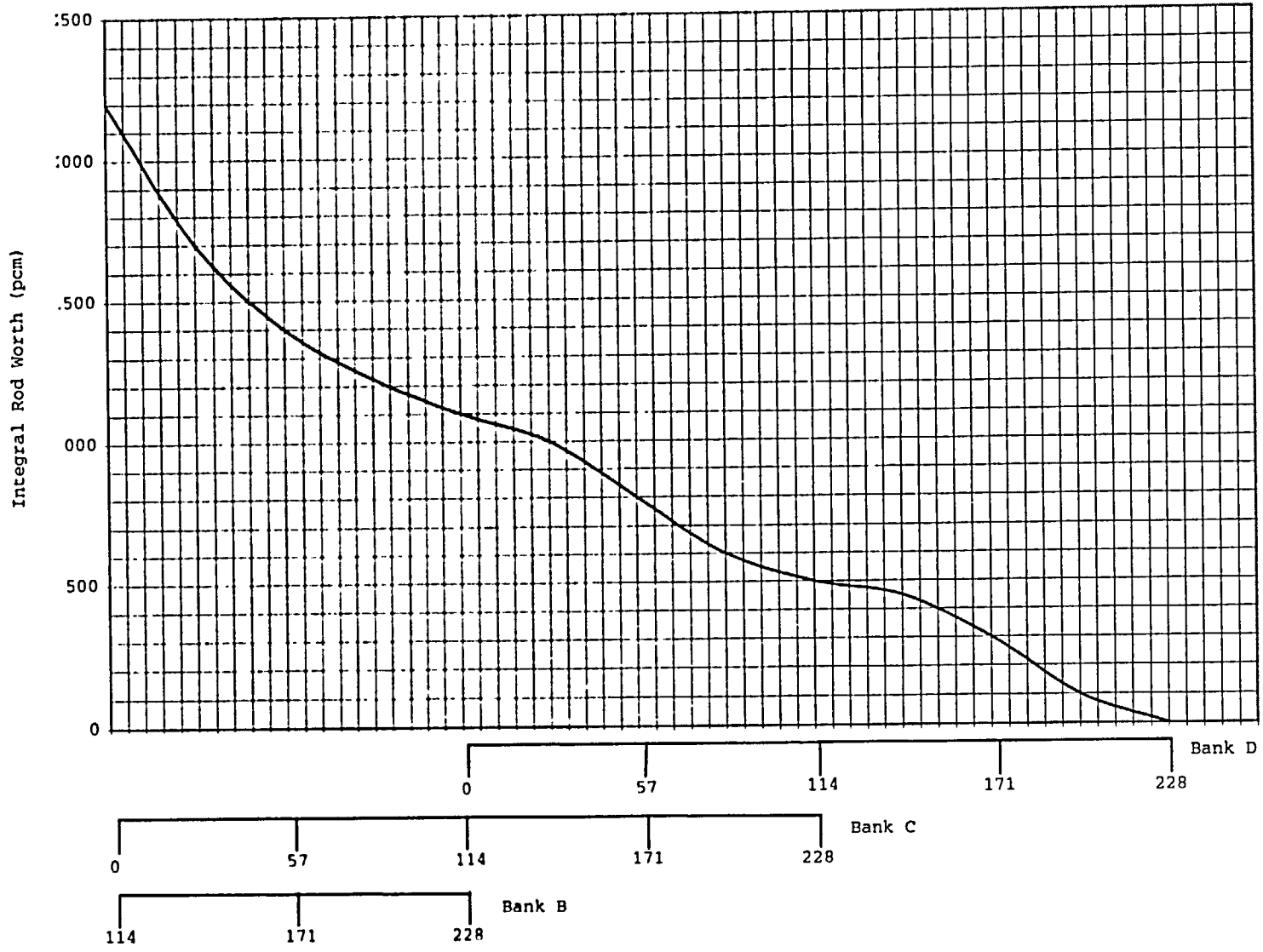

FIGURE 9-6

Integral Rod Worth
HZP, BOL

10. PHYSICS TEST COMPARISONS

Startup physics testing is described in UFSAR Chapter 14. The startup testing information contained in this section is presented to provide the perspective on the benchmarking of measured to predicted results. The predicted results presented are based on the PDQ07/EPRI-NODE-P models. Reference 28 presents the benchmarking results for the CASMO-3/SIMULATE-3 models.

10.1 Introduction

This section presents measurement and calculational techniques and comparisons of calculated and measured results for some key core physics parameters. The physics parameters include hot zero power (HZP) and hot full power (HFP) critical boron concentrations, HZP control rod worths and ejected rod worths, and HZP isothermal temperature coefficients.

The measured data is from the McGuire Nuclear Station, Unit 1 Cycles 1 and 1A, and Unit 2, Cycle 1. (Broken hold down springs on some Burnable Poison rods were found during an outage on McGuire Unit 1 at 191.5 EFPD. During this outage, 94 of 96 Burnable Poison Rod Assemblies were removed from the core. Cycle 1A is the continuation of Cycle 1 but without the Burnable Poison Rods.) The measurement techniques discussed are those currently used at the station. The HZP measurements were taken at beginning-of-cycle (BOC) during the Zero Power Physics Testing. The HFP boron concentration measurements were taken at various time steps throughout the cycles. All calculations were performed with EPRI-NODE-P.

The comparisons of calculated and measured results present the means of the differences between the measured and calculated data and the corresponding standard deviations. The mean and standard deviation are defined as follows:

$$\text{Mean} = \bar{X} = \frac{\Sigma x_i}{n}$$

$$\text{Standard Deviation} = S = \sqrt{\frac{\Sigma(\bar{x}-x_i)^2}{n-1}}$$

where: x_i = value for the ith observation

n = number of observations.

10.2 Critical Boron Concentrations

10.2.1 Measurement Technique

Critical boron concentrations are measured at HZP and HFP by an acid-base titration of a reactor coolant system sample.

The measurement uncertainty for critical boron concentrations is due to (1) error in the titration method and (2) error due to differences between the sample concentration and the core average concentration. Based on conservative estimates of these errors, the total uncertainty associated with the critical boron concentration measurements is less than 20 ppmb.

10.2.2 Calculational Technique

Critical boron concentrations are calculated at HZP and HFP using EPRI-NODE-P in the boron search mode. Since the search does not yield an exactly critical value, fixed boron runs using EPRI-NODE-P are also made to calculate a boron worth, which is then used to correct the calculated boron concentration to exactly critical.

10.2.3 Comparison of Calculated and Measured Results

10.2.3.1 Hot Zero Power Comparison

The calculated and measured critical boron concentrations at HZP and BOC for McGuire Unit 1, Cycles 1 and 1A, and Unit 2, Cycle 1 are compared in Table 10-1. Each entry corresponds to a different control rod position. The mean

of the differences for these three cycles was found to be -7 ppmb with a standard deviation of 16 ppmb.

10.2.3.2 Hot Full Power Comparison

The calculated and measured critical boron concentrations at HFP for McGuire Unit 1, Cycles 1 and 1A, are compared in Table 10-2. The mean of the differences for these cycles is -41 ppmb with a standard deviation of 11 ppmb.

The data displayed in Table 10-2 can be visualized better by examining plots of soluble boron concentration as a function of burnup. These boron letdown curves are shown in Figures 10-1 and 10-2.

10.2.4 Summary

The comparison between EPRI-NODE-P and measured critical boron concentrations at HZP and HFP indicate EPRI-NODE-P can adequately predict soluble boron concentrations.

10.3 Control Rod Worth

10.3.1 Measurement Techniques

Individual control rod bank worths are measured by the boron swap technique. This technique involves a continuous decrease in boron concentration together with an insertion of the control rods in small, discrete steps. The change in reactivity due to each insertion is determined from reactivity computer readings before and after the insertion. The worth of each rod bank is the sum of all the reactivity changes for that bank. Measured bank worths in ppmb can be determined independent of the reactivity computer by using the measured boron endpoints.

10.3.2 Calculational Techniques

Individual and total controlling rod bank worths in terms of reactivity are

calculated by making two EPRI-NODE-P runs. The first is a boron search run with the rod bank(s) out. The boron concentration found in this run is then used in a fixed boron run with the rod bank(s) in. The difference in reactivity between these two runs with constant boron concentration is the rod bank(s) worth.

Bank worths were also calculated using the calculated Boron endpoints. These bank worths are in terms of ppmB.

10.3.3 Comparison of Calculated and Measured Results

A comparison of calculated and measured control rod worths in terms of reactivity is shown in Table 10-3. This table compares the worths of control banks: D, C, B, and A and shutdown banks: E, D, and C at HZP and BOC for McGuire Unit 1, Cycles 1 and 1A, and McGuire Unit 2, Cycle 1. A comparison of calculated and measured control rod worths in terms of ppmB is shown in Table 10-4. This table also compares the worths of control banks: D, C, B, and A and shutdown banks: E, D, and C at HZP and BOC for McGuire Unit 1, Cycles 1 and 1A, and McGuire Unit 2 Cycle 1. Table 10-5 is a comparison of PDQ07 calculated and measured control rod worths.

PDQ07 calculated bank worths agree well to measured with an average difference of 2.7% and a standard deviation of 3.3%. EPRI-NODE-P calculated bank worths similarly agreed well with an average difference of -4.5% and a standard deviation of 5.1%. Rod worths calculated using boron endpoints also agreed well, with an average difference of -2.2% and a standard deviation of 7.9%.

10.3.4 Summary

The comparisons between the calculated and measured control rod worths at HZP indicate that EPRI-NODE-P can adequately predict control rod worths. Tables 10-3 and 10-4 indicate consistent agreement using either reactivity or boron endpoint measurement techniques.

10.4 Ejected Rod Worths

Ejected rod worth is defined here as the measured worth of the worst case ejected rod. No error adjustments have been included.

10.4.1 Measurement Technique

Ejected rod worths are measured by boron swap. The boron swap method is similar to the method used to measure control rod worth. It involves maintaining criticality by varying the boron concentration to compensate for the ejection of the worst case rod. The control rod positions are held constant. As was done for control rod worth, the ejected rod worth is determined from the reactivity computer.

10.4.2 Calculational Techniques

Ejected rod worths are calculated using EPRI-NODE-P to simulate boron swap. A boron search run is first performed to determine the critical boron concentration at the rod group position. The boron concentration as calculated in the EPRI-NODE-P run should be corrected for exact criticality. Using this corrected boron concentration and a constant rod group position, the reactivity is determined with the worst case rod first in and then out. The ejected rod worth is the difference in reactivity between the worst case rod in and out.

10.4.3 Comparison of Calculated and Measured Results

A comparison of calculated and measured ejected rod worth for McGuire Unit 1, Cycle 1, is given in Table 10-6.

10.5 Isothermal Temperature Coefficients

The isothermal temperature coefficient is defined as the change in reactivity per unit change in moderator temperature at hot zero power, i.e.,

$$\alpha_T = \frac{\Delta\rho}{\Delta T}$$

10.5.1 Measurement Techniques

The isothermal temperature coefficient is measured by executing an average moderator temperature ramp to +5°F and then a ramp down to the initial equilibrium critical conditions. During each change, reactivity is measured on the reactivity computer and other pertinent data is measured. After each change, steady state conditions are established. The isothermal temperature coefficient is determined as the change in reactivity between plateaus divided by the change in temperature. Since two different temperature ramps are executed, two coefficients can be determined. The reported isothermal temperature coefficient is an average of these two coefficients.

10.5.2 Calculational Technique

The isothermal temperature coefficient at HZP is calculated using EPRI-NODE-P. Two cases with the same boron concentration and rod positions but different moderator temperatures are run. The isothermal temperature coefficient is the difference in reactivity between the two cases divided by the difference in the moderator temperatures.

10.5.3 Comparison of Calculated and Measured Results

A comparison of calculated and measured isothermal temperature coefficients at HZP and BOC for McGuire Unit 1, Cycles 1 and 1A, and Unit 2, Cycle 1 is presented in Table 10-7. The mean of all the differences was found to be 1.38 pcm/°F with a standard deviation of 1.87 pcm/°F.

10.5.4 Summary

The comparison between calculated and measured isothermal temperature coefficients indicates that EPRI-NODE-P is a good predictor of isothermal temperature coefficients.

TABLE 10-1

McGuire

Critical Boron Concentrations at Hot Zero Power, BOC

Unit	Cycle	Critical Boron Conc. PPM Calculated	Measured	Difference
1	1	1301	1310	-9
		1242	1248	-6
		1123	1128	-5
		1033	1029	4
		972	967	5
		888	891	-3
		822	819	3
		728	723	5
1	1A	1269	1310	-41
		1200	1242	-42
		1090	1125	-35
2	1	1280	1295	-15
		1221	1217	4
		1101	1097	4
		1002	997	5
		944	938	6
		861	860	1
		788	791	-3
		691	694	-3
Mean		----	----	-6.6
Standard Deviation		----	----	15.7

Difference = Calculated - Measured

TABLE 10-2

McGuire 1 Cycle 1-1A

Hot Full Power Critical Boron Concentrations

Unit	EFPD	Critical Boron Conc. PPM Calculated	Measured	Difference
1	24.6	860	880	-20
	34.4	846	865	-19
	39.2	838	864	-26
	49.2	823	862	-39
	82.2	761	801	-40
	90.4	745	790	-45
	99.0	729	771	-42
	101.2	724	762	-38
	126.0	667	724	-57
	154.4	600	650	-50
	180.7	531	591	-60
1A	203.7	782	831	-49
	217.5	713	751	-38
	227.8	673	719	-46
	232.9	653	696	-43
	238.5	631	677	-46
	255.2	566	615	-49
	279.8	473	511	-38
	300.6	395	434	-39
	330.8	281	318	-37
Mean		----	----	-41.1
Standard Deviation		----	----	10.5

Difference = Calculated - Measured

TABLE 10-3

McGuire

Control Rod Worths at Hot Zero Power, BOC

Unit/Cycle	Bank	Rod Worth (PCM) Calculated	Measured	Difference (PCM)	Difference (%)
1/1	CD	606	669	-63	-9.4
	CC	1217	1250	-33	-2.6
	CB	925	996	-71	-7.1
	CA	654	695	-41	-5.9
	SE	884	840	44	5.2
	SD	668	755	-87	-11.5
	SC	961	1011	-50	-4.9
1/1A	CD	685	712	-27	-3.8
	CC	1100	1038	62	6.0
2/1	CD	604	664	-60	-9.0
	CC	1224	1283	-59	-4.6
	CB	1004	1105	-101	-9.1
	CA	618	678	-60	-8.8
	SE	862	853	9	1.1
	SD	738	771	-33	-4.3
	SC	992	1026	-31	-3.0
Mean		----	----	-37.6	-4.5
Standard Deviation		----	----	43.8	5.1

Difference (PCM) = Calculated - Measured

$$\text{Difference}(\%) = \frac{\text{Calculated} - \text{Measured}}{\text{Measured}} \times 100$$

TABLE 10-4

McGuire

Control Rod Worths at Hot Zero Power, BOC

Using Boron Endpoints

Unit/Cycle	Bank	Rod Worth (PPM) Calculated	Measured	Difference (PPM)	Difference (%)
1/1	CD	59	62	-3	-4.8
	CC	119	120	-1	-0.8
	CB	90	99	-9	-9.1
	CA	61	62	-1	-1.6
	SE	84	76	8	10.5
	SD	66	72	-6	-8.3
	SC	94	96	-2	-2.1
1/1A	CD	69	68	1	1.5
	CC	110	117	-7	-6.0
2/1	CD	59	78	-19	-24.4
	CC	120	120	0	0.0
	CB	99	100	-1	-1.0
	CA	58	59	-1	-1.7
	SE	83	78	5	6.4
	SD	73	69	4	5.8
	SC	97	97	0	0.0
Mean		----	----	-2.0	-2.2
Standard Deviation		----	----	6.3	7.9

Difference (PCM) = Calculated - Measured

$$\text{Difference}(\%) = \frac{\text{Calculated} - \text{Measured}}{\text{Measured}} \times 100$$

TABLE 10-5

McGuire

PDQ07 Calculated Rod Worths vs. Measured Rod Worths at HZP, BOC

Unit/Cycle	Bank	Rod Worth (PCM) Calculated	Measured	Difference (PCM)	Difference (%)
1/1	D	644	669	-25	-3.7
	C	1214	1250	-36	-2.9
	B	962	996	-34	-3.4
1/1A	D	667	712	-45	-6.3
	C	1088	1038	50	4.8
2/1	D	637	664	-27	-4.1
	C	1261	1283	-22	-1.7
	B	1090	1105	-15	-1.4
	A	638	678	-40	-5.9
Mean		----	----	-22	-2.7
Standard Deviation		----	----	28	3.3

Difference (PCM) = Calculated - Measured

$$\text{Difference}(\%) = \frac{\text{Calculated} - \text{Measured}}{\text{Measured}} \times 100$$

TABLE 10-6

McGuire 1 Cycle 1
Ejected Rod Worths

Cycle	Location	Worth (PCM) Calculated	Measured	Difference (PCM)
1	D-12	406	432	-26

Difference (PCM) = Calculated - Measured

TABLE 10-7

McGuire

Isothermal Temperature Coefficients at Hot Zero Power, BOC

Unit/Cycle	Control Rod Configuration	Temp. Coeff., (PCM/°F) Calculated	Measured	Difference (PCM/°F)
1	ARO	-1.03	-0.57	-0.46
	D in	-2.09	-2.02	-0.07
	C & D in	-6.03	-5.86	-0.17
	B, C, & D in	-6.08	-6.83	0.75
	A, B, C, & D in	-9.37	-9.72	0.35
1	ARO	-4.51	-1.13	-3.38
	D in	-5.86	-1.98	-3.88
	C & D in	-9.76	-4.83	-4.93
2	ARO	-2.34	-1.41	-0.93
	D in	-3.54	-2.73	-0.81
	C & D in	-7.70	-6.07	-1.63
Mean		----	----	-1.38
Standard Deviation		----	----	1.87

Difference (PCM/°F) = Calculated - Measured

FIGURE 10-1

McGuire 1 Cycle 1
Boron Letdown Curves

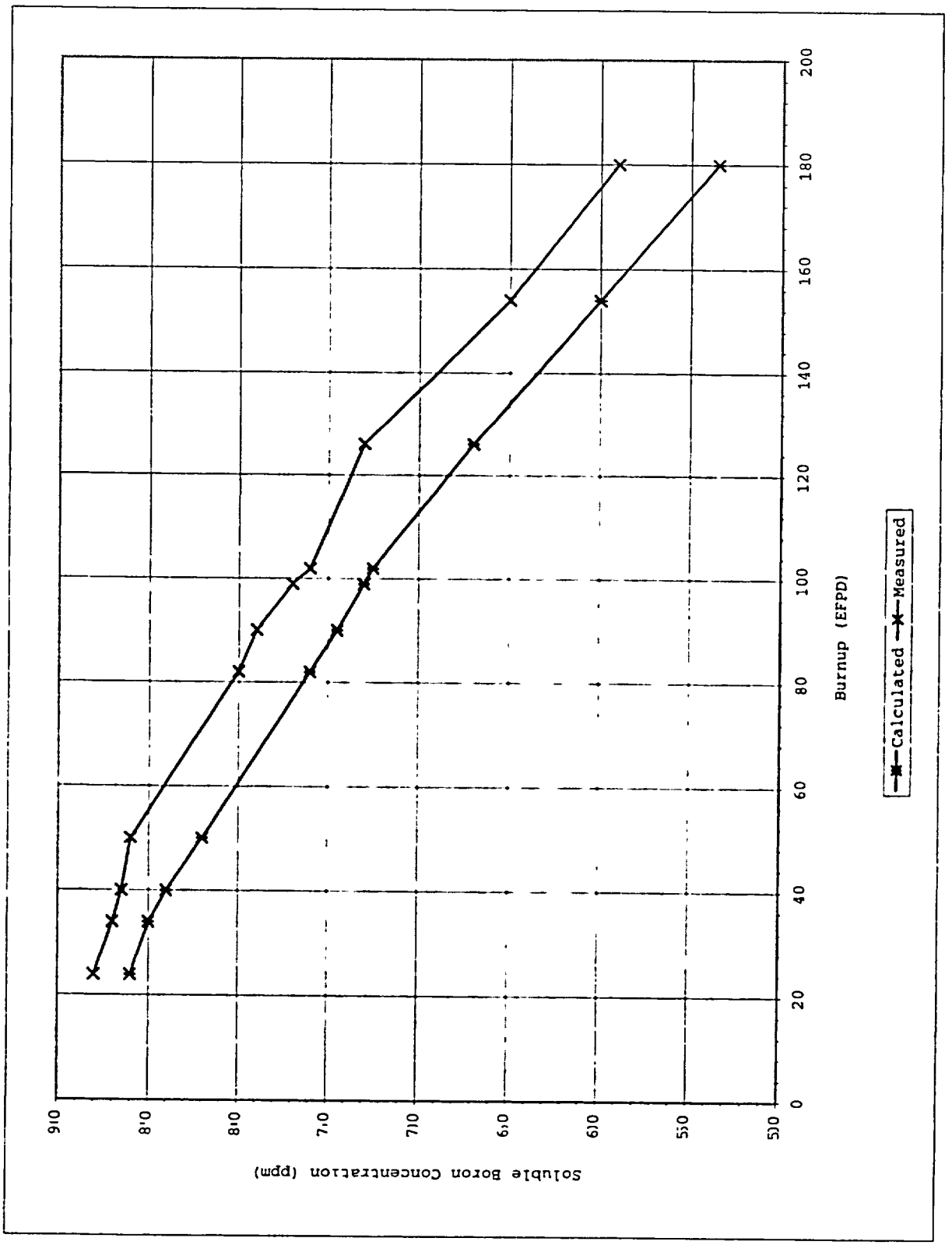

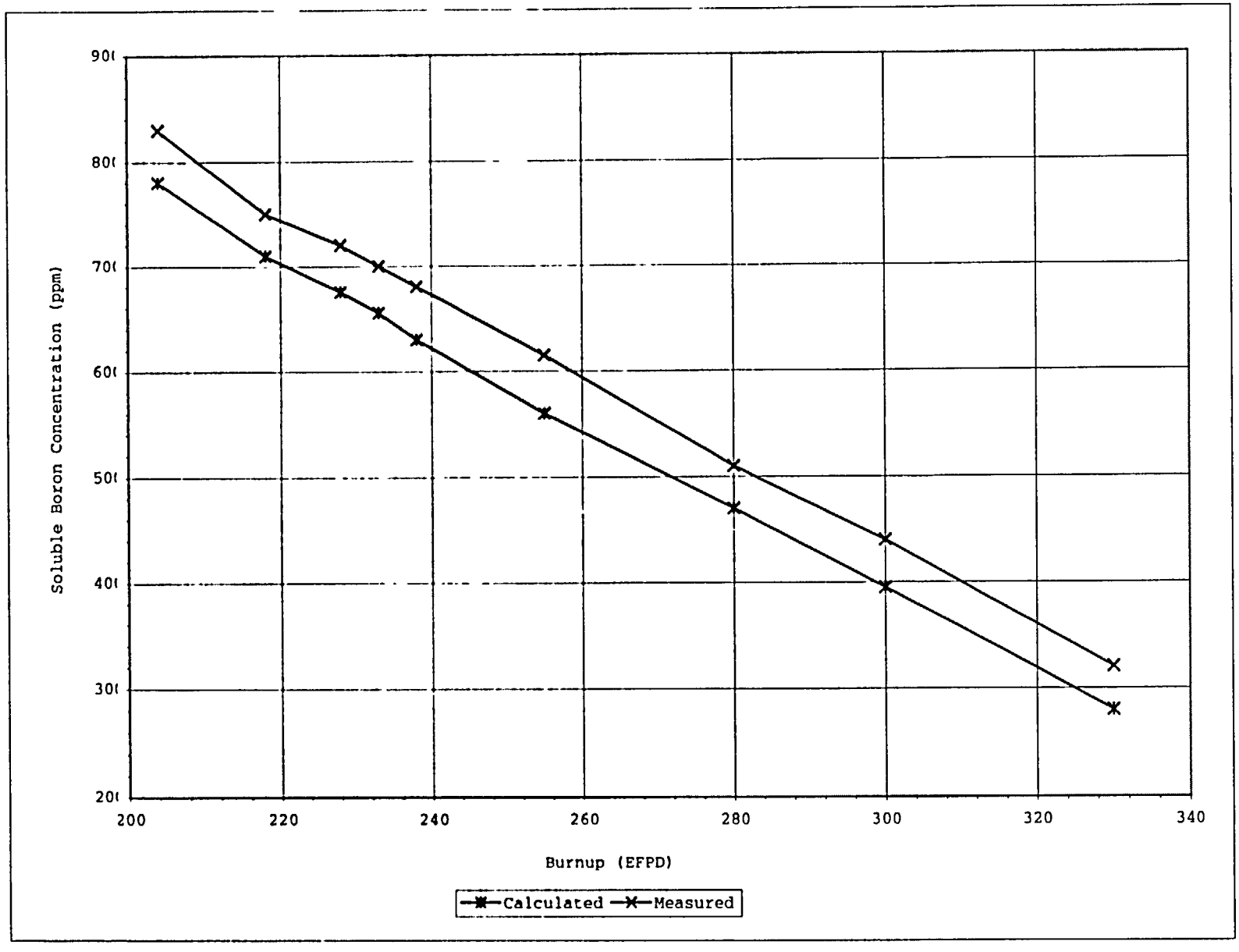

FIGURE 10-2

McGuire 1 Cycle 1A
Boron Letdown Curves

11. POWER DISTRIBUTION COMPARISONS

Power distribution information contained in this section is presented to provide the perspective on the benchmarking of measured to predicted results. The predicted results are based on the PDQ07/EPRI-NODE-P models. Reference 28 presents the benchmarking results for the CASMO-3/SIMULATE-3 models.

11.1 Introduction and Summary

11.1.1 Introduction

The nuclear code employed in this section to calculate three dimensional assembly power calculations is EPRI-NODE-P. Additional two dimensional calculations are performed with PDQ07. The EPRI-NODE-P code has been benchmarked against McGuire Unit 1 Cycle 1 and part of Cycle 1A. It has also been benchmarked against TVA's Sequoyah Unit 1 Cycle 1.

This work encompassed: derivation of measured power distributions for the above cycles, simulations of the above cycles using EPRI-NODE-P, development of fitting procedures for the calculated assembly peak axial powers, and development of a statistical basis for estimating the calculational accuracy of EPRI-NODE-P.

11.1.2 Summary

A data base consisting of McGuire Unit 1 Cycle 1 and part of Cycle 1A, and TVA's Sequoyah Unit 1 Cycle 1, measured and EPRI-NODE-P calculated fuel assembly powers was assembled. Calculated and measured powers were statistically combined to derive 95/95 Observed Nuclear Reliability Factors (ONRF) for EPRI-NODE-P. ONRF's were calculated for assembly radial powers, assembly peak axial powers, and assembly normalized axial powers. The assembly radial power ($F_{\Delta H}$) is defined as the ratio of assembly average power to core average power. The assembly peak axial power (F_Q) is defined as the maximum assembly x-y planar average power along the fuel assembly length

relative to the core average power. The assembly axial power (F_Z) is defined as the ratio of the assembly peak axial power and the assembly radial power ($F_Q/F_{\Delta H}$).

ORNFs of 1.03 for the assembly radial powers, 1.06 for the assembly peak axial powers, and 1.05 for the assembly normalized axial powers were determined.

11.2 Measured Data

11.2.1 Measured Assembly Power Data

The measured power data base comprises assembly power data from McGuire Unit 1, Cycle 1 and part of Cycle 1A, and TVA's Sequoyah Unit 1, Cycle 1. All measured assembly power data are directly traceable to signals from the incore detector system.

11.2.2 Measurement System Description

The incore detector systems at McGuire and Sequoyah consist of 6 movable miniature fission chamber neutron detectors. The detectors are inserted into the bottom of the reactor vessel and driven up through the core to the top. They are then slowly withdrawn through the core. Incore flux maps are obtained by taking voltage signal readings from the detectors as they are withdrawn through the core. This data is then stored on the plant computer.

The detectors travel inside thimbles that are located in the Instrument Guide Tube of the fuel assemblies. There are 58 instrumented assemblies out of a total of 193 fuel assemblies. There are 61 voltage signals recorded axially along each of instrumented fuel assemblies. The instrumented fuel assemblies are shown on Figure 11-1.

The detectors are inter-calibrated by inserting each detector into one reference (calibration) fuel assembly. After each flux map the detector signals are processed by Shanstrom Nuclear Associates Code for Operating

Reactor Evaluation (SNA-CORE)[26]. SNA-CORE uses the 58 x 61 array of signals to calculate peaking factors, (radial powers and assembly peak axial powers) for each of the 193 assemblies. The 193 radial powers and assembly peak axial powers are then averaged into eighth core or quarter core, depending on the cycle. These peaking factors then make up the measured data base. All power measurements were taken at approximately equilibrium xenon conditions. Tables 11-1, 11-2, and 11-3 show the selected reactor state points.

11.3. EPRI-NODE-P Power Distribution Comparisons

11.3.1 EPRI-NODE-P Model

As noted previously, EPRI-NODE-P was used to calculate the three dimensional power distribution data presented in this section. This code can be used for all maneuvering analyses, core follow, and physics test data where three-dimensional core power distributions are required. In this section, comparisons of measured and EPRI-NODE-P calculated values will be shown for both radial powers and assembly peak axial powers. Comparisons were performed on a total of 37 reactor state points covering McGuire Unit 1, Cycle 1 and part of 1A, and Sequoyah Unit 1, Cycle 1.

McGuire Unit 1, Cycle 1 and Sequoyah Unit 1, Cycle 1 were modeled using eighth core symmetry. McGuire Unit 1, Cycle 1A was modeled using quarter core symmetry. Each fuel assembly was modeled with one radial and 12 equidistant axial nodes. The active stack height was set at 144 inches. Control rods could be positioned continuously in this model. Simulations of the McGuire and Sequoyah cores were performed using methods described in Section 3.5 and 5.2.

11.3.2 Fuel Cycle Simulations

Using the EPRI-NODE-P model described in section 11.3.1, McGuire Unit 1, Cycles 1 and part of 1A, and TVA's Sequoyah Unit 1, Cycle 1 were depleted

using thermal and hydraulic feedbacks. The depletions were performed in a core follow mode, utilizing critical boron searches at each exposure step.

McGuire Unit 1, Cycle 1 operated until 191.5 EFPD. Control and shutdown bank locations are shown on Figure 11-2. The core loading pattern is shown on Figure 11-3. During this time the unit was operated mostly at the 50% and 75% power plateaus because of power limitations imposed by steam generator flow impingement problems.

The EPRI-NODE-P radial powers were normalized to PDQ07 depletion at 25 EFPD for McGuire Unit 1, Cycle 1. There were 25 state points for this cycle. These are shown on Table 11-1. Figures 11-6 to 11-30 show comparisons of calculated and measured radial powers. Figure 11-31 to 11-55 show comparisons of calculated and measured assembly peak axial powers.

The data used for McGuire Unit 1, Cycle 1A was through 250 EFPD. Control and shutdown bank locations are the same as those for McGuire Unit 1, Cycle 1. The core loading pattern for cycle 1A was the same as the loading pattern for Cycle 1 except all but 2 burnable poison rods were removed. The two that remained were in core locations H-3 and H-13. The unit was operated mostly at 100% power during this time after the steam generator flow impingement problem was corrected.

The EPRI-NODE-P radial powers were normalized to PDQ07 depletion at 257 EFPD for McGuire Unit 1, Cycle 1A. There were 5 state points for the part of this cycle that was used. These are shown on Table 11-2. Figures 11-56 to 11-60 show comparison of calculated and measured radial powers. Figures 11-61 to 11-65 show comparisons of calculated and measured assembly peak axial powers.

TVA's Sequoyah Unit 1, Cycle 1 operated until the end of cycle which lasted 390 EFPD. Control and shutdown bank locations are shown on Figure 11-4. The core loading pattern is shown on Figure 11-5.

The EPRI-NODE-P radial powers were normalized to PDQ07 depletion at 25 EFPD

for Sequoyah Unit 1, Cycle 1. There were 7 state points for this cycle. These are shown on Table 11-3. Figures 11-66 to 11-72 show comparison of calculated and measured radial powers. Figures 11-73 to 11-79 show comparison of calculated and measured assembly peak axial powers.

11.3.3 Radial Power Methodology

The radial powers are radial peaking factors. Therefore, the radial peaking factors from SNA-CORE are compared directly to the normalized radial powers (P(I,J)) from EPRI-NODE-P.

11.3.4 Assembly Peak Axial Power Methodology

The assembly peak axial powers are peaking factors. There are 61 assembly axial powers for each fuel assembly calculated by SNA-CORE. Of these 61 assembly axial powers, the maximum is chosen for the "measured" assembly peak axial power. The EPRI-NODE-P model calculated 12 nodal axial powers per assembly. The assembly peak axial power could not be compared directly to the maximum nodal power.

Therefore, the nodal axial powers were curve fit using the following equation:

$$P(z) = \sum_{n=1}^{3} A_n \mathrm{Sin}(n\pi z) + B_n \mathrm{Cos}(n\pi z)$$

Where: A_n, B_n = Fourier series coefficients

z = normalized vertical axis variable

n = Fourier sequence number

The 12 level node powers were fit, yielding 61 assembly axial powers for each assembly at each state point. The assembly peak axial power was then selected from the 61 calculated assembly axial powers and the 12 nodal powers.

11.3.5 Conclusions

EPRI-NODE-P yielded consistently good power distributions when compared to measured power distributions. This conclusion applies for both radial and assembly peak axial power comparisons. Although the conclusions in this section are qualitative, quantitative statistical results of these comparisons will be shown in Section 11.5.

11.4 PDQ07 - Power Distribution Comparisons

Radial power distributions from the PDQ07 depletions of McGuire Unit 1, Cycle 1, Cycle 1A, and Sequoyah Unit 1, Cycle 1 were compared to measured radial power distributions from SNA-CORE at various burnups. The PDQ07 model employed a 2-dimensional geometry with two neutron energy groups. (For additional information concerning the use of this code, refer to Section 3.4). All power distributions from PDQ07 were performed at hot full power all rods out. Table 11-4 compares the state points of the measured data to that of PDQ07. Figures 11-80 to 11-86 show the comparisons of the radial powers.

11.5. Statistical Analysis

11.5.1 Observed Nuclear Reliability Factor Derivation

This section will address quantitatively statistics arising from Section 11.3. Normal distribution theory will be used in deriving calculational uncertainties.

In deriving the calculational uncertainty for EPRI-NODE-P, the algebraic difference between a calculated and a measured value forms a normally distributed (refer to Section 11.5.2) random variable.

The difference variable is defined:

$$D_i = C_i - M_i \tag{11-1}$$

where: D is the ith difference; $1 \leq i \leq N$

C is the ith calculated value (radial or assembly peak axial power)

M is the ith measured value (radial or assembly peak axial power)

The mean of the difference as defined in equation 11-2 is:

$$\bar{D} = \bar{C} - \bar{M} \tag{11-2}$$

where: $$\bar{C} = (\sum_{i=1}^{n} C_i) \div n \tag{11-2a}$$

$$\bar{M} = (\sum_{i=1}^{n} M_i) \div n \tag{11-2b}$$

$$\bar{D} = (\sum_{i=1}^{n} D_i) \div n \tag{11-2c}$$

n = number of observations in sample

Now a one sided upper bound factor is derived by employing One Sided Upper Tolerance Limit (OSUTL) methodology. For a normal random variable X with a sample mean X and standard deviation S, the OSUTL of X is defined by:

$$\text{OSUTL}(X) = \bar{X} + K \times S \tag{11-3}$$

where: $$\bar{X} = (\sum_{i=1}^{n} X_i) \div n \tag{11-4}$$

$$S = [(\sum_{i=1}^{n} (X_i - \bar{X})^2) \div (n-1)]^{1/2} \tag{11-5}$$

In equation 11-3, K is the one-sided tolerance factor. Equation 11-3 is

formulated such that a predetermined proportion of the population (P) is below the OSUTL with a confidence factor (α)[25]. K is explicitly dependent on n, P, and α. Following industry practice, P = 95% and α = 95%.

The OSUTL is given for D by:

$$OSUTL(D) = \bar{D} + K \times S(D) \qquad (11\text{-}6)$$

C is a deterministic variable and does not have an OSUTL per se, but a reasonable upper limit to C can be defined by:

$$UL(C) = \bar{M} + OSUTL(D) \qquad (11\text{-}7)$$

$$UL(C) = \bar{M} + \bar{D} + K \times S(D) \qquad (11\text{-}7a)$$

If one substitutes equations 11-2 into equation 11-7 you obtain the following:

$$UL(C) = \bar{M} + \bar{C} - \bar{M} + K \times S(D) \qquad (11\text{-}8)$$

or $$UL(C) = \bar{C} + K \times S(D) \qquad (11\text{-}8a)$$

From equation (11-8a), it is more obvious that the upper limit is a function of the calculated parameter. Also, it is obvious that the standard deviation being associated with the calculated limit is that of the difference distribution. This means that any error in the measurement of the radial or assembly peak axial power as well as any calculational error will be included in the UL(C) parameter. While equation 11-7a and 11-8a are valid, the definition of $\bar{D} = \bar{C} - \bar{M}$ (equation 11-2) leads to UL(C) being smaller if the measured parameter is underpredicted. The conservative solution to this is to subtract $\bar{D}$ in equation 11-7a instead of adding it. This would yield the following equation:

$$UL(C) = \bar{M} + \bar{D} + K \times S(D) \qquad (11\text{-}9)$$

Finally, the Observed Nuclear Reliability Factor (ONRF) is defined as the quotient of UL(C) from equation 11-9 and the mean of the measurements:

$$ONRF = \frac{UL(C)}{\bar{M}} \qquad (11\text{-}10)$$

or

$$ONRF = \frac{\bar{M}-\bar{D}+K\times S(D)}{\bar{M}} \qquad (11\text{-}11)$$

The ONRF from equation 11-11 will be used as a multiplicative factor applied to EPRI-NODE-P calculated powers such that:

$$ONRF \times C \geq M \qquad (11\text{-}12)$$

for 95% of the population and with a confidence factor of 95%. Separate ONRF's are derived for radial and assembly peak axial powers.

This procedure was employed in Reference 3 to statistically evaluate ORNFs for EPRI-NODE-P as part of the Oconee Reload Design Methodology.

11.5.2 Normality Test Results

In analyzing the normality of the difference distributions, C, M data were grouped into the following categories:

1) reactor cycle: McGuire 1, Cycle 1; McGuire 1, Cycle 1A; Sequoyah 1, Cycle 1
2) grouped cycles: All reactor cycles combined
3) type: radial powers or assembly peak axial powers

The difference distributions were analyzed for normality using the D' test from ANSI N15.15 - 1974.[27] Using the engineering judgment that only peaking factors greater than the core average are the area of concern, pairs of C,M where both are $\geq$ 1.0 will be treated. Table 11-5 displays the normality test results. The level of significance was chosen to be .05. Therefore, the D' statistic must be between the .025 and .975 percentage point D' values for normality. Here, 3 out of 4 assembly radial power distributions were normal and 4 assembly peak axial power distributions were normal. The remainder of

the difference distributions yielded D' statistics that were close to the critical values and were therefore classified as nearly normal.

11.5.3 Observed Nuclear Reliability Factors (ONRF) for EPRI-NODE-P

In this subsection the statistical treatment developed in Section 11.5.1 will be utilized to develop ONRF's ($F^R_{\Delta H}$, F^R_Q, and F^R_Z) for McGuire Unit 1, Cycle 1 and part of Cycle 1A, and TVA's Sequoyah Unit 1, Cycle 1, combined.

All pairs of C, M $\geq$ 1.0 from all 37 state points of McGuire Unit 1, Cycle 1 and part of Cycle 1A, and Sequoyah Unit 1, Cycle 1, were obtained. The procedure was applied to radial powers, assembly peak axial powers, and assembly normalized axial powers. The variables shown in equation 11-11 were then derived and the ONRF's calculated.

As an example, for radial ORNF ($F^R_{\Delta H}$)

$\bar{M}$ = 1.131

$\bar{D}$ = 0.002

S(D) = 0.020

N = 846

K = 1.7343 (N = 846, 95%/95%)

Therefore, the ONRF would be:

$$ONRF = \frac{1.131 - 0.002 + (1.7343 \times 0.020)}{1.131} \qquad (11\text{-}13)$$

$$ONRF = 1.029 \qquad (11\text{-}13a)$$

Table 11-6 shows the calculated ORNF's and the data used to calculate them.

11.5.4 Quantitative Comparisons of EPRI-NODE-P to Measurement

By analyzing the variable D as defined in equation 11-1, the accuracy of EPRI-NODE-P can be assessed. Four important statistical properties of D are discussed.

$\bar{D}$ is the mean of the differences between EPRI-NODE-P and measured assembly powers. For McGuire Unit 1, Cycle 1 and part of 1A, and Sequoyah Unit 1, Cycle 1 $\bar{D}$ is 0.002 for radial powers and -0.031 for assembly peak axial powers. The above means were derived from all pairs of C, M $\geq$ 1.0 from all 37 state points. Subsequent statistics are also derived from this consideration.

S(D), the standard deviation of the differences, indicates the spread of the values of D about $\bar{D}$. For the above cycles, S(D) for radial powers is 0.020. S(D) for assembly peak axial powers is 0.028.

The mean of the absolute differences $\overline{ABS(D)}$ and its standard deviation can be combined to give limits on this variable. 95% confidence limits on the means were given by:

$$\overline{ABS(D)}_{U,L} = ABS(D) \pm \frac{t(.05,n) \times S(ABS(D))}{\sqrt{n}} \qquad (11\text{-}14)$$

Equation 11-14 yields

$$\overline{ABS(D)}_{U,L} = 0.018 \pm 0.001$$

for radial powers for C, M pairs $\geq$ 1.0 for all 37 state points and:

$$\overline{ABS(D)}_{U,L} = 0.036 + 0.001$$

for assembly peak axial powers for all C, M pairs $\geq$ 1.0 for all 37 state points.

Tables 11-7 and 11-8 present summary D statistics for radial and assembly peak axial powers, respectively, where C, M $\geq$ 1.0 for all pairs considered.

11.5.5 Relative Percent Differences

The relative percent difference between EPRI-NODE-P calculated values and measured values will be defined:

$$\% \text{ Diff} = \frac{C-M}{M} \times 100 \qquad (11\text{-}15)$$

This section will address relative percent differences derived from:

a) the sample mean
b) the mean of the absolute value

Since negative percent differences represent calculational nonconservatisms, the minimum values will be more important. Relative percent differences for all C, M $\geq$ 1.0 will be discussed.

Combining data for McGuire Unit 1, Cycle 1, and part of Cycle 1A, and Sequoyah Unit 1, Cycle 1, the following results were obtained.

The average percent difference was 0.167 and the absolute 1.555 for radial powers. Also, the average percent difference was -2.195 and the absolute 2.392 for assembly peak axial powers.

Table 11-9 shows summary data for percent differences derived from calculated and measured radial powers. Values are presented by cycle and for all cycles combined. Table 11-10 is similar to Table 11-9 and provides data for assembly peak axial power percent differences.

11.5.6 Conclusions

A statistical analysis of EPRI-NODE-P calculated and plant measured power distributions has been performed. The resulting ONRF's for all C, M pairs $\geq$ 1.0 for all 37 state points are:

$(F_{\Delta H}^{R})$ Assembly Radial ONRF	(F_{Q}^{R}) Assembly Peak Axial ONRF	(F_{Z}^{R}) Assembly Normalized Axial Power ONRF
1.03	1.06	1.05

These values while based upon calculations and measurements performed on McGuire Unit 1, Cycles 1 and part of 1A, and Sequoyah Unit 1, Cycle 1 are applicable to all McGuire and Catawba units for the following reasons:

1. McGuire, Catawba, and Sequoyah have identical incore detector systems.

2. All units are manufactured by the same vendor and use similar fuel.

3. Calculations for all units were performed using the same calculational methods and procedures. Similarly, all calculations performed for McGuire and Catawba will use the same calculational methods and procedures.

As an additional verification of the conservatism in the 1.03 radial and 1.06 assembly peak axial ONRF's, all calculated maximum radial powers were multiplied by 1.03 and compared to measured. Similarly all calculated assembly peak axial powers were multiplied by 1.06 and compared to measured. 29 out of 843 (3.4%) radial powers exceeded the 1.03 x maximum calculated radial power. 43 out of 1038 (4.1%) assembly peak axial powers exceeded the 1.06 x maximum calculated assembly peak axial power. Therefore, the 1.03 radial factor was satisfactory for the entire population. The 1.06 assembly peak axial factor was also satisfactory for the entire population.

For pin power distributions, the uncertainty in the assembly power distribution is statistically combined with the uncertainty in the radial local factor (2% see Section 8.5) and the uncertainty for manufacturing tolerance (3%).

The pin total peak uncertainty factor (F_Q^{SCUF}) is calculated below.

$$F_Q^{SCUF} = 1+\frac{0.031}{1.375}+\sqrt{(0.03)^2+(0.035)^2+(0.02)^2} = 1.073$$

Similary, the pin radial peak uncertainty factor ($F_{\Delta H}^{SCUF}$) is calculated below, not including the bias term.

$$F_{\Delta H}^{SCUF} = 1+\sqrt{(0.03)^2+(0.03)^2+(0.02)^2} = 1.047$$

Finally, the assembly normalized axial peak uncertainty factor (F_Z^{SCUF}) is calculated below.

$$F_Z^{SCUF} = 1+\frac{0.032}{1.251}+\sqrt{(0.022)^2} = 1.048$$

TABLE 11-1

McGuire Unit 1 Cycle 1 State Points

Point #	EFPD	Power (%)	Control Bank D Position (Steps)	Axial Offset (Meas/Calc) (%)
1	1.28	30	213	-4.67 / -4.78
2	5.27	30	170	-10.68 / -9.20
3	7.70	48	200	-7.59 / -6.83
4	11.42	48	164	-11.90 /-11.07
5	37.10	50	186	-8.76 / -7.70
6	41.59	50	201	-5.56 / -6.30
7	48.75	50	201	-6.27 / -6.01
8	59.37	50	201	-5.06 / -5.83
9	75.38	50	198	-6.10 / -5.86
10	80.46	75	213	-8.57 / -6.94
11	91.54	75	213	-7.41 / -6.75
12	104.47	50	215	-4.07 / -3.58
13	112.05	50	215	-1.57 / -3.43
14	115.69	75	217	-5.61 / -6.52
15	118.71	50	180	-8.60 / -7.50
16	122.15	75	215	-5.58 / -6.36
17	130.59	75	215	-7.58 / -6.17
18	135.44	75	215	-5.77 / -5.99
19	139.82	50	180	-8.43 / -6.82
20	151.42	50	215	-0.54 / -2.52
21	146.01	75	215	-4.80 / -5.86
22	150.19	50	215	-0.70 / -2.32
23	162.76	50	215	-4.80 / -2.33
24	173.34	50	215	-0.29 / -2.27
25	185.58	50	215	-0.45 / -2.24

TABLE 11-2

McGuire Unit 1 Cycle 1A State Points

Point #	EFPD	Power (%)	Control Bank D Position (Steps)	Axial Offset (Meas/Calc) (%)
1	198.66	90	217	0.73 / -0.93
2	217.53	100	209	1.35 / -5.05
3	223.35	100	211	-3.51 / -4.92
4	236.23	100	211	-3.44 / -4.89
5	249.75	100	221	-2.51 / -3.77

TABLE 11-3

Sequoyah Unit 1 Cycle 1 State Points

Point #	EFPD	Power (%)	Control Bank D Position (Steps)	Axial Offset (Meas/Calc) (%)
1	71.82	100	200	-7.31 / -9.01
2	101.62	100	218	-4.36 / -6.19
3	133.29	100	216	-3.95 / -5.60
4	166.04	100	210	-2.68 / -5.51
5	231.70	100	216	-1.36 / -3.77
6	290.04	100	216	-1.51 / -3.40
7	378.92	100	222	-1.43 / -2.86

TABLE 11-4

McGuire Unit 1 Cycles 1 and 1A and Sequoyah Unit 1 Cycle 1
State Points for PDQ07 Calculated and Measured Data

			PDQ07 Calculated			Measured		
Pt #	Unit	Cycle	EFPD	Control Bank D Position (Steps)	Power (%)	EFPD	Control Bank D Position (Steps)	Power (%)
1	M1	1	52.2	228	100	48.8	200	50
2	M1	1	104.4	228	100	104.5	218	50
3	M1	1	156.7	228	100	150.2	216	50
4	M1	1A	208.9	228	100	198.7	210	90
5	S1	1	103.6	228	100	101.6	216	100
6	S1	1	155.5	228	100	133.3	216	100
7	S1	1	362.7	228	100	378.9	222	100

TABLE 11-5

Difference Distribution Normality Tests
for C, M ≥ 1.0 - 5% Level of Significance

Assembly Radial Powers

Unit/Cycle	N	D' (P=.025)	D'	D' (P=.975)	Remarks
M1/C1	510	3215.0	3274.7	3275.0	Normal
M1/C1A	190	725.9	746.0	748.1	Normal
S1/C1	146	487.6	491.9	504.6	Normal
All Combined	846	6886.7	7000.9	6986.2	Nearly Normal

Assembly Peak Axial Powers

Unit/Cycle	N	D' (P=.025)	D'	D' (P=.975)	Remarks
M1/C1	642	4546.4	4586.3	4621.7	Normal
M1/C1A	220	904.9	922.9	930.5	Normal
S1/C1	176	646.4	646.4	666.9	Normal
All Combined	1038	9345.5	9379.5	9489.8	Normal

TABLE 11-6

Calculated ONRFs and Associated Data

Assembly Radial Power ONRF ($F^R_{\Delta H}$)

$\bar{M}$	= 1.131
$\bar{D}$	= 0.002
S(D)	= 0.020
N	= 846
K	= 1.7343 (N = 846, 95%/95%)
ONRF($F^R_{\Delta H}$)	= 1.029

Assembly Peak Axial Power ONRF (F^R_Q)

$\bar{M}$	= 1.375
$\bar{D}$	= -0.031
S(D)	= 0.028
N	= 1038
K	= 1.7259 (N = 1038, 95%/95%)
ONRF(F^R_Q)	= 1.058

Assembly Axial Power ONRF (F^R_Z)

$\bar{M}$	= mean value of $(F_Q/F_{\Delta H})$meas.	= 1.251
$\bar{D}$	= mean value of $[(F_Q/F_{\Delta H})$meas. - $(F_Q/F_{\Delta H})$calc.$]$	= 0.032
S(D)	= 0.016	
N	= 846	
K	= 1.7343 (N = 846, 95%/95%)	
ONRF(F^R_Z)	= 1.048	

TABLE 11-7

Difference, Means, and Standard Deviations for Assembly Radial Powers (C, M ≥1.0)

Unit/Cycle	N	$\bar{D}$	S(D)	$\overline{ABS}$	S(ABS(D))
M1/C1	510	-0.001	0.019	0.017	0.008
M1/C1A	190	-0.001	0.025	0.023	0.010
S1/C1	146	0.013	0.012	0.014	0.010
All Combined	846	0.002	0.020	0.018	0.010

TABLE 11-8

Difference, Means, and Standard Deviations for Assembly Peak Axial Powers (C, M ≥1.0)

Unit/Cycle	N	$\bar{D}$	S(D)	$\overline{ABS}$	S(ABS(D))
M1/C1	642	-0.029	0.027	0.032	0.023
M1/C1A	220	-0.039	0.033	0.041	0.029
S1/C1	176	-0.028	0.026	0.031	0.023
All Combined	1038	-0.031	0.028	0.036	0.025

TABLE 11-9

Percent Difference Means

(C, M ≥1.0) - Assembly Radial Powers

Unit/Cycle	Mean % Difference	Mean Absolute % Difference
M1/C1	-0.058	1.452
M1/C1A	0.007	2.043
S1/C1	1.163	1.281
All Combined	0.167	1.555

TABLE 11-10

Percent Difference Means

(C, M ≥1.0) - Assembly Peak Axial Powers

Unit/Cycle	Mean % Difference	Mean Absolute % Difference
M1/C1	-2.001	2.196
M1/C1A	-2.838	3.031
S1/C1	-2.099	2.310
All Combined	-2.195	2.392

FIGURE 11-1

Instrumented Fuel Assemblies

McGuire and Sequoyah

								X								
1							X			X						
2				X			X		X							
3									X		X		X		X	
4			X	X					X							
5						X				X		X		X		
6		X		X			X		X						X	
7					X			X			X			X		
8	W	X		X		X		X			X		X	X	X		Y
9			X							X		X				X
10						X		X					X			
11		X				X			X			X				X
12							X			X			X			
13				X		X			X						X	
14				X				X			X		X			
15						X			X							
								Z								
		R	P	N	M	L	K	J	H	G	F	E	D	C	B	A

FIGURE 11-2

Control and Shutdown Bank Locations
McGuire 1 Cycle 1

								X								
1																
2					SA		B		C		B		SA			
3						SD		SB		SB		SC				
4			SA		D				SE				D		SA	
5				SC										SD		
6			B				C		A		C				B	
7				SB										SB		
8	W		C		SE		A		D		A		SE		C		Y
9				SB										SB		
10			B				C		A		C				B	
11				SD										SC		
12			SA		D				SE				D		SA	
13						SC		SB		SB		SD				
14					SA		B		C		B		SA			
15																
								Z								
		R	P	N	M	L	K	J	H	G	F	E	D	C	B	A

FIGURE 11-3

Core Loading Pattern

McGuire 1 Cycle 1

X

	R	P	N	M	L	K	J	H	G	F	E	D	C	B	A	
1					C	10 C	C	10 C	C	10 C	C					
2			9 C	C	12 C	A	20 C	A	19 C	A	12 C	C	9 C			
3		9 C	C	20 B	A	16 B	A	16 B	A	16 B	A	20 B	C	9 C		
4		C	20 B	B	20 B	A	16 B	A	16 B	A	20 B	B	20 B	C		
5	C	12 C	A	20 B	A	16 B	A	16 B	A	16 B	A	20 B	A	12 C	C	
6	10 C	A	16 B	A	16 B	A	20 B	A	20 B	A	16 B	A	16 B	A	10 C	
7	C	20 C	A	16 B	A	20 B	A	20 B	A	20 B	A	16 B	A	20 C	C	
8 W	10 C	A	16 B	A	16 B	A	20 B	A	20 B	A	16 B	A	16 B	A	10 C	Y
9	C	20 C	A	16 B	A	20 B	A	20 B	A	20 B	A	16 B	A	20 C	C	
10	10 C	A	16 B	A	16 B	A	20 B	A	20 B	A	16 B	A	16 B	A	10 C	
11	C	12 C	A	20 B	A	16 B	A	16 B	A	16 B	A	20 B	A	12 C	C	
12		C	20 B	B	20 B	A	16 B	A	16 B	A	20 B	B	20 B	C		
13		9 C	C	20 B	A	16 B	A	16 B	A	16 B	A	20 B	C	9 C		
14			9 C	C	12 C	A	20 C	A	19 C	A	12 C	C	9 C			
15					C	10 C	C	10 C	C	10 C	C					

Z

A	Region 1 (2.1 w/o)
B	Region 2 (2.6 w/o)
C	Region 3 (3.1 w/o)

Number indicates number of burnable poison rods

FIGURE 11-4

Control and Shutdown Bank Locations
Sequoyah 1 Cycle 1

								X							
1															
2					SA		B		C		B		SA		
3						SD		SB		SB		SC			
4			SA		D				D				D		SA
5				SC										SD	
6			B				C		A		C				B
7				SB										SB	
8	W		C		D		A		D		A		D		C	Y
9				SB										SB	
10			B				C		A		C				B
11				SD										SC	
12			SA		D				D				D		SA
13						SC		SB		SB		SD			
14					SA		B		C		B		SA		
15															
								Z							
	R	P	N	M	L	K	J	H	G	F	E	D	C	B	A

FIGURE 11-5

Core Loading Pattern

Sequoyah 1 Cycle 1

X

	R	P	N	M	L	K	J	H	G	F	E	D	C	B	A	
1					C	10 C	C	10 C	C	10 C	C					
2			9 C	C	9 B	A	12 B	A	12 B	A	9 B	C	9 C			
3		9 C	C	16 B	A	16 B	A	20 B	A	16 B	A	16 B	C	9 C		
4		C	16 B	A	16 B	A	16 B	A	16 B	A	16 B	A	16 B	C		
5	C	9 B	A	16 B	A	20 B	A	20 B	A	20 B	A	16 B	A	9 B	C	
6	10 C	A	16 B	A	20 B	A	20 B	A	20 B	A	20 B	A	16 B	A	10 C	
7	C	12 B	A	16 B	A	20 B	A	12 B	A	20 B	A	16 B	A	12 B	C	
8 W	10 C	A	20 B	A	20 B	A	12 B	A	12 B	A	20 B	A	20 B	A	10 C	Y
9	C	12 B	A	16 B	A	20 B	A	12 B	A	20 B	A	16 B	A	12 B	C	
10	10 C	A	16 B	A	20 B	A	20 B	A	20 B	A	20 B	A	16 B	A	10 C	
11	C	9 B	A	16 B	A	20 B	A	20 B	A	20 B	A	16 B	A	9 B	C	
12		C	16 B	A	16 B	A	16 B	A	16 B	A	16 B	A	16 B	C		
13		9 C	C	16 B	A	16 B	A	20 B	A	16 B	A	16 B	C	9 C		
14			9 C	C	9 B	A	12 B	A	12 B	A	9 B	C	9 C			
15					C	10 C	C	10 C	C	10 C	C					

Z

A — Region 1 (2.1 w/o)

B — Region 2 (2.6 w/o)

C — Region 3 (3.1 w/o)

Number indicates number of burnable poison rods

FIGURE 11-6

McGuire-1 Cy-1 Assembly Radial Powers Calculated vs Measured

1.28 EFPD 30%FP Control Bank D at 213 Steps Withdrawn

	H	G	F	E	D	C	B	A
	1.03	.94	1.11	1.10	1.21	1.08	1.06	.73
8	1.01	.96	1.10	1.12	1.20	1.09	1.05	.73
		1.07	.99	1.18	1.11	1.17	1.01	.80
9		1.05	1.01	1.16	1.14	1.15	1.03	.79
			1.15	1.10	1.19	1.06	1.04	.67
10			1.14	1.13	1.17	1.10	1.01	.68
				1.18	1.04	1.12	1.02	.57
11				1.18	1.06	1.12	1.01	.58
					1.27	.95	.87	
12					1.24	.95	.87	
						1.06	.50	Calculated
13						1.02	.49	Measured

FIGURE 11-7

McGuire-1 Cy-1 Assembly Radial Powers Calculated vs Measured

5.27 EFPD 30%FP Control Bank D at 170 Steps Withdrawn

	H	G	F	E	D	C	B	A
8	.97 .97	.93 .97	1.12 1.12	1.12 1.15	1.23 1.22	1.10 1.12	1.07 1.07	.74 .74
9		1.08 1.06	1.01 1.03	1.20 1.18	1.13 1.16	1.19 1.17	1.02 1.05	.81 .80
10			1.17 1.15	1.11 1.14	1.19 1.17	1.07 1.10	1.04 1.01	.67 .68
11				1.18 1.17	1.02 1.04	1.11 1.09	1.01 .99	.57 .57
12					1.17 1.15	.92 .91	.85 .85	
13						1.03 .98	.49 .48	Calculated Measured

FIGURE 11-8

McGuire-1 Cy-1 Assembly Radial Powers Calculated vs Measured

7.70 EFPD 48%FP Control Bank D at 200 Steps Withdrawn

	H	G	F	E	D	C	B	A
8	1.05 1.05	.97 1.00	1.14 1.14	1.12 1.15	1.22 1.22	1.09 1.10	1.05 1.03	.72 .72
9		1.10 1.09	1.02 1.05	1.21 1.19	1.13 1.15	1.18 1.15	1.00 1.02	.79 .78
10			1.18 1.15	1.12 1.14	1.19 1.17	1.06 1.09	1.03 1.00	.66 .67
11				1.19 1.17	1.04 1.05	1.11 1.10	1.00 .99	.56 .57
12					1.23 1.22	.93 .93	.84 .85	
13						1.02 1.00	.48 .48	Calculated Measured

FIGURE 11-9

McGuire-1 Cy-1 Assembly Radial Powers Calculated vs Measured

11.42 EFPD 48%FP Control Bank D at 164 Steps Withdrawn

	H	G	F	E	D	C	B	A
	.99	.97	1.15	1.14	1.24	1.11	1.07	.73
8	.99	1.00	1.15	1.18	1.24	1.13	1.05	.73
		1.11	1.04	1.22	1.15	1.19	1.02	.80
9		1.09	1.07	1.21	1.18	1.17	1.04	.79
			1.19	1.13	1.20	1.07	1.03	.66
10			1.18	1.17	1.19	1.10	1.00	.67
				1.18	1.02	1.10	.99	.56
11				1.18	1.04	1.07	.98	.56
					1.13	.90	.83	
12					1.12	.88	.82	
						.99	.47	Calculated
13						.94	.46	Measured

FIGURE 11-10

McGuire-1 Cy-1 Assembly Radial Powers Calculated vs Measured

37.10 EFPD 50%FP Control Bank D at 186 Steps Withdrawn

	H	G	F	E	D	C	B	A
	1.07	1.03	1.17	1.16	1.23	1.10	1.04	.71
8	1.10	1.07	1.18	1.18	1.23	1.10	1.03	.70
		1.14	1.08	1.22	1.15	1.17	1.00	.77
9		1.15	1.11	1.21	1.17	1.14	1.01	.76
			1.20	1.15	1.19	1.07	1.01	.64
10			1.21	1.19	1.18	1.09	.98	.65
				1.19	1.05	1.09	.98	.54
11				1.20	1.05	1.06	.97	.55
					1.17	.92	.81	
12					1.15	.90	.81	
						.98	.47	Calculated
13						.94	.46	Measured

FIGURE 11-11

McGuire-1 Cy-1 Assembly Radial Powers Calculated vs Measured

41.59 EFPD 50%FP Control Bank D at 201 Steps Withdrawn

	H	G	F	E	D	C	B	A
	1.10	1.04	1.18	1.16	1.22	1.10	1.03	.70
8	1.10	1.08	1.18	1.21	1.22	1.11	1.01	.70
		1.15	1.08	1.22	1.15	1.14	1.00	.76
9		1.15	1.12	1.21	1.18	1.14	1.01	.75
			1.20	1.15	1.19	1.07	1.00	.64
10			1.19	1.19	1.18	1.09	.96	.64
				1.19	1.06	1.09	.97	.54
11				1.19	1.08	1.07	.96	.54
					1.20	.93	.81	
12					1.18	.91	.80	
						.98	.47	Calculated
13						.94	.46	Measured

FIGURE 11-12

McGuire-1 Cy-1 Assembly Radial Powers Calculated vs Measured

48.75 EFPD 50%FP Control Bank D at 201 Steps Withdrawn

	H	G	F	E	D	C	B	A
	1.11	1.05	1.18	1.17	1.22	1.10	1.03	.70
8	1.11	1.09	1.19	1.21	1.22	1.12	1.01	.70
		1.15	1.09	1.22	1.15	1.16	1.00	.76
9		1.15	1.12	1.21	1.19	1.14	1.01	.75
			1.20	1.16	1.19	1.07	1.00	.64
10			1.19	1.19	1.18	1.09	.96	.64
				1.19	1.07	1.09	.97	.54
11				1.19	1.08	1.07	.95	.54
					1.20	.93	.81	
12					1.18	.91	.80	
						.98	.47	Calculated
13						.94	.46	Measured

FIGURE 11-13

McGuire-1 Cy-1 Assembly Radial Powers Calculated vs Measured

59.37 EFPD 50%FP Control Bank D at 201 Steps Withdrawn

	H	G	F	E	D	C	B	A
8	1.12 1.12	1.07 1.10	1.18 1.19	1.17 1.21	1.22 1.22	1.10 1.12	1.02 1.01	.69 .70
9		1.16 1.16	1.10 1.13	1.22 1.21	1.16 1.18	1.15 1.14	1.00 1.01	.75 .75
10			1.20 1.19	1.16 1.19	1.19 1.17	1.07 1.09	.99 .96	.63 .64
11				1.19 1.18	1.07 1.07	1.08 1.06	.97 .95	.54 .54
12					1.19 1.17	.93 .92	.80 .80	
13						.97 .95	.46 .46	Calculated Measured

FIGURE 11-14

McGuire-1 Cy-1 Assembly Radial Powers Calculated vs Measured

75.38 EFPD 50%FP Control Bank D at 198 Steps Withdrawn

	H	G	F	E	D	C	B	A
8	1.12 1.12	1.09 1.11	1.19 1.18	1.18 1.21	1.21 1.20	1.11 1.13	1.02 1.00	.69 .69
9		1.17 1.15	1.12 1.14	1.22 1.20	1.16 1.19	1.15 1.13	1.00 1.02	.75 .74
10			1.21 1.19	1.17 1.20	1.18 1.17	1.07 1.10	.98 .96	.63 .64
11				1.19 1.18	1.08 1.09	1.08 1.06	.96 .95	.53 .54
12					1.18 1.16	.93 .92	.80 .80	
13						.96 .94	.46 .46	Calculated Measured

FIGURE 11-15

McGuire-1 Cy-1 Assembly Radial Powers Calculated vs Measured

80.46 EFPD 75%FP Control Bank D at 213 Steps Withdrawn

	H	G	F	E	D	C	B	A	
	1.17	1.11	1.20	1.19	1.21	1.10	1.01	.68	
8	1.16	1.14	1.20	1.22	1.20	1.11	1.00	.70	
		1.18	1.13	1.22	1.17	1.14	.99	.74	
9		1.17	1.15	1.21	1.19	1.12	1.01	.74	
			1.21	1.18	1.18	1.07	.98	.63	
10			1.19	1.19	1.17	1.09	.95	.64	
				1.19	1.09	1.07	.95	.53	
11				1.18	1.09	1.05	.95	.53	
					1.19	.93	.79		
12					1.17	.92	.80		
						.95	.46		Calculated
13						.94	.46		Measured

FIGURE 11-16

McGuire-1 Cy-1 Assembly Radial Powers Calculated vs Measured

91.54 EFPD 75%FP Control Bank D at 213 Steps Withdrawn

	H	G	F	E	D	C	B	A	
	1.17	1.12	1.20	1.19	1.20	1.11	1.00	.68	
8	1.15	1.15	1.20	1.22	1.19	1.11	.99	.70	
		1.19	1.14	1.22	1.17	1.14	.99	.73	
	9	1.17	1.16	1.20	1.19	1.11	1.01	.73	
			1.21	1.18	1.18	1.08	.97	.63	
		10	1.19	1.21	1.16	1.10	.94	.63	
				1.19	1.09	1.07	.95	.53	
			11	1.18	1.11	1.05	.95	.53	
					1.18	.94	.79		
				12	1.17	.93	.79		
						.94	.46		Calculated
					13	.93	.46		Measured

FIGURE 11-17

McGuire-1 Cy-1 Assembly Radial Powers Calculated vs Measured

104.47 EFPD 50%FP Control Bank D at 215 Steps Withdrawn

	H	G	F	E	D	C	B	A
	1.16	1.12	1.19	1.18	1.19	1.10	1.00	.68
8	1.15	1.14	1.19	1.22	1.19	1.12	.99	.69
		1.17	1.13	1.20	1.16	1.13	1.00	.74
9		1.17	1.15	1.19	1.19	1.11	1.02	.73
			1.20	1.18	1.17	1.08	.97	.63
10			1.18	1.19	1.16	1.10	.95	.64
				1.18	1.10	1.07	.96	.53
11				1.16	1.10	1.06	.95	.53
					1.20	.95	.80	
12					1.18	.94	.80	
						.96	.46	Calculated
13						.94	.46	Measured

FIGURE 11-18

McGuire-1 Cy-1 Assembly Radial Powers Calculated vs Measured

112.05 EFPD 50%FP Control Bank D at 215 Steps Withdrawn

	H	G	F	E	D	C	B	A
	1.16	1.12	1.19	1.18	1.19	1.10	1.00	.68
8	1.14	1.14	1.18	1.21	1.19	1.12	.99	.70
		1.17	1.14	1.20	1.16	1.13	1.00	.74
9		1.16	1.15	1.19	1.19	1.11	1.01	.74
			1.19	1.18	1.17	1.08	.97	.63
10			1.18	1.20	1.15	1.10	.95	.64
				1.18	1.10	1.07	.97	.53
11				1.17	1.10	1.06	.95	.53
					1.20	.96	.80	
12					1.18	.94	.80	
						.96	.46	Calculated
13						.95	.47	Measured

FIGURE 11-19

McGuire-1 Cy-1 Assembly Radial Powers Calculated vs Measured

115.69 EFPD 75%FP Control Bank D at 217 Steps Withdrawn

	H	G	F	E	D	C	B	A	
	1.18	1.14	1.20	1.19	1.19	1.11	1.00	.68	
8	1.16	1.16	1.20	1.22	1.19	1.12	.99	.69	
		1.19	1.15	1.21	1.17	1.13	1.00	.73	
9		1.18	1.16	1.19	1.19	1.11	1.01	.73	
			1.20	1.18	1.17	1.08	.97	.63	
10			1.19	1.20	1.15	1.10	.95	.64	
				1.18	1.10	1.07	.95	.53	
11				1.17	1.10	1.05	.95	.53	
					1.18	.95	.79		
12					1.17	.94	.80		
						.94	.46		Calculated
13						.94	.46		Measured

FIGURE 11-20

McGuire-1 Cy-1 Assembly Radial Powers Calculated vs Measured

118.71 EFPD 50%FP Control Bank D at 180 Steps Withdrawn

	H	G	F	E	D	C	B	A
8	1.09 1.08	1.11 1.13	1.19 1.18	1.20 1.23	1.20 1.19	1.12 1.14	1.02 1.01	.70 .72
9		1.17 1.15	1.15 1.16	1.21 1.19	1.17 1.20	1.14 1.12	1.02 1.04	.75 .75
10			1.20 1.18	1.18 1.20	1.17 1.15	1.09 1.11	.98 .96	.63 .65
11				1.17 1.16	1.08 1.09	1.06 1.04	.96 .96	.53 .54
12					1.12 1.10	.93 .92	.79 .79	
13						.94 .92	.46 .46	Calculated Measured

FIGURE 11-21

McGuire-1 Cy-1 Assembly Radial Powers Calculated vs Measured

122.15 EFPD 75%FP Control Bank D at 215 Steps Withdrawn

	H	G	F	E	D	C	B	A
8	1.17 1.15	1.14 1.16	1.20 1.19	1.19 1.22	1.19 1.18	1.11 1.12	1.00 .99	.68 .70
9		1.19 1.17	1.15 1.17	1.20 1.18	1.17 1.19	1.13 1.10	1.00 1.02	.73 .73
10			1.20 1.18	1.18 1.21	1.17 1.15	1.08 1.10	.97 .94	.63 .64
11				1.18 1.17	1.10 1.11	1.07 1.05	.96 .95	.53 .53
12					1.18 1.17	.95 .94	.79 .79	
13						.94 .93	.46 .47	Calculated Measured

FIGURE 11-22

McGuire-1 Cy-1 Assembly Radial Powers Calculated vs Measured

130.59 EFPD 75%FP Control Bank D at 215 Steps Withdrawn

	H	G	F	E	D	C	B	A
	1.17	1.15	1.19	1.19	1.18	1.11	1.00	.68
8	1.16	1.16	1.18	1.22	1.17	1.13	.99	.70
		1.19	1.15	1.20	1.17	1.12	1.00	.73
9		1.17	1.17	1.18	1.18	1.10	1.01	.73
			1.20	1.18	1.16	1.08	.97	.63
10			1.18	1.20	1.14	1.10	.94	.64
				1.17	1.11	1.07	.96	.53
11				1.17	1.11	1.05	.95	.53
					1.18	.96	.79	
12					1.17	.95	.80	
						.94	.46	Calculated
13						.94	.47	Measured

FIGURE 11-23

McGuire-1 Cy-1 Assembly Radial Powers Calculated vs Measured

135.44 EFPD 75%FP Control Bank D at 215 Steps Withdrawn

	H	G	F	E	D	C	B	A
8	1.17 1.16	1.15 1.17	1.19 1.19	1.19 1.22	1.18 1.17	1.11 1.12	1.00 .99	.68 .70
9		1.18 1.17	1.16 1.17	1.20 1.18	1.17 1.19	1.12 1.10	1.00 1.02	.73 .73
10			1.19 1.18	1.18 1.20	1.16 1.15	1.08 1.10	.97 .94	.63 .64
11				1.17 1.16	1.11 1.11	1.07 1.05	.96 .95	.53 .53
12					1.18 1.17	.96 .95	.79 .80	
13						.95 .94	.46 .47	Calculated Measured

FIGURE 11-24

McGuire-1 Cy-1 Assembly Radial Powers Calculated vs Measured

139.82 EFPD 50%FP Control Bank D at 180 Steps Withdrawn

	H	G	F	E	D	C	B	A
8	1.09 1.08	1.12 1.14	1.18 1.18	1.19 1.23	1.19 1.19	1.12 1.14	1.01 1.01	.70 .71
9		1.17 1.15	1.15 1.17	1.20 1.19	1.17 1.20	1.13 1.12	1.03 1.04	.75 .75
10			1.19 1.18	1.18 1.20	1.16 1.14	1.09 1.11	.98 .96	.64 .65
11				1.16 1.15	1.09 1.09	1.06 1.04	.97 .95	.54 .54
12					1.11 1.11	.94 .93	.79 .79	
13						.94 .92	.46 .46	Calculated Measured

FIGURE 11-25

McGuire-1 Cy-1 Assembly Radial Powers Calculated vs Measured

141.52 EFPD 50%FP Control Bank D at 215 Steps Withdrawn

	H	G	F	E	D	C	B	A
	1.16	1.13	1.18	1.18	1.17	1.11	1.00	.69
8	1.15	1.16	1.18	1.21	1.17	1.12	.99	.70
		1.17	1.14	1.19	1.16	1.12	1.01	.74
9		1.16	1.16	1.17	1.18	1.10	1.02	.74
			1.18	1.18	1.16	1.08	.97	.63
10			1.17	1.20	1.14	1.10	.95	.64
				1.17	1.11	1.07	.97	.53
11				1.16	1.11	1.06	.96	.53
					1.19	.97	.80	
12					1.17	.96	.81	
						.96	.47	Calculated
13						.95	.47	Measured

FIGURE 11-26

McGuire-1 Cy-1 Assembly Radial Powers Calculated vs Measured

146.01 EFPD 75%FP Control Bank D at 215 Steps Withdrawn

	H	G	F	E	D	C	B	A
	1.17	1.15	1.19	1.19	1.17	1.11	1.00	.68
8	1.16	1.18	1.18	1.22	1.17	1.12	.98	.70
		1.18	1.16	1.19	1.16	1.12	1.01	.74
9		1.17	1.18	1.18	1.19	1.09	1.02	.73
			1.19	1.18	1.16	1.09	.97	.63
10			1.17	1.21	1.14	1.10	.94	.64
				1.17	1.11	1.07	.96	.53
11				1.16	1.12	1.04	.95	.53
					1.18	.96	.79	
12					1.16	.95	.79	
						.95	.46	Calculated
13						.93	.47	Measured

FIGURE 11-27

McGuire-1 Cy-1 Assembly Radial Powers Calculated vs Measured

150.19 EFPD 50%FP Control Bank D at 215 Steps Withdrawn

	H	G	F	E	D	C	B	A
	1.16	1.14	1.17	1.18	1.17	1.11	1.00	.69
8	1.14	1.16	1.17	1.21	1.16	1.12	.99	.71
		1.17	1.15	1.18	1.16	1.12	1.01	.74
9		1.15	1.16	1.16	1.19	1.10	1.03	.74
			1.18	1.17	1.15	1.09	.97	.63
10			1.16	1.20	1.14	1.11	.95	.65
				1.16	1.11	1.07	.97	.54
11				1.16	1.12	1.05	.96	.54
					1.19	.98	.80	
12					1.17	.97	.80	
						.97	.47	Calculated
13						.95	.48	Measured

FIGURE 11-28

McGuire-1 Cy-1 Assembly Radial Powers Calculated vs Measured

162.76 EFPD 50%FP Control Bank D at 215 Steps Withdrawn

	H	G	F	E	D	C	B	A
	1.15	1.14	1.17	1.18	1.16	1.11	1.00	.69
8	1.14	1.17	1.17	1.21	1.16	1.13	.99	.70
		1.16	1.15	1.17	1.16	1.11	1.02	.74
9		1.15	1.17	1.16	1.18	1.09	1.02	.74
			1.17	1.17	1.15	1.09	.97	.64
10			1.16	1.20	1.13	1.11	.94	.65
				1.16	1.12	1.07	.97	.54
11				1.15	1.12	1.05	.96	.54
					1.19	.98	.80	
12					1.17	.97	.80	
						.97	.47	Calculated
13						.95	.48	Measured

FIGURE 11-29

McGuire-1 Cy-1 Assembly Radial Powers Calculated vs Measured

173.34 EFPD 50%FP Control Bank D at 215 Steps Withdrawn

	H	G	F	E	D	C	B	A	
	1.15	1.14	1.16	1.17	1.15	1.11	1.00	.69	
8	1.13	1.17	1.16	1.21	1.14	1.13	.99	.71	
		1.16	1.15	1.17	1.16	1.11	1.02	.74	
9		1.14	1.17	1.15	1.18	1.09	1.03	.74	
			1.17	1.17	1.14	1.09	.97	.64	
10			1.15	1.19	1.12	1.11	.94	.65	
				1.15	1.12	1.07	.98	.54	
11				1.14	1.12	1.05	.96	.54	
					1.18	.99	.81		
12					1.16	.98	.81		
						.97	.47		Calculated
13						.95	.49		Measured

FIGURE 11-30

McGuire-1 Cy-1 Assembly Radial Powers Calculated vs Measured

185.58 EFPD 50%FP Control Bank D at 215 Steps Withdrawn

	H	G	F	E	D	C	B	A
	1.15	1.14	1.16	1.17	1.15	1.11	1.00	.70
8	1.13	1.16	1.15	1.20	1.14	1.12	.99	.72
		1.16	1.15	1.16	1.15	1.11	1.03	.75
9		1.14	1.16	1.14	1.18	1.09	1.04	.74
			1.16	1.17	1.14	1.09	.97	.64
10			1.14	1.19	1.12	1.11	.95	.66
				1.15	1.12	1.07	.98	.54
11				1.14	1.13	1.06	.97	.54
					1.18	.99	.81	
12					1.17	.99	.81	
						.97	.48	Calculated
13						.96	.49	Measured

FIGURE 11-31

McGuire-1 Cy-1 Assembly Peak Axial Powers Calculated vs Measured

1.28 EFPD 30%FP Control Bank D at 213 Steps Withdrawn

	H	G	F	E	D	C	B	A
	1.41	1.27	1.50	1.48	1.63	1.46	1.43	.99
8	1.40	1.32	1.50	1.52	1.62	1.47	1.42	1.00
		1.45	1.34	1.60	1.50	1.59	1.36	1.09
9		1.43	1.38	1.57	1.54	1.55	1.40	1.08
			1.56	1.49	1.61	1.43	1.41	.91
10			1.55	1.54	1.59	1.49	1.37	.92
				1.60	1.42	1.52	1.38	.77
11				1.60	1.45	1.52	1.37	.78
					1.74	1.29	1.18	
12					1.71	1.29	1.18	
						1.45	.68	Calculated
13						1.39	.67	Measured

FIGURE 11-32

McGuire-1 Cy-1 Assembly Peak Axial Powers Calculated vs Measured

5.27 EFPD 30%FP Control Bank D at 170 Steps Withdrawn

	H	G	F	E	D	C	B	A
8	1.50 1.48	1.33 1.40	1.56 1.58	1.53 1.61	1.68 1.71	1.50 1.55	1.47 1.47	1.01 1.03
9		1.50 1.51	1.39 1.45	1.65 1.65	1.55 1.62	1.63 1.62	1.40 1.45	1.11 1.12
10			1.61 1.62	1.54 1.61	1.65 1.66	1.47 1.54	1.44 1.42	.93 .95
11				1.65 1.67	1.46 1.50	1.56 1.57	1.41 1.40	.79 .80
12					1.81 1.76	1.33 1.33	1.20 1.21	
13						1.47 1.43	.69 .69	Calculated Measured

FIGURE 11-33

McGuire-1 Cy-1 Assembly Peak Axial Powers Calculated vs Measured

7.70 EFPD 48%FP Control Bank D at 200 Steps Withdrawn

	H	G	F	E	D	C	B	A	
	1.46	1.33	1.54	1.52	1.65	1.47	1.42	.97	
8	1.47	1.38	1.56	1.58	1.66	1.50	1.40	.99	
		1.49	1.38	1.63	1.52	1.58	1.35	1.06	
9		1.50	1.43	1.62	1.58	1.57	1.39	1.07	
			1.59	1.52	1.62	1.43	1.39	.89	
10			1.58	1.57	1.61	1.49	1.36	.91	
				1.61	1.42	1.51	1.35	.76	
11				1.62	1.45	1.51	1.35	.77	
					1.71	1.27	1.14		
12					1.71	1.28	1.16		
						1.39	.66		Calculated
13						1.37	.66		Measured

FIGURE 11-34

McGuire-1 Cy-1 Assembly Peak Axial Powers Calculated vs Measured

11.42 EFPD 48%FP Control Bank D at 164 Steps Withdrawn

	H	G	F	E	D	C	B	A
	1.54	1.38	1.59	1.57	1.70	1.51	1.45	.99
8	1.54	1.46	1.64	1.66	1.73	1.57	1.46	1.01
		1.55	1.43	1.67	1.57	1.63	1.38	1.09
9		1.57	1.51	1.70	1.65	1.63	1.45	1.10
			1.64	1.56	1.66	1.47	1.42	.91
10			1.67	1.65	1.68	1.55	1.41	.94
				1.66	1.47	1.54	1.38	.77
11				1.69	1.52	1.56	1.39	.80
					1.76	1.30	1.16	
12					1.75	1.32	1.19	
						1.41	.67	Calculated
13						1.40	.67	Measured

FIGURE 11-35

McGuire-1 Cy-1 Assembly Peak Axial Powers Calculated vs Measured

37.10 EFPD 50%FP Control Bank D at 186 Steps Withdrawn

	H	G	F	E	D	C	B	A	
	1.52	1.40	1.57	1.55	1.63	1.46	1.37	.93	
8	1.58	1.50	1.64	1.62	1.67	1.50	1.40	.95	
		1.53	1.44	1.62	1.53	1.54	1.33	1.01	
9		1.61	1.53	1.66	1.60	1.56	1.38	1.03	
			1.60	1.54	1.59	1.43	1.33	.85	
10			1.67	1.64	1.63	1.50	1.34	.89	
				1.59	1.43	1.46	1.30	.72	
11				1.66	1.48	1.48	1.33	.75	
					1.65	1.25	1.09		
12					1.66	1.26	1.13		
						1.32	.63		Calculated
13						1.32	.64		Measured

FIGURE 11-36

McGuire-1 Cy-1 Assembly Peak Axial Powers Calculated vs Measured

41.59 EFPD 50%FP Control Bank D at 201 Steps Withdrawn

	H	G	F	E	D	C	B	A
8	1.50 1.55	1.39 1.49	1.55 1.61	1.53 1.64	1.60 1.65	1.44 1.51	1.35 1.37	.92 .95
9		1.52 1.57	1.43 1.52	1.60 1.64	1.52 1.60	1.52 1.53	1.31 1.37	1.00 1.01
10			1.58 1.62	1.52 1.61	1.57 1.60	1.41 1.48	1.31 1.30	.84 .86
11				1.57 1.62	1.42 1.48	1.44 1.45	1.28 1.29	.71 .73
12					1.62 1.64	1.24 1.25	1.07 1.09	
13						1.30 1.29	.62 .62	Calculated Measured

FIGURE 11-37

McGuire-1 Cy-1 Assembly Peak Axial Powers Calculated vs Measured

48.75 EFPD 50%FP Control Bank D at 201 Steps Withdrawn

	H	G	F	E	D	C	B	A
	1.50	1.40	1.54	1.53	1.58	1.44	1.33	.91
8	1.56	1.50	1.62	1.64	1.64	1.51	1.36	.94
		1.51	1.43	1.59	1.51	1.50	1.30	.99
9		1.57	1.52	1.64	1.60	1.53	1.36	1.01
			1.57	1.52	1.55	1.40	1.29	.83
10			1.62	1.61	1.59	1.47	1.30	.86
				1.56	1.41	1.42	1.27	.70
11				1.61	1.47	1.44	1.28	.72
					1.60	1.23	1.06	
12					1.63	1.25	1.09	
						1.28	.61	Calculated
13						1.29	.62	Measured

FIGURE 11-38

McGuire-1 Cy-1 Assembly Peak Axial Powers Calculated vs Measured

59.37 EFPD 50%FP Control Bank D at 201 Steps Withdrawn

	H	G	F	E	D	C	B	A	
	1.49	1.41	1.53	1.52	1.56	1.43	1.31	.89	
8	1.54	1.47	1.59	1.60	1.61	1.48	1.33	.92	
		1.51	1.44	1.57	1.50	1.48	1.29	.97	
9		1.55	1.50	1.60	1.56	1.50	1.33	.99	
			1.55	1.51	1.53	1.39	1.27	.82	
10			1.58	1.57	1.55	1.44	1.27	.84	
				1.54	1.41	1.40	1.25	.69	
11				1.57	1.43	1.41	1.26	.71	
					1.58	1.22	1.04		
12					1.60	1.23	1.07		
						1.26	.60		Calculated
13						1.27	.61		Measured

FIGURE 11-39

McGuire-1 Cy-1 Assembly Peak Axial Powers Calculated vs Measured

75.38 EFPD 50%FP Control Bank D at 198 Steps Withdrawn

	H	G	F	E	D	C	B	A	
	1.48	1.41	1.51	1.51	1.53	1.41	1.28	.87	
8	1.51	1.46	1.54	1.57	1.55	1.46	1.29	.90	
		1.49	1.43	1.54	1.48	1.45	1.27	.95	
	9	1.51	1.48	1.56	1.53	1.46	1.31	.96	
			1.53	1.50	1.50	1.37	1.24	.80	
		10	1.54	1.55	1.51	1.42	1.24	.83	
				1.51	1.40	1.37	1.23	.68	
			11	1.53	1.42	1.38	1.24	.69	
					1.54	1.21	1.02		
				12	1.56	1.22	1.05		
						1.23	.59		Calculated
					13	1.24	.61		Measured

FIGURE 11-40

McGuire-1 Cy-1 Assembly Peak Axial Powers Calculated vs Measured

80.46 EFPD 75%FP Control Bank D at 213 Steps Withdrawn

	H	G	F	E	D	C	B	A
	1.49	1.42	1.51	1.50	1.51	1.39	1.26	.86
8	1.54	1.48	1.55	1.57	1.54	1.44	1.29	.90
		1.49	1.43	1.52	1.47	1.43	1.25	.93
9		1.53	1.48	1.56	1.53	1.45	1.30	.96
			1.52	1.48	1.48	1.36	1.22	.79
10			1.53	1.53	1.50	1.41	1.23	.82
				1.49	1.38	1.35	1.21	.67
11				1.51	1.40	1.36	1.22	.68
					1.52	1.19	1.00	
12					1.53	1.20	1.04	
						1.20	.58	Calculated
13						1.22	.60	Measured

FIGURE 11-41

McGuire-1 Cy-1 Assembly Peak Axial Powers Calculated vs Measured

91.54 EFPD 75%FP Control Bank D at 213 Steps Withdrawn

	H	G	F	E	D	C	B	A	
	1.47	1.41	1.49	1.48	1.48	1.38	1.25	.85	
8	1.50	1.47	1.52	1.56	1.50	1.41	1.26	.89	
		1.47	1.43	1.50	1.45	1.41	1.24	.92	
9		1.50	1.48	1.52	1.51	1.41	1.28	.93	
			1.50	1.47	1.46	1.34	1.21	.78	
10			1.51	1.53	1.47	1.39	1.20	.80	
				1.47	1.37	1.33	1.19	.66	
11				1.49	1.40	1.33	1.20	.67	
					1.50	1.19	.99		
12					1.50	1.19	1.01		
						1.19	.57		Calculated
13						1.19	.59		Measured

FIGURE 11-42

McGuire-1 Cy-1 Assembly Peak Axial Powers Calculated vs Measured

104.47 EFPD 50%FP Control Bank D at 215 Steps Withdrawn

	H	G	F	E	D	C	B	A
	1.43	1.38	1.44	1.45	1.44	1.35	1.22	.84
8	1.47	1.44	1.49	1.53	1.48	1.40	1.24	.86
		1.43	1.39	1.45	1.42	1.37	1.23	.90
	9	1.46	1.45	1.49	1.48	1.39	1.27	.92
			1.45	1.44	1.41	1.32	1.18	.77
		10	1.46	1.48	1.44	1.38	1.19	.79
				1.43	1.36	1.31	1.18	.65
			11	1.44	1.38	1.33	1.19	.66
					1.47	1.18	.98	
				12	1.49	1.18	1.00	
						1.18	.57	Calculated
					13	1.18	.58	Measured

FIGURE 11-43

McGuire-1 Cy-1 Assembly Peak Axial Powers Calculated vs Measured

112.05 EFPD 50%FP Control Bank D at 215 Steps Withdrawn

	H	G	F	E	D	C	B	A
	1.41	1.38	1.43	1.43	1.42	1.34	1.20	.83
8	1.44	1.42	1.47	1.51	1.46	1.39	1.23	.86
		1.42	1.39	1.43	1.41	1.35	1.22	.90
9		1.44	1.43	1.47	1.47	1.37	1.26	.91
			1.43	1.42	1.40	1.31	1.17	.77
10			1.46	1.48	1.43	1.36	1.18	.79
				1.41	1.35	1.29	1.18	.65
11				1.45	1.37	1.32	1.19	.66
					1.46	1.18	.97	
12					1.48	1.18	1.00	
						1.17	.57	Calculated
13						1.19	.59	Measured

FIGURE 11-44

McGuire-1 Cy-1 Assembly Peak Axial Powers Calculated vs Measured

115.69 EFPD 75%FP Control Bank D at 217 Steps Withdrawn

	H	G	F	E	D	C	B	A
	1.45	1.40	1.45	1.45	1.44	1.35	1.21	.83
8	1.47	1.44	1.48	1.50	1.46	1.38	1.22	.86
		1.44	1.41	1.46	1.42	1.37	1.23	.90
9		1.46	1.44	1.47	1.46	1.37	1.25	.90
			1.45	1.44	1.42	1.32	1.18	.77
10			1.46	1.47	1.42	1.35	1.17	.78
				1.43	1.36	1.30	1.17	.65
11				1.43	1.35	1.30	1.17	.65
					1.46	1.18	.97	
12					1.47	1.17	.99	
						1.16	.56	Calculated
13						1.17	.58	Measured

FIGURE 11-45

McGuire-1 Cy-1 Assembly Peak Axial Powers Calculated vs Measured

118.71 EFPD 50%FP Control Bank D at 180 Steps Withdrawn

	H	G	F	E	D	C	B	A	
	1.46	1.41	1.46	1.46	1.45	1.37	1.23	.85	
8	1.48	1.47	1.50	1.54	1.48	1.43	1.26	.89	
		1.45	1.42	1.47	1.44	1.38	1.25	.92	
	9	1.47	1.47	1.49	1.50	1.40	1.30	.94	
			1.46	1.45	1.43	1.34	1.20	.78	
		10	1.48	1.52	1.45	1.40	1.20	.82	
				1.44	1.37	1.32	1.20	.66	
			11	1.47	1.41	1.34	1.21	.68	
					1.49	1.20	.99		
				12	1.51	1.22	1.02		
						1.20	.58		Calculated
					13	1.21	.60		Measured

FIGURE 11-46

McGuire-1 Cy-1 Assembly Peak Axial Powers Calculated vs Measured

122.15 EFPD 75%FP Control Bank D at 215 Steps Withdrawn

	H	G	F	E	D	C	B	A
	1.44	1.40	1.44	1.44	1.42	1.34	1.21	.83
8	1.45	1.44	1.46	1.49	1.43	1.38	1.21	.86
		1.43	1.40	1.44	1.41	1.36	1.22	.89
9		1.44	1.44	1.45	1.45	1.35	1.24	.90
			1.44	1.43	1.40	1.32	1.17	.76
10			1.44	1.47	1.40	1.35	1.15	.78
				1.42	1.35	1.29	1.17	.65
11				1.42	1.36	1.28	1.16	.65
					1.45	1.18	.96	
12					1.45	1.17	.98	
						1.16	.56	Calculated
13						1.15	.58	Measured

FIGURE 11-47

McGuire-1 Cy-1 Assembly Peak Axial Powers Calculated vs Measured

130.59 EFPD 75%FP Control Bank D at 215 Steps Withdrawn

	H	G	F	E	D	C	B	A	
	1.43	1.39	1.43	1.43	1.41	1.34	1.20	.83	
8	1.45	1.43	1.44	1.49	1.42	1.38	1.22	.86	
		1.42	1.39	1.43	1.40	1.34	1.22	.89	
9		1.44	1.44	1.45	1.43	1.34	1.25	.90	
			1.43	1.42	1.39	1.31	1.16	.76	
10			1.45	1.47	1.39	1.35	1.16	.79	
				1.41	1.35	1.29	1.16	.64	
11				1.42	1.36	1.29	1.17	.66	
					1.44	1.17	.96		
12					1.46	1.18	.99		
						1.15	.56		Calculated
13						1.17	.58		Measured

FIGURE 11-48

McGuire-1 Cy-1 Assembly Peak Axial Powers Calculated vs Measured

135.44 EFPD 75%FP Control Bank D at 215 Steps Withdrawn

	H	G	F	E	D	C	B	A
8	1.42 1.44	1.39 1.43	1.42 1.45	1.42 1.48	1.40 1.41	1.33 1.36	1.19 1.20	.82 .85
9		1.41 1.43	1.39 1.42	1.42 1.43	1.40 1.43	1.34 1.34	1.22 1.23	.89 .89
10			1.42 1.42	1.42 1.45	1.38 1.38	1.31 1.33	1.16 1.14	.76 .77
11				1.40 1.40	1.34 1.34	1.28 1.27	1.16 1.15	.64 .64
12					1.44 1.43	1.17 1.16	.96 .97	
13						1.15 1.15	.56 .57	Calculated Measured

FIGURE 11-49

McGuire-1 Cy-1 Assembly Peak Axial Powers Calculated vs Measured

139.82 EFPD 50%FP Control Bank D at 180 Steps Withdrawn

	H	G	F	E	D	C	B	A	
	1.42	1.38	1.42	1.43	1.40	1.34	1.21	.84	
8	1.48	1.46	1.48	1.51	1.45	1.41	1.24	.88	
		1.41	1.39	1.42	1.41	1.35	1.24	.91	
9		1.47	1.46	1.47	1.47	1.38	1.28	.92	
			1.42	1.42	1.39	1.32	1.17	.77	
10			1.47	1.49	1.43	1.38	1.19	.80	
				1.40	1.35	1.29	1.19	.65	
11				1.44	1.41	1.32	1.20	.67	
					1.45	1.19	.98		
12					1.50	1.21	1.01		
						1.18	.57		Calculated
13						1.20	.60		Measured

FIGURE 11-50

McGuire-1 Cy-1 Assembly Peak Axial Powers Calculated vs Measured

141.52 EFPD 50%FP Control Bank D at 215 Steps Withdrawn

	H	G	F	E	D	C	B	A
	1.37	1.35	1.37	1.38	1.36	1.30	1.16	.81
8	1.43	1.42	1.44	1.48	1.42	1.37	1.20	.85
		1.37	1.35	1.38	1.36	1.30	1.20	.87
	9	1.42	1.42	1.44	1.44	1.34	1.24	.90
			1.38	1.38	1.35	1.28	1.13	.75
		10	1.43	1.46	1.39	1.34	1.16	.78
				1.36	1.32	1.25	1.14	.63
			11	1.41	1.35	1.29	1.17	.66
					1.41	1.16	.94	
				12	1.45	1.18	.99	
						1.14	.56	Calculated
					13	1.17	.59	Measured

FIGURE 11-51

McGuire-1 Cy-1 Assembly Peak Axial Powers Calculated vs Measured

146.01 EFPD 75%FP Control Bank D at 215 Steps Withdrawn

	H	G	F	E	D	C	B	A
8	1.41 1.43	1.38 1.44	1.40 1.43	1.41 1.47	1.38 1.40	1.32 1.36	1.19 1.19	.82 .85
9		1.40 1.42	1.38 1.43	1.40 1.42	1.39 1.43	1.32 1.32	1.21 1.23	.88 .89
10			1.40 1.41	1.40 1.45	1.37 1.37	1.30 1.33	1.15 1.14	.76 .78
11				1.38 1.39	1.34 1.35	1.27 1.26	1.16 1.15	.64 .64
12					1.43 1.42	1.17 1.16	.95 .97	
13						1.14 1.14	.56 .58	Calculated Measured

FIGURE 11-52

McGuire-1 Cy-1 Assembly Peak Axial Powers Calculated vs Measured

150.19 EFPD 50%FP Control Bank D at 215 Steps Withdrawn

	H	G	F	E	D	C	B	A	
	1.36	1.34	1.36	1.38	1.35	1.29	1.16	.81	
8	1.39	1.40	1.40	1.44	1.38	1.35	1.18	.84	
		1.36	1.34	1.36	1.35	1.29	1.19	.87	
9		1.38	1.39	1.39	1.41	1.30	1.22	.88	
			1.36	1.37	1.34	1.27	1.13	.74	
10			1.39	1.43	1.35	1.32	1.13	.77	
				1.35	1.31	1.24	1.14	.63	
11				1.37	1.34	1.25	1.15	.64	
					1.40	1.16	.94		
12					1.41	1.16	.97		
						1.13	.55		Calculated
13						1.14	.58		Measured

FIGURE 11-53

McGuire-1 Cy-1 Assembly Peak Axial Powers Calculated vs Measured

162.76 EFPD 50%FP Control Bank D at 215 Steps Withdrawn

	H	G	F	E	D	C	B	A	
	1.35	1.33	1.35	1.36	1.33	1.28	1.15	.80	
8	1.39	1.39	1.39	1.43	1.36	1.33	1.17	.83	
		1.34	1.33	1.35	1.34	1.28	1.18	.86	
9		1.37	1.38	1.38	1.39	1.29	1.21	.87	
			1.35	1.36	1.32	1.26	1.12	.74	
10			1.37	1.42	1.34	1.31	1.12	.77	
				1.34	1.30	1.23	1.13	.63	
11				1.36	1.32	1.24	1.14	.64	
					1.38	1.15	.93		
12					1.40	1.15	.96		
						1.12	.55		Calculated
13						1.14	.58		Measured

FIGURE 11-54

McGuire-1 Cy-1 Assembly Peak Axial Powers Calculated vs Measured

173.34 EFPD 50%FP Control Bank D at 215 Steps Withdrawn

	H	G	F	E	D	C	B	A
	1.35	1.33	1.33	1.35	1.32	1.28	1.14	.80
8	1.36	1.39	1.37	1.42	1.34	1.34	1.17	.84
		1.33	1.33	1.33	1.33	1.27	1.18	.86
9		1.35	1.38	1.36	1.39	1.28	1.22	.88
			1.34	1.35	1.31	1.26	1.11	.74
10			1.35	1.41	1.33	1.31	1.12	.77
				1.32	1.30	1.23	1.13	.62
11				1.34	1.33	1.24	1.14	.64
					1.38	1.15	.93	
12					1.39	1.17	.96	
						1.12	.55	Calculated
13						1.14	.58	Measured

FIGURE 11-55

McGuire-1 Cy-1 Assembly Peak Axial Powers Calculated vs Measured

185.58 EFPD 50%FP Control Bank D at 215 Steps Withdrawn

	H	G	F	E	D	C	B	A
	1.34	1.32	1.32	1.34	1.30	1.27	1.13	.80
8	1.35	1.37	1.35	1.40	1.33	1.32	1.16	.84
		1.32	1.32	1.32	1.32	1.26	1.18	.86
9		1.34	1.36	1.34	1.38	1.27	1.21	.87
			1.32	1.34	1.30	1.25	1.11	.74
10			1.34	1.39	1.31	1.30	1.11	.77
				1.31	1.30	1.22	1.13	.62
11				1.33	1.32	1.24	1.14	.64
					1.37	1.15	.93	
12					1.39	1.17	.96	
						1.12	.55	Calculated
13						1.13	.58	Measured

FIGURE 11-56

McGuire-1 Cy-1A Assembly Radial Powers Calculated vs Measured

198.66 EFPD 90%FP Control Bank D at 217 Steps Withdrawn

	H	G	F	E	D	C	B	A
8	1.12 1.08	1.20 1.22	1.11 1.08	1.16 1.18	1.07 1.05	1.13 1.18	1.00 .99	.76 .79
9	1.20 1.21	1.12 1.08	1.19 1.20	1.09 1.05	1.15 1.18	1.07 1.04	1.14 1.17	.76 .76
10	1.10 1.06	1.18 1.19	1.09 1.06	1.16 1.19	1.08 1.06	1.13 1.15	.96 .93	.70 .71
11	1.13 1.16	1.07 1.04	1.15 1.17	1.10 1.07	1.19 1.21	1.06 1.03	1.02 1.03	.54 .54
12	1.01 .99	1.11 1.13	1.06 1.04	1.18 1.20	1.18 1.16	1.12 1.13	.82 .83	
13	.96 .98	1.00 .98	1.09 1.13	1.04 1.02	1.11 1.11	1.01 1.01	.56 .57	
14	.92 .91	1.07 1.11	.93 .90	1.00 1.00	.81 .81	.56 .57		
15	.71 .73	.72 .72	.67 .69	.53 .52	Calculated Measured			

FIGURE 11-57

McGuire-1 Cy-1A Assembly Radial Powers Calculated vs Measured

217.53 EFPD 100%FP Control Bank D at 209 Steps Withdrawn

	H	G	F	E	D	C	B	A
8	1.10 1.06	1.19 1.21	1.10 1.08	1.15 1.18	1.07 1.05	1.13 1.17	1.00 .99	.76 .79
9	1.19 1.20	1.11 1.07	1.18 1.19	1.08 1.05	1.15 1.17	1.07 1.04	1.13 1.17	.76 .77
10	1.09 1.06	1.17 1.18	1.09 1.05	1.16 1.17	1.08 1.05	1.12 1.15	.96 .94	.71 .72
11	1.13 1.16	1.07 1.04	1.15 1.17	1.09 1.07	1.17 1.19	1.05 1.02	1.02 1.03	.55 .55
12	1.02 1.00	1.11 1.13	1.06 1.04	1.17 1.19	1.15 1.13	1.10 1.11	.82 .83	
13	.98 .99	1.01 .98	1.10 1.13	1.04 1.02	1.10 1.10	1.00 1.00	.57 .58	
14	.94 .93	1.09 1.12	.94 .92	1.01 1.02	.82 .82	.56 .57		
15	.73 .76	.74 .74	.69 .71	.54 .54	Calculated Measured			

FIGURE 11-58

McGuire-1 Cy-1A Assembly Radial Powers Calculated vs Measured
223.35 EFPD 100%FP Control Bank D at 211 Steps Withdrawn

	H	G	F	E	D	C	B	A
8	1.09 1.06	1.18 1.21	1.10 1.08	1.15 1.18	1.07 1.05	1.13 1.18	1.00 .99	.77 .79
9	1.18 1.20	1.11 1.07	1.17 1.19	1.08 1.05	1.14 1.17	1.07 1.05	1.13 1.17	.77 .77
10	1.09 1.07	1.17 1.19	1.09 1.05	1.15 1.17	1.08 1.05	1.12 1.14	.96 .93	.71 .72
11	1.13 1.17	1.07 1.04	1.14 1.17	1.09 1.07	1.17 1.19	1.05 1.02	1.02 1.02	.55 .55
12	1.02 1.01	1.11 1.13	1.06 1.04	1.17 1.19	1.16 1.14	1.10 1.11	.82 .82	
13	.99 .99	1.02 .99	1.10 1.13	1.04 1.01	1.10 1.10	1.00 .99	.57 .58	
14	.95 .93	1.09 1.12	.95 .92	1.01 1.02	.82 .82	.57 .57		
15	.74 .76	.74 .74	.69 .71	.54 .54	Calculated Measured			

FIGURE 11-59

McGuire-1 Cy-1A Assembly Radial Powers Calculated vs Measured

236.23 EFPD 100%FP Control Bank D at 211 Steps Withdrawn

	H	G	F	E	D	C	B	A
8	1.09 1.06	1.17 1.21	1.09 1.08	1.14 1.17	1.07 1.05	1.13 1.17	1.00 .99	.77 .80
9	1.17 1.20	1.10 1.07	1.16 1.18	1.07 1.05	1.14 1.16	1.07 1.04	1.13 1.17	.77 .77
10	1.08 1.06	1.16 1.18	1.08 1.05	1.15 1.17	1.07 1.05	1.12 1.14	.97 .94	.71 .73
11	1.13 1.16	1.06 1.04	1.14 1.16	1.08 1.06	1.17 1.18	1.05 1.02	1.02 1.02	.55 .56
12	1.03 1.01	1.11 1.13	1.06 1.04	1.16 1.18	1.15 1.13	1.10 1.10	.83 .82	
13	1.00 1.00	1.02 .99	1.10 1.13	1.04 1.01	1.10 1.10	1.00 .99	.57 .58	
14	.96 .94	1.10 1.12	.95 .93	1.01 1.02	.82 .82	.57 .58		
15	.75 .77	.75 .75	.70 .72	.55 .55	Calculated Measured			

FIGURE 11-60

McGuire-1 Cy-1A Assembly Radial Powers Calculated vs Measured
249.75 EFPD 100%FP Control Bank D at 221 Steps Withdrawn

	H	G	F	E	D	C	B	A
8	1.10 1.07	1.17 1.20	1.08 1.06	1.13 1.15	1.06 1.05	1.12 1.16	1.00 .99	.77 .80
9	1.17 1.19	1.09 1.06	1.15 1.17	1.07 1.05	1.13 1.17	1.06 1.04	1.13 1.15	.77 .77
10	1.08 1.06	1.15 1.17	1.07 1.05	1.14 1.17	1.07 1.05	1.12 1.14	.97 .93	.72 .72
11	1.12 1.17	1.06 1.04	1.13 1.15	1.08 1.05	1.17 1.18	1.05 1.03	1.02 1.03	.56 .55
12	1.03 1.03	1.11 1.14	1.06 1.02	1.17 1.17	1.17 1.14	1.10 1.11	.83 .83	
13	1.01 1.00	1.03 1.00	1.10 1.14	1.05 1.02	1.10 1.09	1.00 1.00	.58 .59	
14	.96 .95	1.10 1.13	.96 .94	1.02 1.03	.83 .81	.58 .58		
15	.76 .78	.76 .75	.71 .73	.55 .56	Calculated Measured			

FIGURE 11-61

McGuire-1 Cy-1A Assembly Peak Axial Powers Calculated vs Measured

198.66 EFPD 90%FP Control Bank D at 217 Steps Withdrawn

	H	G	F	E	D	C	B	A
8	1.34 1.34	1.41 1.51	1.30 1.33	1.35 1.44	1.25 1.27	1.29 1.41	1.13 1.19	.86 .94
9	1.41 1.50	1.32 1.33	1.38 1.47	1.27 1.29	1.33 1.42	1.23 1.25	1.30 1.40	.86 .91
10	1.29 1.31	1.37 1.46	1.28 1.30	1.35 1.45	1.26 1.29	1.29 1.39	1.09 1.11	.79 .86
11	1.32 1.43	1.25 1.27	1.34 1.43	1.28 1.32	1.37 1.47	1.21 1.25	1.17 1.24	.61 .65
12	1.18 1.21	1.28 1.37	1.23 1.26	1.36 1.45	1.37 1.41	1.28 1.36	.94 1.00	
13	1.11 1.19	1.15 1.17	1.25 1.36	1.19 1.22	1.27 1.34	1.15 1.21	.64 .69	
14	1.04 1.08	1.22 1.32	1.05 1.08	1.14 1.21	.92 .98	.64 .69		
15	.81 .87	.82 .86	.76 .83	.60 .63	Calculated Measured			

FIGURE 11-62

McGuire-1 Cy-1A Assembly Peak Axial Powers Calculated vs Measured
217.53 EFPD 100%FP Control Bank D at 209 Steps Withdrawn

	H	G	F	E	D	C	B	A
8	1.33 1.31	1.43 1.48	1.30 1.33	1.37 1.42	1.26 1.26	1.34 1.39	1.18 1.18	.90 .94
9	1.42 1.47	1.31 1.31	1.40 1.44	1.27 1.27	1.36 1.40	1.26 1.24	1.36 1.38	.90 .91
10	1.29 1.30	1.39 1.44	1.28 1.27	1.37 1.42	1.27 1.26	1.33 1.36	1.13 1.11	.83 .86
11	1.34 1.41	1.25 1.26	1.36 1.41	1.28 1.29	1.41 1.44	1.24 1.21	1.21 1.22	.64 .65
12	1.19 1.21	1.31 1.36	1.25 1.25	1.40 1.43	1.41 1.36	1.32 1.31	.97 .98	
13	1.14 1.19	1.18 1.17	1.30 1.34	1.23 1.21	1.32 1.31	1.19 1.18	.67 .68	
14	1.10 1.10	1.29 1.32	1.10 1.09	1.19 1.21	.97 .97	.67 .68		
15	.86 .90	.87 .87	.81 .84	.63 .64	Calculated Measured			

FIGURE 11-63

McGuire-1 Cy-1A Assembly Peak Axial Powers Calculated vs Measured

223.35 EFPD 100%FP Control Bank D at 211 Steps Withdrawn

	H	G	F	E	D	C	B	A
8	1.32 1.33	1.41 1.49	1.29 1.32	1.36 1.43	1.25 1.28	1.33 1.45	1.17 1.21	.90 .97
9	1.41 1.48	1.30 1.31	1.39 1.45	1.26 1.28	1.35 1.43	1.25 1.28	1.35 1.42	.90 .93
10	1.28 1.30	1.38 1.45	1.27 1.28	1.36 1.43	1.26 1.28	1.33 1.40	1.13 1.13	.83 .87
11	1.33 1.42	1.25 1.27	1.35 1.42	1.28 1.30	1.40 1.47	1.24 1.25	1.21 1.23	.64 .66
12	1.19 1.21	1.31 1.36	1.24 1.26	1.39 1.45	1.40 1.43	1.32 1.36	.97 .99	
13	1.14 1.19	1.18 1.19	1.29 1.37	1.22 1.24	1.31 1.35	1.19 1.21	.67 .69	
14	1.10 1.12	1.29 1.35	1.10 1.11	1.19 1.23	.96 .98	.66 .69		
15	.87 .91	.87 .88	.81 .85	.63 .65	Calculated Measured			

FIGURE 11-64

McGuire-1 Cy-1A Assembly Peak Axial Powers Calculated vs Measured
236.23 EFPD 100%FP Control Bank D at 211 Steps Withdrawn

	H	G	F	E	D	C	B	A
8	1.29 1.32	1.39 1.47	1.27 1.31	1.34 1.42	1.24 1.27	1.32 1.43	1.17 1.20	.90 .96
9	1.39 1.45	1.28 1.30	1.37 1.43	1.25 1.27	1.33 1.41	1.24 1.27	1.34 1.41	.90 .93
10	1.26 1.28	1.36 1.42	1.26 1.27	1.34 1.41	1.25 1.27	1.32 1.38	1.12 1.12	.83 .87
11	1.32 1.41	1.23 1.26	1.34 1.40	1.26 1.29	1.38 1.45	1.23 1.24	1.20 1.22	.64 .66
12	1.18 1.21	1.30 1.36	1.24 1.25	1.38 1.44	1.38 1.41	1.31 1.34	.97 .98	
13	1.15 1.19	1.18 1.19	1.29 1.36	1.22 1.23	1.30 1.34	1.18 1.20	.67 .69	
14	1.11 1.12	1.30 1.34	1.10 1.11	1.19 1.22	.96 .98	.67 .69		
15	.88 .91	.88 .89	.82 .86	.64 .65	Calculated Measured			

FIGURE 11-65

McGuire-1 Cy-1A Assembly Peak Axial Powers Calculated vs Measured

249.75 EFPD 100%FP Control Bank D at 221 Steps Withdrawn

	H	G	F	E	D	C	B	A
8	1.26 1.26	1.35 1.40	1.24 1.24	1.31 1.36	1.21 1.25	1.29 1.38	1.15 1.18	.89 .95
9	1.35 1.41	1.25 1.26	1.33 1.39	1.22 1.24	1.30 1.39	1.22 1.23	1.32 1.37	.89 .91
10	1.23 1.25	1.33 1.39	1.23 1.25	1.31 1.38	1.22 1.25	1.29 1.35	1.11 1.09	.83 .85
11	1.29 1.39	1.21 1.24	1.31 1.36	1.23 1.24	1.35 1.41	1.20 1.22	1.18 1.20	.64 .65
12	1.17 1.22	1.28 1.34	1.21 1.20	1.35 1.38	1.35 1.37	1.28 1.32	.95 .97	
13	1.15 1.18	1.17 1.18	1.27 1.35	1.20 1.22	1.28 1.30	1.16 1.17	.66 .68	
14	1.10 1.12	1.29 1.34	1.09 1.12	1.18 1.22	.95 .96	.66 .67		
15	.88 .91	.88 .88	.82 .86	.64 .66	Calculated Measured			

FIGURE 11-66

Sequoyah-1 Cy-1 Assembly Radial Powers Calculated vs Measured

71.82 EFPD 100%FP Control Bank D at 200 Steps Withdrawn

	H	G	F	E	D	C	B	A
	1.14	1.09	1.19	1.12	1.16	1.05	1.01	.69
8	1.12	1.05	1.17	1.11	1.15	1.05	1.01	.71
		1.18	1.12	1.20	1.16	1.14	1.00	.75
9		1.16	1.11	1.19	1.16	1.13	1.01	.77
			1.20	1.13	1.19	1.09	.98	.64
10			1.18	1.12	1.18	1.09	.98	.66
				1.19	1.13	1.10	.93	.53
11				1.18	1.13	1.08	.92	.56
					1.10	.98	.82	
12					1.09	.99	.86	
						.98	.48	Calculated
13						1.02	.51	Measured

FIGURE 11-67

Sequoyah-1 Cy-1 Assembly Radial Powers Calculated vs Measured

101.62 EFPD 100%FP Control Bank D at 218 Steps Withdrawn

	H	G	F	E	D	C	B	A	
	1.17	1.11	1.20	1.15	1.18	1.06	1.00	.69	
8	1.14	1.06	1.16	1.13	1.17	1.06	1.00	.71	
		1.19	1.15	1.21	1.17	1.13	1.00	.74	
	9	1.16	1.12	1.18	1.16	1.12	1.01	.76	
			1.20	1.15	1.18	1.09	.97	.63	
		10	1.18	1.13	1.17	1.09	.97	.65	
				1.19	1.14	1.08	.92	.53	
			11	1.17	1.13	1.08	.91	.55	
					1.11	.99	.81		
				12	1.11	1.00	.85		
						.97	.48		Calculated
					13	1.02	.51		Measured

FIGURE 11-68

Sequoyah-1 Cy-1 Assembly Radial Powers Calculated vs Measured

133.30 EFPD 100%FP Control Bank D at 216 Steps Withdrawn

	H	G	F	E	D	C	B	A
	1.17	1.13	1.20	1.17	1.18	1.08	.99	.68
8	1.14	1.08	1.17	1.14	1.16	1.07	.99	.70
		1.19	1.17	1.20	1.18	1.12	1.00	.73
9		1.17	1.14	1.19	1.17	1.12	1.01	.76
			1.21	1.16	1.17	1.09	.96	.63
10			1.18	1.14	1.17	1.09	.96	.65
				1.18	1.14	1.07	.91	.53
11				1.16	1.13	1.06	.91	.55
					1.09	.99	.80	
12					1.09	1.00	.84	
						.96	.47	Calculated
13						1.01	.51	Measured

FIGURE 11-69

Sequoyah-1 Cy-1 Assembly Radial Powers Calculated vs Measured

166.04 EFPD 100%FP Control Bank D at 210 Steps Withdrawn

	H	G	F	E	D	C	B	A	
	1.15	1.13	1.20	1.18	1.16	1.09	.99	.69	
8	1.13	1.09	1.17	1.15	1.14	1.08	.99	.71	
		1.19	1.18	1.20	1.18	1.12	1.00	.74	
9		1.16	1.15	1.19	1.17	1.11	1.01	.76	
			1.20	1.17	1.17	1.10	.96	.63	
10			1.18	1.15	1.16	1.09	.96	.66	
				1.18	1.14	1.06	.91	.53	
11				1.16	1.13	1.06	.91	.55	
					1.08	.99	.80		
12					1.08	1.00	.84		
						.96	.48		Calculated
13						1.00	.51		Measured

FIGURE 11-70

Sequoyah-1 Cy-1 Assembly Radial Powers Calculated vs Measured

231.70 EFPD 100%FP Control Bank D at 216 Steps Withdrawn

	H	G	F	E	D	C	B	A	
	1.12	1.11	1.17	1.18	1.15	1.10	.99	.71	
8	1.10	1.08	1.14	1.16	1.13	1.09	.99	.72	
		1.16	1.18	1.17	1.17	1.11	1.01	.75	
9		1.13	1.16	1.16	1.17	1.09	1.02	.76	
			1.18	1.18	1.15	1.10	.96	.65	
10			1.16	1.16	1.14	1.10	.96	.67	
				1.16	1.14	1.06	.92	.54	
11				1.14	1.14	1.05	.92	.56	
					1.08	1.01	.81		
12					1.07	1.02	.84		
						.96	.49		Calculated
13						1.00	.53		Measured

FIGURE 11-71

Sequoyah-1 Cy-1 Assembly Radial Powers Calculated vs Measured

292.04 EFPD 100%FP Control Bank D at 216 Steps Withdrawn

	H	G	F	E	D	C	B	A	
	1.08	1.09	1.14	1.17	1.13	1.11	1.00	.73	
8	1.07	1.07	1.12	1.15	1.11	1.10	.99	.74	
		1.13	1.17	1.15	1.16	1.10	1.03	.76	
9		1.11	1.15	1.14	1.16	1.08	1.03	.78	
			1.15	1.17	1.13	1.11	.97	.67	
10			1.14	1.16	1.12	1.11	.97	.69	
				1.14	1.14	1.06	.94	.56	
11				1.12	1.13	1.05	.93	.58	
					1.07	1.03	.82		
12					1.06	1.04	.85		
						.97	.50		Calculated
13						1.00	.55		Measured

FIGURE 11-72

Sequoyah-1 Cy-1 Assembly Radial Powers Calculated vs Measured

378.92 EFPD 100%FP Control Bank D at 222 Steps Withdrawn

	H	G	F	E	D	C	B	A
8	1.06 1.02	1.06 1.04	1.10 1.08	1.14 1.14	1.11 1.09	1.12 1.10	1.01 1.00	.76 .77
9		1.09 1.07	1.14 1.13	1.12 1.10	1.14 1.14	1.09 1.07	1.04 1.05	.79 .80
10			1.12 1.10	1.14 1.14	1.11 1.09	1.11 1.11	.99 .98	.71 .73
11				1.11 1.09	1.13 1.13	1.06 1.05	.96 .96	.59 .60
12					1.08 1.06	1.05 1.06	.84 .87	
13						.98 1.02	.53 .58	Calculated Measured

FIGURE 11-73

Sequoyah-1 Cy-1 Assembly Peak Axial Powers Calculated vs Measured

71.82 EFPD 100%FP Control Bank D at 200 Steps Withdrawn

	H	G	F	E	D	C	B	A	
	1.48	1.40	1.51	1.45	1.51	1.35	1.26	.87	
8	1.55	1.42	1.57	1.50	1.60	1.42	1.33	.93	
		1.50	1.44	1.53	1.48	1.44	1.27	.94	
9		1.56	1.48	1.59	1.56	1.51	1.34	1.02	
			1.52	1.44	1.50	1.38	1.23	.80	
10			1.57	1.49	1.57	1.45	1.29	.86	
				1.51	1.44	1.38	1.17	.67	
11				1.57	1.51	1.43	1.21	.74	
					1.41	1.26	1.03		
12					1.50	1.32	1.13		
						1.25	.60		Calculated
13						1.36	.67		Measured

FIGURE 11-74

Sequoyah-1 Cy-1 Assembly Peak Axial Powers Calculated vs Measured

101.62 EFPD 100%FP Control Bank D at 218 Steps Withdrawn

	H	G	F	E	D	C	B	A
	1.44	1.37	1.46	1.41	1.45	1.30	1.20	.83
8	1.46	1.35	1.48	1.44	1.50	1.36	1.26	.88
		1.45	1.41	1.47	1.43	1.37	1.21	.89
9		1.47	1.42	1.50	1.47	1.42	1.27	.96
			1.47	1.41	1.43	1.32	1.16	.76
10			1.48	1.42	1.48	1.37	1.22	.82
				1.44	1.39	1.31	1.11	.64
11				1.48	1.43	1.35	1.14	.69
					1.35	1.21	.98	
12					1.40	1.25	1.06	
						1.18	.57	Calculated
13						1.27	.64	Measured

FIGURE 11-75

Sequoyah-1 Cy-1 Assembly Peak Axial Powers Calculated vs Measured

133.30 EFPD 100%FP Control Bank D at 216 Steps Withdrawn

	H	G	F	E	D	C	B	A	
	1.40	1.35	1.43	1.40	1.41	1.29	1.17	.81	
8	1.42	1.33	1.44	1.41	1.45	1.33	1.21	.85	
		1.42	1.40	1.43	1.40	1.32	1.18	.87	
9		1.43	1.40	1.46	1.44	1.37	1.23	.92	
			1.43	1.39	1.39	1.30	1.13	.74	
10			1.44	1.39	1.42	1.33	1.17	.79	
				1.40	1.36	1.26	1.08	.62	
11				1.42	1.38	1.29	1.10	.66	
					1.30	1.18	.95		
12					1.34	1.22	1.03		
						1.14	.56		Calculated
13						1.23	.62		Measured

FIGURE 11-76

Sequoyah-1 Cy-1 Assembly Peak Axial Powers Calculated vs Measured

166.04 EFPD 100%FP Control Bank D at 210 Steps Withdrawn

	H	G	F	E	D	C	B	A
	1.37	1.33	1.40	1.39	1.38	1.28	1.15	.81
8	1.37	1.29	1.39	1.38	1.39	1.29	1.17	.84
		1.39	1.40	1.40	1.39	1.30	1.17	.86
9		1.38	1.37	1.42	1.40	1.32	1.20	.90
			1.40	1.38	1.36	1.28	1.11	.74
10			1.40	1.36	1.38	1.30	1.13	.78
				1.37	1.34	1.24	1.06	.62
11				1.36	1.34	1.25	1.08	.66
					1.28	1.17	.93	
12					1.30	1.19	1.00	
						1.12	.56	Calculated
13						1.19	.61	Measured

FIGURE 11-77

Sequoyah-1 Cy-1 Assembly Peak Axial Powers Calculated vs Measured

231.70 EFPD 100%FP Control Bank D at 216 Steps Withdrawn

	H	G	F	E	D	C	B	A	
	1.27	1.26	1.32	1.35	1.31	1.26	1.12	.80	
8	1.28	1.24	1.31	1.34	1.31	1.26	1.13	.83	
		1.31	1.35	1.33	1.34	1.25	1.15	.85	
9		1.30	1.33	1.33	1.35	1.26	1.17	.88	
			1.33	1.34	1.29	1.26	1.08	.74	
10			1.33	1.33	1.30	1.27	1.10	.77	
				1.30	1.30	1.19	1.05	.62	
11				1.30	1.30	1.21	1.06	.65	
					1.23	1.16	.92		
12					1.25	1.18	.98		
						1.10	.56		Calculated
13						1.15	.62		Measured

FIGURE 11-78

Sequoyah-1 Cy-1 Assembly Peak Axial Powers Calculated vs Measured

292.04 EFPD 100%FP Control Bank D at 216 Steps Withdrawn

	H	G	F	E	D	C	B	A
	1.23	1.22	1.28	1.32	1.27	1.26	1.12	.82
8	1.24	1.23	1.28	1.33	1.29	1.26	1.14	.85
		1.26	1.31	1.29	1.31	1.23	1.16	.87
	9	1.28	1.32	1.31	1.34	1.24	1.18	.89
			1.29	1.31	1.26	1.25	1.08	.76
		10	1.31	1.32	1.28	1.27	1.11	.79
				1.27	1.28	1.18	1.06	.64
			11	1.28	1.30	1.20	1.07	.66
					1.21	1.17	.92	
				12	1.24	1.19	.97	
						1.10	.57	Calculated
					13	1.15	.63	Measured

FIGURE 11-79

Sequoyah-1 Cy-1 Assembly Peak Axial Powers Calculated vs Measured

378.92 EFPD 100%FP Control Bank D at 222 Steps Withdrawn

	H	G	F	E	D	C	B	A
8	1.19 1.22	1.20 1.22	1.24 1.27	1.30 1.34	1.26 1.28	1.27 1.29	1.15 1.17	.86 .90
9		1.23 1.26	1.29 1.33	1.26 1.30	1.30 1.34	1.23 1.25	1.19 1.22	.89 .93
10			1.26 1.29	1.30 1.33	1.25 1.28	1.26 1.30	1.11 1.14	.80 .84
11				1.26 1.28	1.28 1.32	1.20 1.23	1.09 1.11	.67 .69
12					1.22 1.26	1.19 1.24	.94 1.00	
13						1.11 1.19	.59 .67	Calculated Measured

FIGURE 11-80

McGuire-1 Cy-1 PDQ07 Assembly Radial Powers Calculated vs Measured

PDQ07 - 52.2 EFPD vs Core Meas - 48.8 EFPD

	H	G	F	E	D	C	B	A
8	1.16 1.12	1.10 1.09	1.20 1.19	1.20 1.21	1.23 1.23	1.12 1.12	1.01 1.01	.68 .71
9		1.18 1.15	1.12 1.13	1.23 1.22	1.18 1.19	1.15 1.14	1.00 1.02	.74 .75
10			1.22 1.20	1.19 1.19	1.20 1.18	1.09 1.10	.97 .97	.63 .64
11				1.20 1.19	1.08 1.08	1.08 1.07	.94 .96	.53 .54
12					1.22 1.18	.92 .92	.80 .81	
13						.96 .95	.46 .46	Calculated Measured

FIGURE 11-81

McGuire-1 Cy-1 PDQ07 Assembly Radial Powers Calculated vs Measured

PDQ07 - 104.4 EFPD vs Core Meas - 104.5 EFPD

	H	G	F	E	D	C	B	A
8	1.17 1.15	1.13 1.15	1.19 1.19	1.20 1.23	1.20 1.19	1.12 1.12	1.00 1.00	.69 .70
9		1.18 1.17	1.14 1.16	1.21 1.20	1.18 1.19	1.13 1.12	1.01 1.02	.74 .74
10			1.20 1.18	1.19 1.20	1.18 1.16	1.09 1.11	.96 .96	.64 .64
11				1.19 1.17	1.10 1.11	1.07 1.07	.94 .96	.54 .53
12					1.21 1.18	.94 .94	.80 .80	
13						.96 .94	.47 .47	Calculated Measured

FIGURE 11-82

McGuire-1 Cy-1 PDQ07 Assembly Radial Powers Calculated vs Measured

PDQ07 - 156.7 EFPD vs Core Meas - 150.2 EFPD

	H	G	F	E	D	C	B	A
8	1.17 1.15	1.15 1.17	1.18 1.17	1.19 1.21	1.17 1.17	1.12 1.13	1.00 1.00	.70 .71
9		1.17 1.15	1.15 1.17	1.18 1.17	1.17 1.19	1.12 1.10	1.02 1.03	.75 .74
10			1.18 1.16	1.18 1.20	1.16 1.14	1.10 1.11	.96 .95	.65 .65
11				1.17 1.16	1.11 1.12	1.07 1.06	.95 .96	.55 .54
12					1.20 1.17	.96 .97	.81 .81	
13						.96 .95	.49 .48	Calculated Measured

FIGURE 11-83

McGuire-1 Cy-1A PDQ07 Assembly Radial Powers Calculated vs Measured

PDQ07 - 208.9 EFPD vs Core Meas - 198.7 EFPD

	H	G	F	E	D	C	B	A
8	1.10 1.08	1.22 1.23	1.08 1.09	1.17 1.19	1.05 1.06	1.16 1.18	.99 .99	.78 .79
9	1.22 1.22	1.09 1.08	1.20 1.20	1.06 1.06	1.17 1.18	1.05 1.05	1.18 1.17	.76 .76
10	1.07 1.07	1.19 1.19	1.06 1.06	1.18 1.19	1.06 1.06	1.16 1.16	.95 .93	.72 .72
11	1.14 1.17	1.04 1.04	1.17 1.18	1.08 1.08	1.22 1.22	1.04 1.04	1.03 1.03	.54 .54
12	.98 .99	1.12 1.13	1.04 1.04	1.21 1.21	1.20 1.17	1.15 1.13	.83 .83	
13	.96 .99	.98 .98	1.12 1.14	1.03 1.02	1.14 1.12	1.02 1.01	.58 .58	
14	.91 .91	1.11 1.11	.91 .91	1.01 1.01	.82 .82	.58 .57		
15	.73 .74	.72 .72	.69 .70	.53 .53	Calculated Measured			

FIGURE 11-84

Sequoyah-1 Cy-1 PDQ07 Assembly Radial Powers Calculated vs Measured

PDQ07 - 103.6 EFPD vs Core Meas - 101.6 EFPD

	H	G	F	E	D	C	B	A	
8	1.16 1.14	1.08 1.07	1.17 1.17	1.13 1.13	1.18 1.17	1.08 1.07	1.01 1.00	.71 .71	
9		1.17 1.16	1.12 1.12	1.19 1.19	1.17 1.17	1.14 1.13	1.02 1.01	.77 .77	
10			1.18 1.18	1.13 1.13	1.18 1.18	1.10 1.10	.97 .98	.65 .66	
11				1.18 1.18	1.15 1.14	1.09 1.08	.91 .92	.55 .56	
12					1.13 1.11	1.00 1.00	.84 .85		
13						1.01 1.02	.50 .51		Calculated Measured

FIGURE 11-85

Sequoyah-1 Cy-1 PDQ07 Assembly Radial Powers Calculated vs Measured

PDQ07 - 155.5 EFPD vs Core Meas - 133.3 EFPD

	H	G	F	E	D	C	B	A	
	1.17	1.11	1.18	1.16	1.17	1.09	1.00	.71	
8	1.13	1.09	1.18	1.16	1.15	1.08	.99	.71	
		1.18	1.16	1.19	1.18	1.12	1.02	.76	
9		1.17	1.16	1.19	1.18	1.12	1.01	.77	
			1.19	1.16	1.17	1.10	.96	.65	
10			1.19	1.16	1.17	1.10	.96	.66	
				1.17	1.15	1.07	.90	.55	
11				1.16	1.14	1.06	.92	.56	
					1.11	1.00	.82		
12					1.08	1.00	.84		
						.99	.50		Calculated
13						1.00	.52		Measured

FIGURE 11-86

Sequoyah-1 Cy-1 PDQ07 Assembly Radial Powers Calculated vs Measured

PDQ07 - 362.7 EFPD vs Core Meas - 378.9 EFPD

	H	G	F	E	D	C	B	A
	1.04	1.04	1.09	1.15	1.11	1.13	1.01	.77
8	1.03	1.04	1.09	1.14	1.09	1.10	1.01	.78
		1.07	1.14	1.11	1.16	1.09	1.06	.80
9		1.07	1.14	1.11	1.15	1.08	1.05	.81
			1.11	1.15	1.11	1.12	.98	.72
10			1.11	1.14	1.10	1.12	.99	.73
				1.11	1.15	1.06	.95	.60
11				1.10	1.13	1.05	.96	.61
					1.08	1.05	.85	
12					1.07	1.07	.87	
						1.01	.57	Calculated
13						1.03	.59	Measured